Design, Fabrication and Performance Investigation of a Centrifugal Reaction Water Turbine for Low Head and Low Flow Application

BY

KIPLANGAT C. KONONDEN

A THESIS SUBMITTED TO THE SCHOOL OF ENGINEERING, DEPARTMENT OF MECHANICAL AND PRODUCTION ENGINEERING IN PARTIAL FULFILMENT OF THE REQUIREMENTS FOR AWARD OF THE MASTER OF SCIENCE DEGREE IN ENERGY STUDIES

MOI UNIVERSITY

APRIL, 2019

DECLARATION

Declaration by Student

I certify that except where due acknowledged, the work here in is that of the author alone; the work has not been submitted previously, in whole or in part, to qualify for any other academic award; the content of the thesis is the result of work which has been carried out since the official commencement date of the approved research program; any editorial work, paid or unpaid, carried out by a third party is acknowledged; and, ethics procedures and guidelines have been followed. No part of this project should be reproduced without prior written permission of the author and/or Moi University.

Sign:_____   Date:_____

Kiplangat C. Kononden
TEC/PGMP/05/14

Declaration by the Supervisors

This thesis has been submitted with our approval as university supervisors.

Sign:_____   Date:_____
Prof. Augustine Makokha
Dpt. of Energy
Moi University

Sign:_____   Date:_____
Prof. Cox Sitters
Dpt. of Civil and Structural Eng.
Moi University

DEDICATION

I dedicate this this thesis to my parents Mr. and Mrs. David Kipkononden Towett.

ACKNOWLEDGEMENT

ABSTRACT

There are few small to medium scale low head and low flow hydro turbines commercially available, but they are very expensive and inefficient for micro power generation. Therefore, there is an intrinsic need of micro-hydro turbines that can encourage the exploitation of hydropower available in Africa's' small rivers and streams. The main aim of this research was to design, fabricate and test a simple, low head and low flow micro-hydro turbine model, that operate with relatively high efficiency while maintaining low cost of manufacturing. Continuum mechanics approach was adopted where the design of the single arm reaction turbine was derived from a mathematical model that was based on the balance equations formulated in a rotating control volume. Once the fabrication was complete, experimental tests were conducted on the model turbine. The tests assessed the power output and efficiency by varying the head, orifice diameter as well as the arm radius. Output power was determined from the operating torque and angular speed of the turbine. A rope brake dynamometer was attached to the turbine to find the torque and a digital tachometer was used to measure the operating angular speed. Power output of each experiment was examined in relation to the specific variables using quantitative analysis. Using the collected data, the coefficient of performance was determined. Experimental results showed that; angular speed increases with increase in the water mass flow rate. Flow-rate also increased with the increase in the radial arm length. The radial arm length affects the operating angular velocity, output torque as well as the overall turbine efficiency. The optimum nozzle to main conduit cross-sectional area ratio that gives the optimum efficiency is in the range of 0.18 to 0.24. The research achieved to build a non-complex turbine with an optimum efficiency of 83% and 40% at a head of 1.85 m and 11.5 m respectively. Theoretical efficiency was found to be 93.4%. The research concluded that the semicircular centrifugal reaction water turbine is a fairly suitable type of turbine for low head and low to medium flow application. The research recommended that an arm conduit with a larger and varying cross-sectional area could be used so as to allow higher discharge and scaling up of the turbine. However further research is still needed on how water from the reservoir gets into the turbine and exits.

TABLE OF CONTENTS

LIST OF TABLES

LIST OF FIGURES

NOMENCLATURE

A_1 Conduit's cross-sectional area (m^2)

A_N Nozzle cross-sectional area (m^2)

β Nozzle projection angle (deg)

c.A   Cross-sectional area (m^2)

F   Turbine force (N)

f   Coefficient of friction (-)

g   Acceleration due to gravity (m/s^2)

H   Supply head (m)

H_a Absolute operating head (m)

H_c Centrifugal Head (m)

k   Is aproportionality factor depending on the roughness and other losses in the turbine conduit and nozzle (-)

K   Non-dimensional factor representing the ratio of the head due to angular acceleration to the head due to gravitational acceleration (-)

$\dot{m}$ Mass flow rate of water flowing through the turbine (kg/s)

ρ Density of water (kg/m^3)

P   Power (W)

P_i Input power (W)

P_O Output power (W)

Q Volume flow rate of water (m^3/s)

r   Conduits cross-sectional radius (m)

r_1 Pulley radius (m)

r_d Rope radius (m)

r_p Effective pulley radius (m)

R   Turbine arm radius (m)

R_e Reynolds number (-)

T   General Turbine torque (Nm)

T_a Absolute output torque (Nm)

T_c Torque due to centrifugal force (Nm)

T_g Torque due to gravity only (Nm)

T_f Frictional torque (Nm)

T_N Nozzle torque (Nm)

u   Tangential velocity of the nozzles (m/s)

ω Turbine angular velocity (rad/s)

W   Weight in Newton (N)

W_0 Dead load (N)

v   Water flow velocity (m/s)

v_a Absolute flow velocity (m/s)

v_e Exit flow velocity (m/s)

v_r Relative flow velocity (m/s)

t Time (s)

N   Rotational speed (rpm)

n   Main pipe to nozzle cross-section area ratio (-)

η Turbine efficiency (-)

CHAPTER ONE

INTRODUCTION

1.1 Introduction to Energy

Energy is a crucial component when performing a certain work. Energy sources are classified into renewable and non-renewable energy sources. Renewable energy sources include; Biomass Energy, Wind Energy, Solar Energy, Geothermal Energy, Hydro energy. Non-renewable energy sources comprises of fossil fuel among others.

Electricity is a secondary source of energy, generated through consumption of primary energy sources, namely; renewable energy, fossil fuels and nuclear energy.

All animals including man use chemical energy in their bodies to perform various duties. Sometimes times this was achieved through the use of slave labour as an energy source. As time passed, man came up with ways to harvest the naturally available energy and used it to perform certain piece of work, particularly heavy work. Natural energy exploitation has since then developed.

The application of fire was the earliest form to release energy from biomass, for example using wood from trees. This method is still widely used in Kenya. The main uses of fire are/were; cooking food, warming houses/caves, as a source of light and making better tools. Various methods of deriving heat from biomass have since then developed.

For the past four and half millenniums the energy sector has experienced numerous scientific developments. To begin with, is wind energy; the first known use was in 2500 BC when people used sails to navigate the Nile River. Persians had already been using windmills for 400 years by 900 AD in order to pump water and grind grain (Derry & Williams, 1993). Windmills may have even been developed in China before

1 AD, but the earliest documentation was written at around 1219 AD. Cretans were using "literally hundreds of sail-rotor windmills to pump water for crops and livestock." (Kothari *et al.*, 2011).

Wind energy is closely followed by direct solar heat energy. It was used for heating and drying of substances.

Hydro Energy was also one of the utmost innovations. Water-falls as a source of energy is known from ancient times. It was used to turn water wheels for grinding purposes. During the 19th century industrial revolution, wooden water wheels were replaced by turbines.

The other major discovery in the field of energy is the use of fossil fuels to provide heat and light. Fossil fuels include coal and all the oil and natural gas products. Introduction of petroleum products has seen the field of science experience massive developments, particularly the transport sector.

Despite the presence of all the above forms of energy one particular type of energy has been noted to be consumed in large quantities. Electricity is one of the recent forms of energy to be discovered. Electricity itself is derived from other forms of energy, as they are converted into electric current.

Burning of fossil fuels is the primary source of extra greenhouse gases which includes CO_2. These gases help to trap heat from the sun, keeping the earth warm. This process is famously known as greenhouse effect and is responsible for the earth's climate change.

The consequences of climate change include changes in wind and current patterns, leading to more droughts, more floods, hotter temperatures in some places and, ironically, colder temperatures in others (Najafi *et al.,* 2o15).

As a result of the creeping environmental pollution, due to excess use of fossil fuels, scientists have been forced to come up with new energy sources. Many researchers are directing their attention to what is now referred as renewable energy sources. Renewable energy is actually the energy obtained from natural and persistent flows of energy occurring in the immediate environment. An obvious example is solar energy. Note that the energy is already passing through the environment as a current or flow, irrespective of there being a device to intercept and harness this power. Such energy may also be called Green Energy or Sustainable Energy (Twidell & Weir, 2006). Renewable energy should also have no/minimal effects on the environment.

Owing to thorough researches, splendid sources of energy have been discovered. This includes Biogas, Bioethanol, biodiesel, Hydrolysis, electromagnetic energy which is still under research, and the highly used nuclear energy.

Nuclear fission is as a result of splitting the atoms apart to produce smaller atoms, and consequently energy is released. Nuclear fission is used in nuclear power plants to generate electricity through the splitting of the nuclei of uranium atoms, especially U-235.

On the other hand, when atoms are joined together to form a larger atom is commonly referred to as nuclear fusion. The sun produces energy through nuclear fusion where the nuclei of hydrogen atoms are fused into helium atoms. Fusion power offers the prospect of an almost inexhaustible source of energy for future generations, but it also presents so far insurmountable scientific and engineering challenges. Today, many

countries take part in fusion research to some extent, led by the European Union, the USA, Russia and Japan, with vigorous programs also underway in China, Brazil, Canada, and Korea (http://www.world-nuclear.org/information-library/current-and-future-generation/nuclear-fusion-power.aspx, 6/1/2017)

Unfortunately, nuclear power generation has by-product wastes. These by-products are spent fuels, radioactive waste and heat. The primary environmental concerns for nuclear power are spent fuels and radioactive wastes (http://www.azocleantech.com/article.aspx?ArticleID=60, 6/1/2017).

Despite all the hard work to reduce the cost of energy as well as to increase its availability, energy cost is still relatively high.

From various literatures hydro energy contributes the highest percentage towards electricity generation in the renewable realm and is evenly distributed across the world (Sternberg, 2008). This means that there is need for the most efficient and reliable machines for this application. Turbines are more often than not, used for the transformation of hydro energy to mechanical energy. Most historians consider turbines as the prime hauliers of civilization for the last eight centuries.

1.2 Introduction to Small Scale Hydro-Power generation

At the moment Hydro-power is one of the most conventional and broadly used renewable resource for generation of electricity and other commercial activities. Most of the early generation of electricity were often derived from hydro-turbines. The capacity of the total worldwide installations has since then grown at about 5% per year. Hydro-power as at 2007 accounted for about 20% of world's electricity generation (Twidell and Weir 2006). China, Canada, Brazil, and the United States were the leaders in hydroelectric production as at 2008 (Sternberg, 2008).

In Africa though, Hydro-power accounts for more than 38% of total electricity generation (Secretariat, 2014). This is because there are many big rivers reliable for hydro power generation. Nevertheless the big rivers are becoming more and more vulnerable due to the changing climates among other factors like environmental and socio-economic concerns (Mango *et al*., 2011). This has necessitated the move to small hydro power generation. The limitation to this move is attributed to following factors; lack of access to appropriate technologies in the small-hydro category, lack of infrastructure for manufacturing, installation and operation. There is also the lack of local capacity to design and develop small hydropower system for Africa's remote areas (Kaunda *et al*., 2012).

Hydroelectricity as at 2015 accounted for about 40% of Kenya's electricity mix, becoming the most commonly used form of renewable energy, as shown in Table 2.2. Kenya's total installed large hydropower capacity is 743 MW. However Kenya currently generates less than 30MW from micro-hydro resources, which is insignificant compared to the estimated potentials of about 3000Mw form medium to small rivers and streams (www.erc.go.ke, 5/08/2015).

As by the ministry of energy, various factors have lead to the low exploitation of small-scale hydro-electricity which includes the following; High cost of installation averaging about KES 250,000 per KW, insufficient data for medium to small rivers hydrology, climatical changes, and hardly reliable small hydro power components from the local fabricators and suppliers (www.erc.go.ke, 5/08/2015).

To alleviate these shortcomings, the Government of Kenya is carrying out a programmed feasibility studies to understand the various potential micro-hydro power sites and there capacities across the country. This research on a centrifugal reaction

water turbine for low heads and low volume flow rates hopes to improve the exploitation of small-scale hydro-electricity.

Figure 1.1 shows the World's Hydropower scenario as at 2004. Technically exploitable potential is 14000 TWh/year, economically exploitable potential is 8000 TWh/year, present hydro power generation is 2800 TWh/year and world electricity production is 18580 TWh/year (Taylor, 2004).
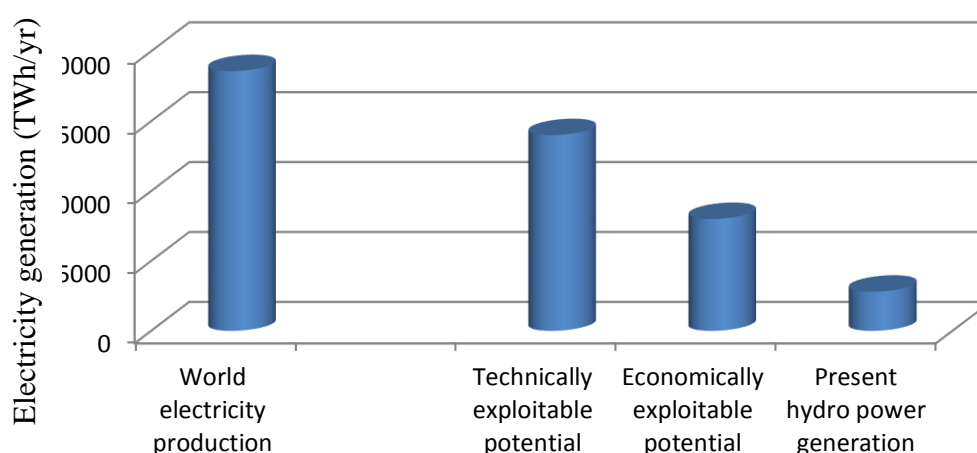
Figure 1.1: World's Hydropower scenario as at 2004 (Taylor, 2004)

Another research done in Kenya revealed that Pico hydro power plants (i.e. power less than 15 kW) are able to supply electricity to households at a fraction of the cost to the end-user compared with either solar PV or using car batteries charged at grid connected charging stations (Maher *et al*., 2003).

Recently initiatives have seen the light in a number of countries in Africa to revive the hydropower sector, either through international development agencies or through private sector led initiatives. In Central Africa (Rwanda), East Africa (Kenya and Tanzania) while in southern Africa (Malawi, Mozambique and Zimbabwe) most of those initiative are focusing on implementing small scale hydropower projects (Mango *et al*., 2012).

Table 1.1: Africa's Hydro Status (Kaunda et al., 2012)

COUNTRIES	Current electricity production (MW)	Hydro generation	Current Micro-hydro generation	Micro-hydro Potentials
Kenya	~ 2000+	~ 790 MW	~ 30 MW	~ 3,000 MW
Benin	~ 350	~ 170 MW		~ 1500 MW
Tanzania	~ 1500	~ 900 MW	~38 MW	
Ethiopia	~ 2150	~ 1200 MW		~ 18,000 MW
Ghana	~ 2700	~ 1300 MW		~ 5,000 MW
Mali	~ 340	~ 170 MW		
Mozambique	~2308	~ 2200 MW	~150 MW	~ 2500 MW+
Rwanda	~ 97	~ 57 MW		~1500 MW
Senegal	~ 780	~ 75 MW		
Uganda	~ 822	~ 750 MW		

In a small-scale hydro-power scheme, water is taken from the river by diverting it through an intake at a barrier as shown in figure 1.2. For high and medium-head setup water may first be passed horizontally to the fore-bay tank by a small canal. The waters are directed to a settling dam at the fore-bay, to allow solid particles to settle-down before descending to the turbine. Otherwise the solid particles will destroy the turbine. A rigid conduit known as a 'penstock' transmits the water from the fore-bay to the turbine, which is situated in the powerhouse together with the generator and control apparatus. From the turbine, the waters are discharged down a 'tail-race' channel back into the river. Figure 1.2 shows the Main components of a Hydro power Scheme.
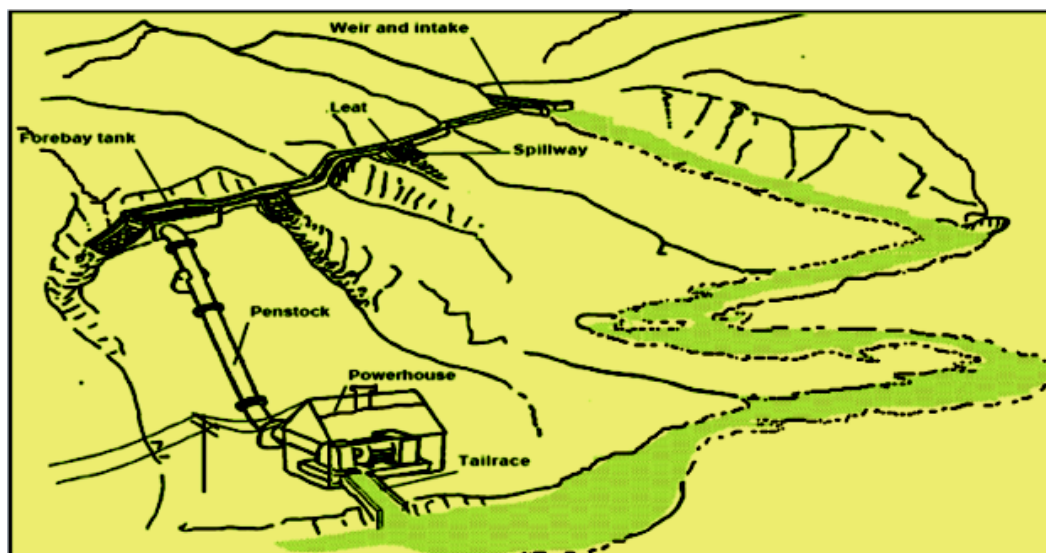
Figure 1.2: Main components of Hydro power Scheme (http://edugen.wiley.com, 05/08/2015)

When harvesting hydro-power, turbine machines are used. A Turbine is a machine that converts hydro's kinetic energy to mechanical energy in form of a contained rotating shaft. The rotating shaft can then be used to drive a generator which in turn produces electrical energy. Otherwise the rotating shaft can be used directly for supplementary mechanical application, and a good example is irrigation activities (Calvert, 2003).

1.3 Problem Statement

For the last one and half centuries hydroelectric production comes mostly from large projects, with dams that require a large reservoir of water to supply the turbine generator. Since most of the best locations for this type of hydro power around the world and even in Africa are already being used, research and development for hydro power is moving towards micro-hydro systems, which require less water to operate and can supply electricity to smaller communities or individual homes.

Currently there are a few companies who manufacture turbines and supply equipment for generation of electricity from micro hydro sources. Most of the low head micro hydroelectric units available use impulse type turbines for energy conversion (Date, 2009). From the turbines literature review, it is clear that impulse turbines are suitable for high head and low volume flow rate applications only. When impulse turbines are used for low head operation their energy conversion efficiency drops drastically to even less than 60% (Harvey, 2005, Waddell, 1999).

Furthermore the current turbines are complex to manufacture, more so in the ordinary workshops since most of them require moulding processes and dedicated machines to fabricate (Toshiba, 2010). This alone, contributes a lot to the high cost of the turbine. For example the unit cost of a 7kW cross flow turbine (i.e. excluding alternator and drive unit) meant for micro-hydro application, is approximately KES 500,000 (Harvey, 2005). This figure falls to KES 200,000 when manufactured in a local workshop.

Maintenance of these turbines too presents a big challenge particularly in developing countries (Barr, 2013). This leads to relatively high operation cost for micro hydro power.

1.4 Justification and Significance of Study

Hydropower is an example of renewable energy and it is the most reliable base-load energy source. Nevertheless, there is huge untapped technically exploitable hydro energy potential of about 14,000TWh (Taylor, 2004, Basar, 2011) waiting to be utilized throughout the world. Most of this untapped hydropower comes from Micro-hydro power sources.

There are few small to medium scale low head and low volume flow rate hydro turbines commercially available, but they are very expensive and inefficient for micro power generation at individual level. Therefore, there is an inherent need for a simple, low cost, efficient, low head and low volume flow rate hydro turbine that can encourage the exploitation of hydropower available in Africa's' small rivers, streams at individual level.

Simple, low cost with high efficiency water turbine will solve a number of the drawbacks faced in micro hydro-power investments.

The other benefit is that this turbine is economical and portable.

1.5 Objectives

1.5.1 General Objectives

To design, fabricate and investigate the performance characteristics of a simple, centrifugal, reaction water turbine structure.

1.5.2 Specific Objectives

   i.   To design and fabricate a single arm, centrifugal, reaction water turbine system structure.

   ii.   To determine the most efficient nozzle to main pipe ratio and the overall efficiency of the turbine.

  iii.   To determine the relation between the arm length (arm radius) and the output power and find the optimum arm length at optimum nozzle to main pipe ratio for low head and high head.

1.6 Scope

The project is an extension of other experiments in the field of turbines with the main aim of designing, fabricating and test running a centrifugal reaction turbine structure and finally collecting data that will form a guide line for future manufacture of the actual turbine system.

In this research a single arm, centrifugal reaction turbine design and its manufacture method was proposed, including the actual construction of the turbine. The turbine design emphasised on low-cost fabrication of the prototype. The research further went ahead to fabricate and carried out a performance analysis of the single arm centrifugal reaction water turbine.

This research was more of a laboratory study of a single arm reaction turbine structure. The turbine's performance characteristics was analysed so as to find the viability of this particular design for micro-hydro applications.

The potential application of this turbine is more likely in remote and economically poor areas. Consequently the materials used for fabrication are those which are generally available. Standard plumbing pipes and fittings of steel/iron or plastic are easily available these days.

1.7 Limitations

The research concentrates only on converting the potential/kinetic energy of the water into mechanical energy and does not pay attention to the various uses of this mechanical energy which poses another challenge.

This research does not pay attention to the process by which the water reaches the turbine from the river (reservoir, penstock design, housing for turbine). Furthermore the research does not pay attention to the process by which the water flows back to the river.

CHAPTER TWO

LITERATURE REVIEW

2.1 A Preview of Fluid Machines

Fluid machines are categorised into two main categories; power absorbing machines (cases where work is done on fluids) and the other one is power producing machines (cases where work is done by fluid). Figure 2.1 is a diagram showing the two main groupings of fluid machines with their examples.

```
                        ┌─────────────────┐
                        │ Fluid Machines  │
                        └─────────────────┘
              ┌────────────────┴────────────────┐
    ┌───────────────────┐            ┌───────────────────┐
    │ Work done on the  │            │ Work done by the  │
    └───────────────────┘            └───────────────────┘
              │                                │
    ┌───────────────────┐            ┌──────────────────────────┐
    │ Power absorbing   │            │ Power producing machines │
    └───────────────────┘            └──────────────────────────┘
              │                                │
    ┌────────────────────────┐       ┌──────────────┐
    │ Pumps, fans, compressors│      │   Turbines   │
    └────────────────────────┘       └──────────────┘
```
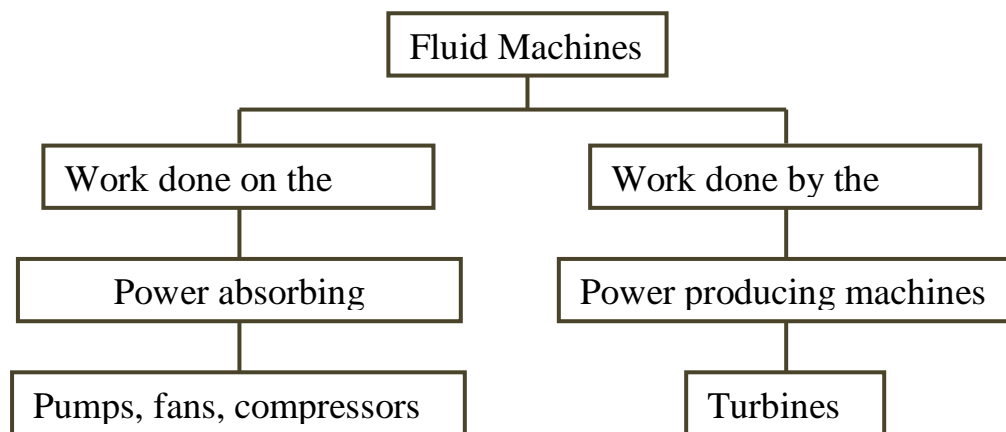
Figure 2.1: Fluid Machines classification

The kinetic energy of a liquid or air can either be added or extracted from it. To add flow energy to a liquid, a pump is used or a compressor when working with gaseous substances. When extracting energy from a liquid for example water, turbines are utilised or wind turbines in the case of wind energy. Fluid machines are used in a wide range of mechanical activities, which includes; hydro and thermal power stations, propulsion of aircrafts and ships among others.

Fluid machines can also be classified, according to their mode of operation i.e. Positive displacement machines, Rotodynamic machines.

In positive displacement machines, a liquid or gas is haggard into a fixed space bounded by a compact wall then potted in it, and ultimately forced out from space.

The cycle is repeated all over again. The speed of the machine (in this case a pump) determines the flow rate of the fluid. Positive displacement fluid machines include; gear pumps, vane pumps reciprocating pumps.

On the other hand, Rotodynamic machines are designed to contain a free flow space situated between the inlet of the machine and all the way to the outlet. As the fluid flow within the machine there is a pressure variations which causes the flow of fluid to either increase when work is done fluids (as in the case of pumps) or decrease when work is done by the fluid (as in the case of turbine) . Rotodynamic machines include; centrifugal blowers, centrifugal pumps and hydraulic turbines among others.

Fluid machines can as well be classification based on the geometry of the flow-course. In a radial flow machines the main flow is perpendicular to the rotating axis and moves radialy in or outward. An axial flow machine guides the flow parallel to the rotating axis, i.e. in axial direction. A mixed flow machine combines the two. Figure 2.2 is a chart that shows a summary of various fluid machines classifications in detail.
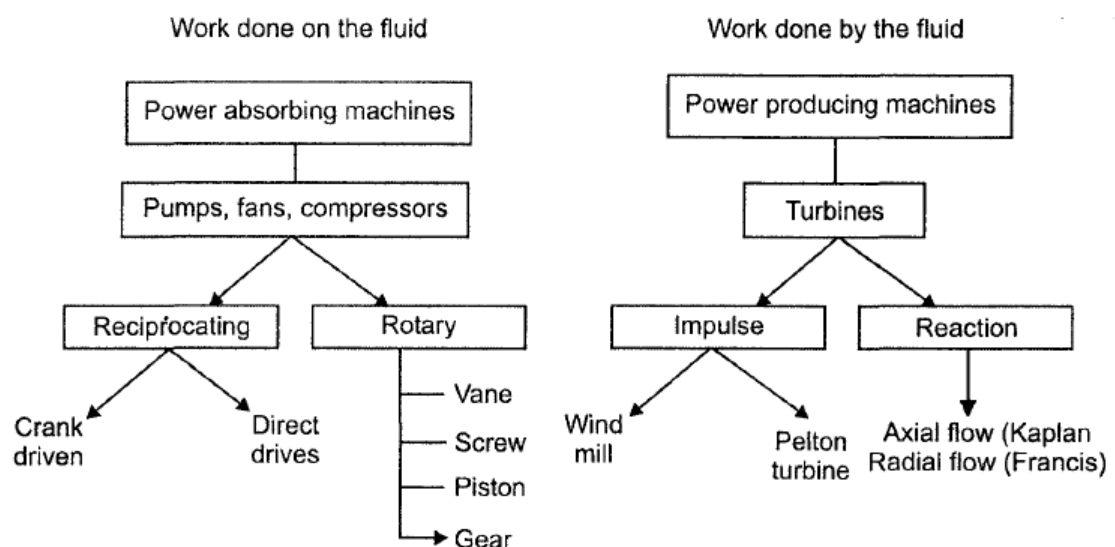
Figure 2.2: Fluid Machines classifications. (Husain et al., 2008)

2.2 Turbines in General

A Turbine is a machine that converts the kinetic energy of a flowing fluid, to mechanical energy in form of a contained rotating shaft. The rotating shaft can then be used to drive an electric generator or direct mechanical application. For the past two and half millennium turbine technology has experienced tremendous transformation.

The word "turbine" was derived from the Latin word for "whirling" or a "vortex" introduced by a French engineer Claude Bourdin. He used the word 'turbine' to describe the theme of an 1826 engineering competition for a water power source (Strandh, 1979).

Turbines can be classified according to its applications, in relation to the type of fluid involved. The common types of turbines include; wind turbine, steam/gas turbine and water turbine. All the three turbines are different but have similar designs and even similar mathematical modelling. Wind turbines find its application in wind farms, where they are used to harvest the kinetic energy of moving air (wind) into a mechanical rotating shaft.

Steam turbines find their applications in thermal power plants. When water is heated in a closed container usually known as boiler, it is possible to obtain large quantities of steam at a relatively high pressure. If an outlet is created the pressurized vapours will expand to a lower pressure zone. By so doing the internal energy contained in the vapours is transform into kinetic energy, which can be converted to mechanical rotating shaft using a steam turbine. However steam is a compressible fluid and its density depends on its pressure which is not the case with water. Furthermore, steam is much less dense than most liquids. High velocities are therefore deemed essential

for large energy transfer. As at 2015, steam turbines provided over 70% of electric power (Twidell & Weir, 2015).

Last but not least are Water Turbines. For thousands of years water wheels have been used to convert the energy contained in falling water directly into mechanical rotary power. Water wheels are fairly efficient, but do not have the ability to handle varying head applications. Water turbines were developed in the 1800's during the industrial revolution era to skirt these limitations and improve the efficiency of the then machinery.

2.3 Conventional Water Turbines

Typically there are two types of water turbines. There is the impulse type turbine and the reaction type turbine. Impulse turbine is a rotating structure (known as impeller) acted upon by the force of moving water. The high velocity jets of water are directed to hit the vanes which are mounted on the impeller hence causing a rotational motion. Examples of impulse turbine are; Pelton, Turgo, Cross-flow turbines. On the other hand a reaction turbine takes advantage of the Newton's third law of motion which is the action and reaction principle. The pressure possessed by the water is applied on the rotor blades and is converted to torque. Examples of reaction turbines includes; Francis, Kaplan, Archimedes screw turbines.
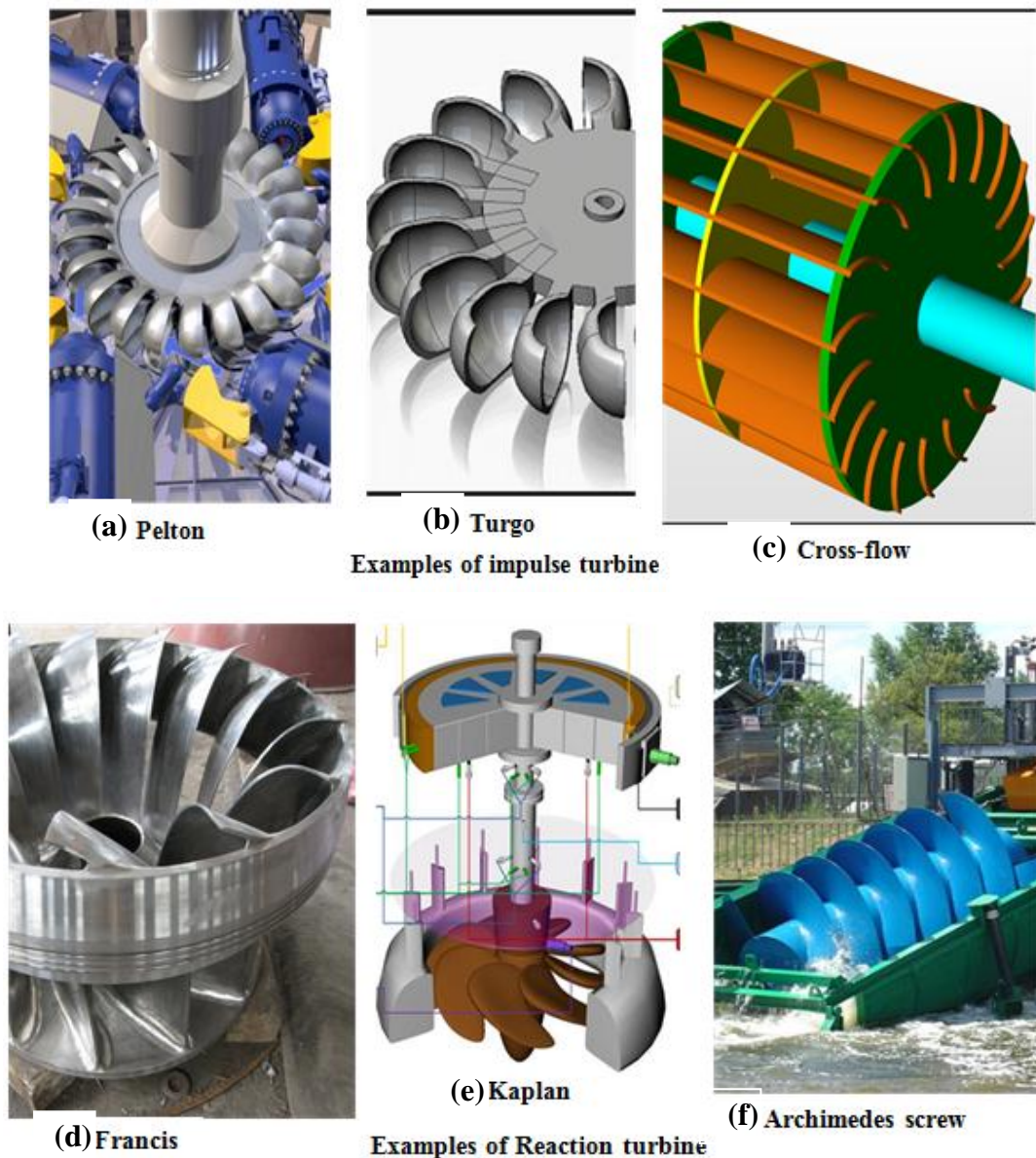
Figure 2.3: Impulse and reaction turbines. (Husain et al., 2008)

2.4 Efficiencies and Operating Conditions of the Various Water Turbines

The table 2.1 shows a summary of most turbines. It includes the appropriate application of each and every type. The table also illustrate the best head (H) for each type of turbine.

Table 2.1: Turbine classification (Kothandaraman & Rudramoorthy, 2007)

Type of Turbine	Classification		
	High Head (>50M)	*Medium(10 – 50M)*	*Low (<10M)*
Impulse Turbine	• Pelton • Turgo	• Cross flow • Multi-jet Pelton • Turgo	• Cross flow
Reaction Turbine		• Francis	• Kaplan • Archimedes Screw

The diagram in figure 2.4 shows graphs of load efficiency characteristics in relation to volume flow rate. Q_0 is the designed flow rate of the turbine while Q is the actual operating flow rate.
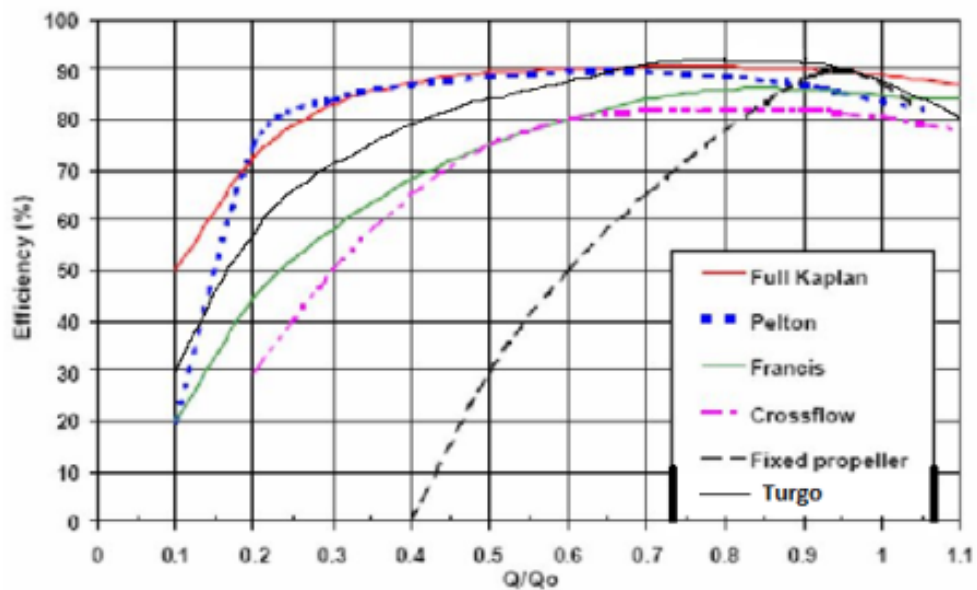
Figure 2.4: Load efficiency characteristics of hydraulic turbines (Kothandaraman & Rudramoorthy 2007)

The diagram in figure 2.5 illustrates the head and volume flow rate operating conditions for the various impulse and reaction turbines. Pelton, Francis and Kaplan turbine are the most widely used turbines since they cover a larger area (http://www.3helixpower.com/hydropower/types-of-turbines/ 8/8/2015).
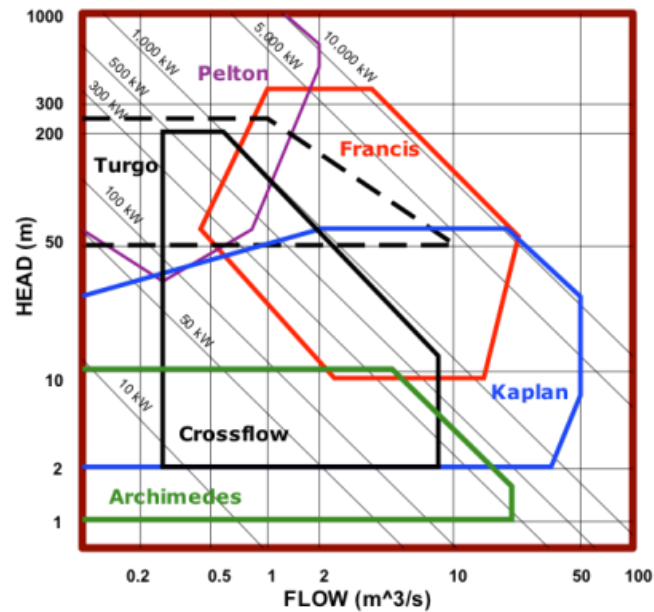
Figure 2.5: Operating areas of the various turbines in terms of head and volume flow rate (http://www.3helixpower.com/hydropower/types-of-turbines/ 8/8/2015)

2.5 Small-Scale Reaction Water Turbines

2.5.1 Introduction

This section focuses on the history and advancement in the small scale reaction water turbine sometimes referred as simple reaction water turbine. Most of these simple reaction water turbines are used in micro hydro application while most of the hydro plants worldwide are medium to large scale. It is for this reason why they are not famous (Akbarzadeh, 2001).

2.5.2 Some historical reaction water turbines

2.5.2.1 Hero's turbine

The earliest ever historically recorded outward-flow turbine is said to be discovered almost 2000 years ago during the first century AD by Hero of Alexandria (Shepherd, 1956). It consists of a hollowed metal sphere with nozzles pointing in opposite direction tangentially to the sphere along the same axis. A sealed boiler generates the steam with two tubes connected to both the sphere and the boiler. This will cause the

steam to flow into the sphere and coming out of the nozzle therefore resulting in a rotation of the. While the turbine didn't produce power, he demonstrated that steam power could be used to operate machinery (Date, 2009). An illustration is shown below. Figure 2.6 show a sketch of Hero's turbine.
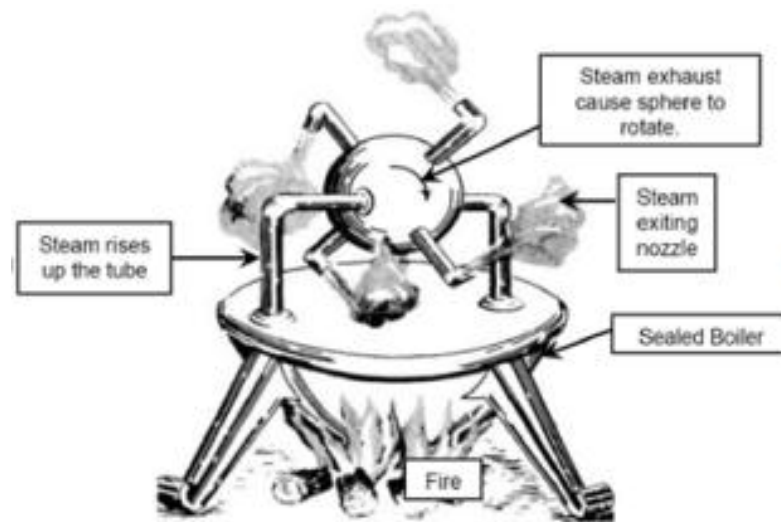
Figure 2.6: Hero's turbine (Shepherd, 1956)

2.5.2.2 Barker's mill

In the late 17th century Barker an English engineer reinvented and modified the Hero's turbine design to work with potential energy of water stored in dam or reservoir, which is called as Barker's mill (Daugherty *et al*., 1954, Duncan *et al*., 1970). Barker's mill was one of the earliest inventions as an outward-flow reaction turbine. Figure 2.7 shows a sketch of Barker's mill. In Barker's mill, fluid enters the centre of the rotor via an inlet at the top. A reaction force is created when the fluid exits the nozzle tangentially causing a movement in reverse direction and making the rotor rotate about a defined axis where the rotation mechanism can produce power (Daugherty *et al*., 1954).
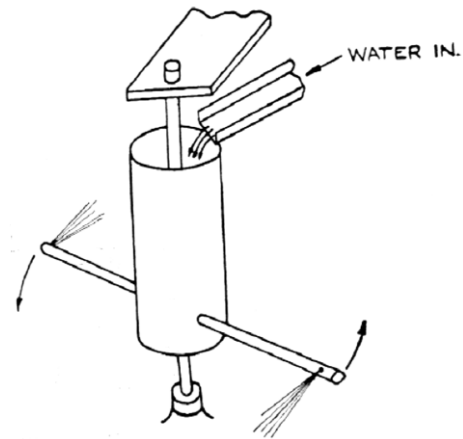
Figure 2.7: Barker's Mill (Shepherd, 1956)

2.5.2.3 Ján Andrej Segner turbine (1750's)

In the mid-1700s Ján Andrej Segner developed a reactive water turbine. It had a vertical axis and was a precursor to modern water turbines. The arms had a ninety degree bend at the tips. It was a very simple machine that is still produced today for use in small hydro sites. Figure 2.8 shows a snapshot of Segner reaction water turbine design.
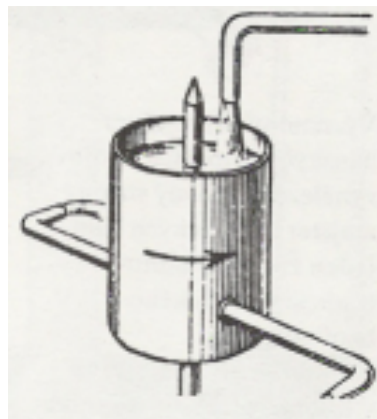
Figure 2.8: Segner's reaction water turbine (Date, 2009)

Segner worked with Euler on some of the early mathematical theories of turbine design. And in 1820, Jean-Victor Poncelet developed an inward-flow reaction turbine.

It was somehow an improvement of Andrej's design. During 1826 Benoit Fourneyron developed an outward-flow turbine. This was an efficient machine (~80%) that sent water through a runner with blades curved in one dimension. The stationary outlet also had curved guides (Date, 2009).

Later in 1844 Uriah A. Boyden developed an outward flow turbine that enhanced on the performance of the Fourneyron turbine. Its runner shape was similar to that of a Francis turbine.

2.5.2.4 Pupil's turbine

Around 1775 Pupil made some further improvements on barkers mill. He modified the entry point of the fluid switching from top to bottom entry. Unlike the earlier design when all the loads have to bear by the thrust bearings supporting the moving parts, this innovation resulted in the load of the head being in the opposite direction to the load of moving parts of the turbine as the rising pressure from below counters this load thus acting like a cushion (Date, 2009). Figure 2.9 shows a sketch of Pupil's turbine.
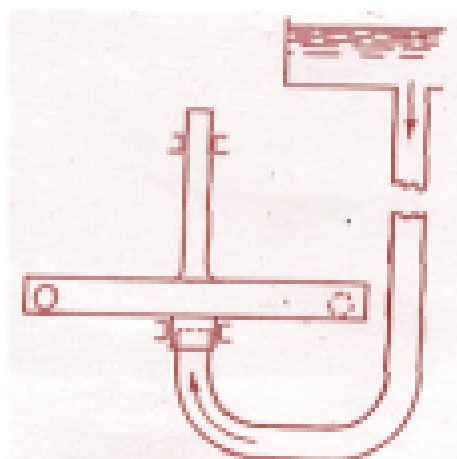
Figure 2.9: Pupil's turbine (Date, 2009)

2.5.2.5 Whitlaw's turbine

In 1832 James Whitlaw proposed some improvements to Barker's mill. By 1839, James Whitlaw invented the "Scotch mill" which also had relatively similar characteristics to the Barker's mill with the exception of the nozzle arm (Date & Akbarzadeh, 2009). Whitlaw redesigned the arm making it curve, therefore creating a higher exit velocity, believing that it increases the efficiency of the turbine (Wilson, 1974). Figure 2.10 shows a sketch of Whitlaw turbine.
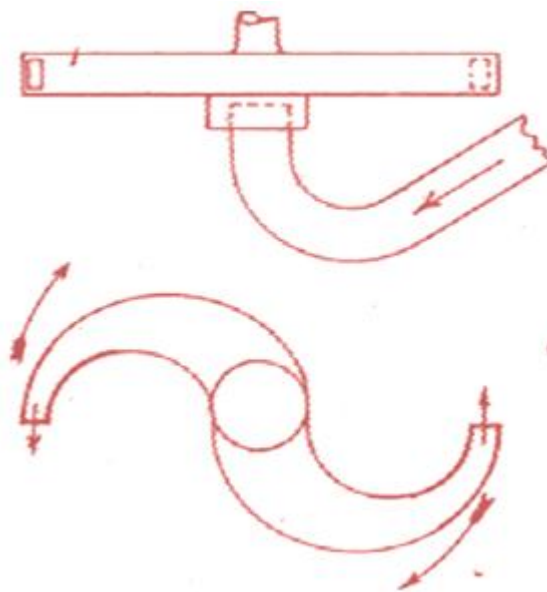
Figure 2.10: Whitlaw's Turbine (Wilson, 1974)

Since then, better and more efficient turbines such as Francis, Fourneyron and Thomson have been invented. In present times, Barker's mill is deemed to be obsolete and not economically viable to be used any more (Duncan, 1970).

Recently Akbarzadeh reviewed this obsolete Hero's turbine design in his paper named "parametric analysis of the simple reaction water turbine" (Akbarzadeh, 2001). The analysis showed that to large extent the simple reaction water turbine is misunderstood. In his paper Akbarzadeh have identified the main geometric and

operational parameters. He has further developed governing equation for the ideal case of zero frictional losses using principles of conservation of mass, momentum and energy.

2.5.3 Some modern simple reaction water turbine

2.5.3.1 Split reaction turbine design (2009)

This type of turbine was being researched by Abhijit Date B.Eng. (School of Aerospace, Mechanical and Manufacturing Engineering Science, Engineering and Technology Portfolio RMIT University). Figure 2.11 shows a three 3D view of the Date split reaction turbine.
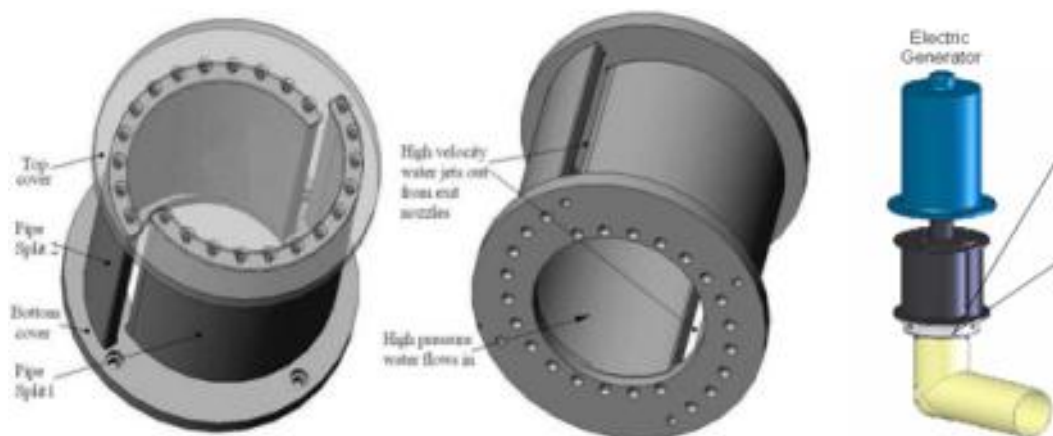
Figure 2.11: Split reaction turbine design (Date, 2009)

As much as subsequent years have seen modifications to increase the efficiency of the Barker's mill turbine design, some scientist regard it as obsolete and not economically viable to be used any more (Duncan, 1970). However some writers like Akbarzadeh et al seems to dispute such views (Akbarzadeh, 2001). They claim that a simple reaction turbine design like that of Barker's and Whitlaw's are highly misunderstood underutilized and almost forgotten other than for garden sprinklers.

2.5.3.2 Gorlov helical turbine

The Gorlov helical turbine (GHT) is a water turbine evolved from the Darrieus cross flow turbine design by altering it to have helical blades/foils. GHT uses the Bernoulli principal in its operation and is able to rotate in the same angular direction despite the direction of water flow. This is especially advantageous for tidal and wave energy systems (Gorlov, 1998). Figure 2.12 shows the design of Gorlov helical turbine.
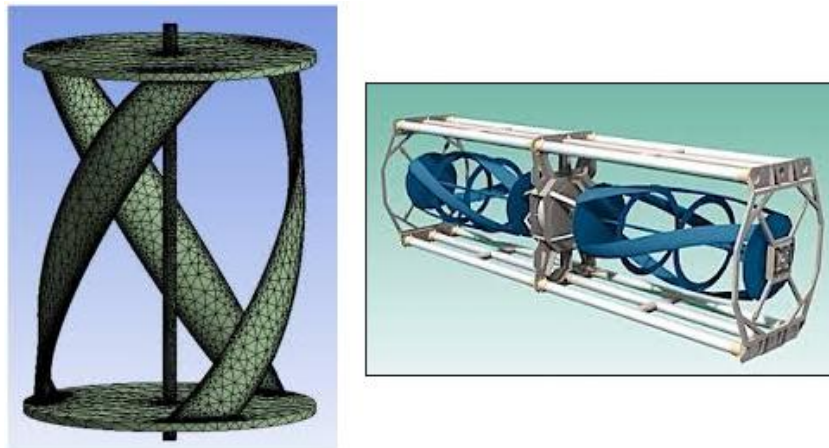
Figure 2.12: Gorlov helical turbine (Gorlov, 1998)

2.5.3.3 Transverse horizontal axis water turbine for tidal waves

The Transverse horizontal axis water turbine (THAWT) is usually referred as a tidal turbine. Its design makes it easy to scale and requires fewer foundations. It too applies the Bernoulli principal in its operation. The THAWT device can be installed horizontally to look like the cross-flow turbine. However the blades are oriented in such a way that they covert the kinetic energy of water into uniform torque along the rotor (McCulloch, 2011). The direction of rotation is dependent on the direction of water flow. Figure 2.13 shows the design of Transverse horizontal axis water turbine.
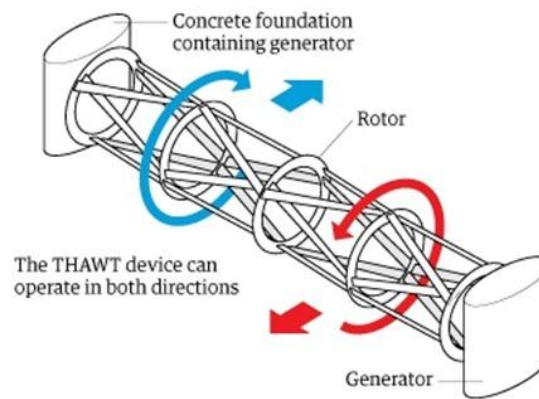
Figure 2.13: Transverse horizontal axis water turbine (McCulloch, 2011)

2.6 Commercially Available Low Head Hydro Machines

Currently there are a view companies who are specialized in manufacturing turbines for generation of electricity from micro hydro sources. For this reason most of the low head micro-hydroelectric units available use impulse type turbines for energy conversion (Date et al, 2009). However when impulse turbines are used for low head operation their energy conversion efficiency drops drastically to even less than 60% (Harvey, 2005, Waddell, 1999).

Due to low cost impulse turbines like Pelton, Cross flow and Turgo are often used even at low to very low head sites (Akbarzadeh, 2001) not putting into consideration there wanting efficiency. Pelton and Turgo turbine cannot be used when the available head is less then 3m, in this case a Cross flow turbine can convert that low head hydro energy within efficiency of about 60% (Harvey, 2005). Even so the prices of this turbine are still relatively high (Date, 2009). Table 2.5 shows the specific cost of various turbines along with their power size. The cost does not include the alternator and drive unit but rather the turbine itself.

Table 2.5: Table of cost of different turbines (Harvey, 2005)

Cost of turbines in units of US $1000 excluding alternator and drive						
Shaft power kW	Crossflow	Francis	Single-jet Pelton	Multi-jet Pelton	Turgo	Propeller
2	1 – 2	4 – 6	1 – 4	1 – 3	2 – 4	4 – 6
5	2 – 6	8 – 10	2 – 8	2 – 6	5 – 8	8 – 10
10	2 – 10	15 – 20	2 – 15	2 – 10	8 – 14	15 – 20
20	3 – 14	20 – 30	3 – 20	3 – 15	12 – 20	20 – 30
50	5 – 30	25 – 70	5 – 50	5 – 30	35 – 50	25 – 70
100	30 – 50	40 – 100	40 – 80	15 – 60	55 – 80	40 – 100
150	50 – 80	60 – 120	60 – 100	30 – 80	80 – 100	60 – 120

2.7 Analysis of Some Symple Reaction Water Turbines

2.7.1 Multiple exits simple reaction turbine

This rather ad-hoc analysis was done by A. Akbarzadeh (Akbarzadeh, 2001) and later

by Abhijit Date (Date, 2009). Consider the system in figure 2.14.
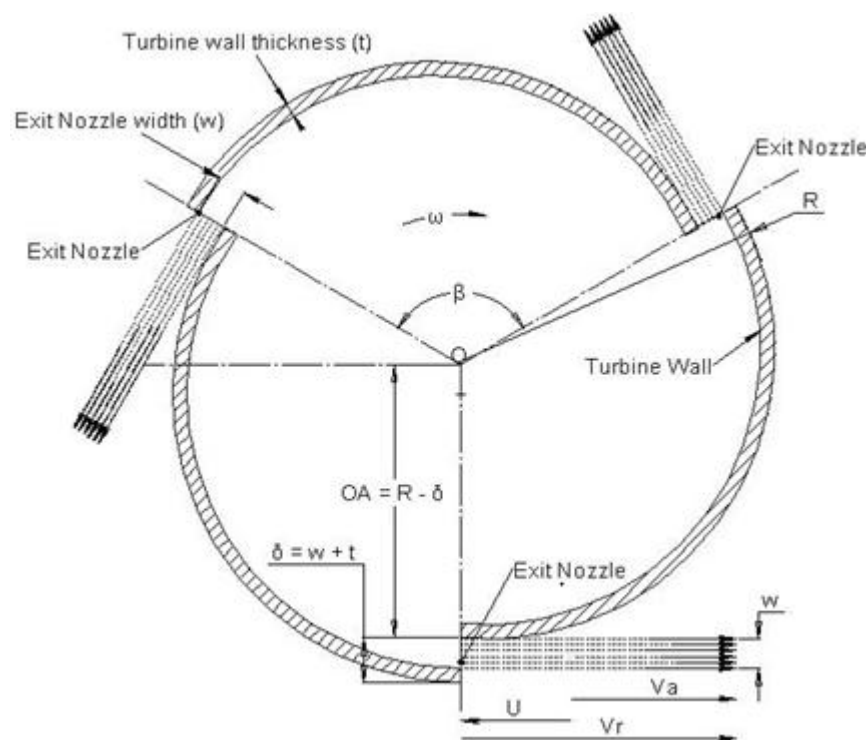
Figure 2.14: Velocity diagram of multiple exits simple reaction turbine rotor

In case of a simple reaction turbine, two components of acting pressures were

assumed that govern the flow of water through the turbine. The main operating head

is created due to physical difference between the water level in the reservoir and the

position of the turbine. The secondary head is created due to angular speed of the turbine which causes a centrifugal pumping effect as discussed by A. Akbarzadeh (Akbarzadeh, 2001).

$$H_c = \frac{\omega^2 R^2}{2g} \qquad \{eqn\ 2.1\}$$

In this case, H_c is the centrifugal head in meters and is proportional to the angular speed of the turbine. Assuming ideal condition where there are no fluid frictional losses, the relative kinetic energy would be equal to sum of potential energy and energy due to centrifugal head (Akbarzadeh, 2001).

$$V_r = \sqrt{2gH + \omega^2 R^2} \qquad \{eqn\ 2.2\}$$

To estimate the torque T due to action and reaction principle produced by the jets of water leaving the turbine we apply conservation of momentum principle which gives;

$$T = \dot{m}V_a R = \rho Q V_a R \qquad \{eqn\ 2.3\}$$

But power can be defined as a product of torque T and angular speed ω in radians per sec.

Power output;

$$P = T\omega = [\dot{m}V_a R].\omega \qquad \{eqn\ 2.4\}$$

After the power output is defined, an energy balance equation can be written for a simple reaction turbine assuming the ideal situation without any losses. Upon applying the conservation of energy principle to this situation, the total rate of potential energy $P.E.P = \dot{m}gh$ supplied to the turbine at any given rotational speed would be equal to the mechanical power output plus the kinetic energy lost as a result of absolute velocity of the water jet leaving the turbine $K.E.P = \frac{1}{2}\dot{m}.V_a^2$. Therefore, we can write the energy balance equation as follows,

$$P = T\omega = \dot{m}gh - \frac{1}{2}\dot{m}.V_a{}^2 \qquad \qquad \{eqn\ 2.5\}$$

The efficiency η of the simple reaction turbine to convert the potential energy available in the water from the reservoir to mechanical power can be written as follows;

$$\eta = \frac{P}{\dot{m}gh} \qquad \qquad \{eqn\ 2.6\}$$

2.7.2 Lawn Sprinkler

This analysis was done by (Calvert, 2003). Figure 2.15 shows a sketch of a two-armed runner of a rotating lawn sprinkler along with its velocity diagram.
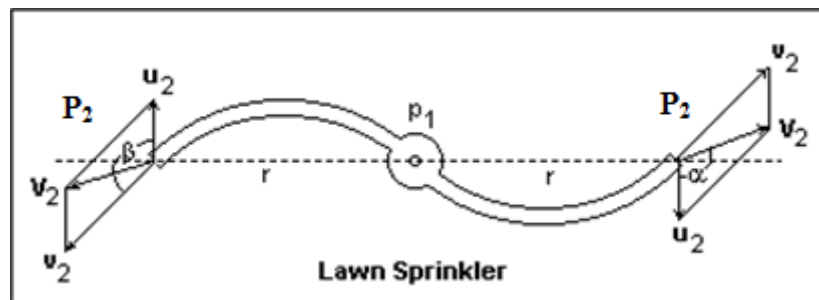
Figure 2.15: Lawn sprinkler and its velocity diagram (Calvert, 2003)

The jet at the end of an arm is projected at an angle β with a perpendicular normal to the radius from the centre of rotation, in the direction of the rotational velocity $u_2 = \omega r$. The space velocity V_2 is the vector sum of v_2 and u_2, which makes an angle α with u_2. When the runner is stopped, V_2. As the runner speeds up, V_2 moves closer to a radial direction. When it reaches the radial direction, there is no longer a component normal to the radius and, therefore, no accelerating torque. It is easy to see that the torque will be a maximum when the runner is stalled.

To find v_2 in terms of p_1, Bernoulli's theorem is used. However, energy is not conserved between the axial point 1 and point 2 at the end of the arm, since the water

does work in passing from one point to the other. There is a reaction force of magnitude ρV_2 in the opposite direction to V_2. The movement of point 2 is in the direction of u_2, so the rate of doing work is given by equation 2.7.

$$P = \rho V_2 u_2 \cos\alpha \qquad \qquad \{eqn\ 2.7\}$$

Dividing by ρg to express this work as head, it is found that a head of $V_2 u_2 \cos\alpha/g$ must be subtracted from the difference of the heads at points 2 and 1. Since $z_2 = z_1$ point 1, and $Presure = 0$ at point 2 (using gauge pressures), this leads to the following equation;

$$\frac{V_2{}^2}{2g} = \frac{p1}{\rho g} - V_2 * u_2 \cos\frac{\alpha}{g}. \qquad \qquad \{eqn\ 2.8\}$$

From the vector triangles, it found that (dropping the subscript 2 for the moment) leads to;

$$V^2 = u^2 + v^2 - 2uv\cos(180° - \beta) = u^2 + v^2 + 2uv\cos\beta \qquad \{eqn\ 2.9\}$$

However,

$$V\cos\alpha = v\cos\beta + u \qquad \qquad \{eqn\ 2.10\}$$

Substituting for V^2 and $V^2\cos\alpha$ in the above equation leads to;

$$v^2 = 2gh + u^2 \qquad \qquad \{eqn\ 2.11\}$$

In equation 2.11, h is the supply head, which may include approach velocity if it is to be considered.

Having equation 2.11, equation 2.9 and equation 2.10 can be expressed as a function of u_2, or as a function of the angular velocity ω. In particular the component of V perpendicular to the radius is $V' = V\cos\alpha = v\cos\beta + u$. The corresponding reaction force is obtained by multiplying by ρ, and by the total discharge Av, where A is the total area of the jets on all arms. Therefore force;

$$F = -\rho A v V' = -\rho A v \left(v \cos \beta + u\right) \qquad \{eqn\ 2.12\}$$

The torque, then, is

$$T = -\rho A v r \left(v \cos \beta + u\right) \qquad \{eqn\ 2.13\}$$

Where $v = \sqrt{(2gh + u^2)}$ and $u = \omega r$

Therefore power is given,

$$P = T * \omega = -\rho A v r \left(v - u\right) * \omega \qquad \{eqn\ 2.14\}$$

NB: For the turbine in this research $\beta = 180°$

Calvert concluded that if much interest was on power than in watering, β could be made $180°$, and the area of the jets could be increased, partly by multiplying the number of jets. If the angular velocity of the runner could be such that $v^2 = 2gh + u^2$, the efficiency of the turbine would be at maximum.

CHAPTER THREE

TURBINE ANALYSIS, DESIGN AND CONSTRUCTION

3.1 Introduction

This chapter of the study presents the relevant methods that were used during the research. It discusses the materials, research design, fabrication design, research instruments and equipment that were used in the study.

The design of the turbine in this research is similar to that of Whitlaw's turbine with the difference being that; the semicircular conduit has a uniform cross-sectional area that runs from the centre all the way to the nozzle, as well as a complete semicircular path, and a smooth 90^0 bend conduit with a uniform cross-sectional area joining the semicircular conduit and the inlet pipe. This is not the case with Whitlaw's turbine. Whitlaw's turbine is made of a varying cross-sectional with no smooth bend between the arms and the inlet pipe.

Instead of an ad-hoc method a systematic method laid down in continuum mechanics was adopted in deriving the mathematical model that predicts the power output as a function of the design and operating conditions of the turbine. Another new aspect is that emphasis is put on determining the most efficient main conduit to nozzle cross-sectional area ratio for a particular height for this type of a reaction turbine.

This research was done by performing experiments on a turbine model that was fabricated at Moi University, Civil and structural department, Fluid laboratory.

3.2 Working principle

Due to potential energy contained in the water at the upper storage tank, the waters flows downwards trough the delivery pipe (mini-penstock). As the water falls downwards and flows into the turbine through the lip seal they are made to follow a

semicircular curved path and exits at the nozzle. As a result, centrifugal acceleration along the curved conduit as well as action and reaction principle at the nozzle takes place causing the free arm to move forward. Since the arm is pivoted at the centre, it only has the option of revolving in a clockwise direction.

The balance equations for continuity, moment of momentum and energy have to be evaluated to derive the relations for the generated torque, power and efficiency of the turbine as a function of rotational speed, radial arm length and other input parameters such as rate of flow and supplied water head. These equations have to be derived for the moving turbine arm, which necessitates the introduction of a transport theorem for a moving control volume.

3.3 Continuum Analysis of Fluid Flow Including a Moving Control Volume

3.3.1 Continuum mechanics approach

Continuum mechanics approach is the analysis of the kinematics and the mechanical behaviour of materials modelled as a continuous mass rather than as discrete particles. In continuum mechanics an object is modelled in such a way that the matter of the object completely fills the space it occupies. Fundamental physical laws such as the conservation of mass, the conservation of momentum, the conservation of moment of momentum and the conservation of energy may be applied to such models to derive differential equations describing the behaviour of such objects, and some information about the particular subject material is added through constitutive relations (Schedule, 2011).

In order to understand the derivation of the balance equations with respect to a moving control volume, some basic understanding is required of vector analysis.

3.3.2 Guide lines for vector analysis

3.3.2.1 Vector definition

Vector is a dimensionless quantity with a magnitude and direction. An arrow '→' on top of a symbol is used to denote a vector. Examples of vectors are velocity $\vec{v}$, force $\vec{f}$, and displacement $\vec{u}$ (Hirsch, 2007). The magnitude or norm of a vector $\vec{u}$ is denoted by $\|\vec{u}\|$. In a drawing, a vector has a working line with an arrow of a certain length showing the direction and the magnitude of the vector.

3.3.2.2 Vector operations

Addition and subtraction

Two vectors $\vec{u}$ and $\vec{v}$ are added by shifting one of the vectors, along the working line and parallel to it, i.e. without changing its orientation, until a "tail" and a "head" are connected (figure 3.1).
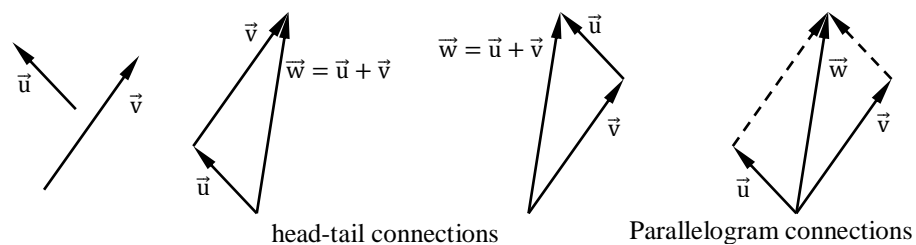
Figure 3.1: Addition of vectors (Sitters, 2014)

The sum of the two vectors is the vector from the free "tail" to the free "head".

A parallelogram construction for summing up two vectors is used frequently as well and leads to the same result. However, this procedure omits the order of the carried out operations.

Multiplication of a vector by a scalar

When a vector $\vec{u}$ is multiplied by a scalar α a new vector $\vec{v}$ is formed having the same working line and a new magnitude equal to the absolute value of the scalar α multiplied by the magnitude of $\vec{u}$, i.e.
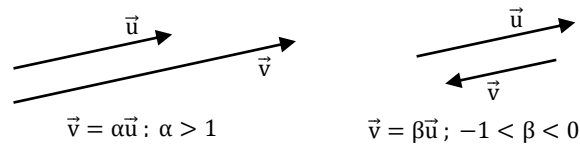
$$\vec{v} = \alpha\vec{u} \; ; \; \|\vec{v}\| = |\alpha|\|\vec{u}\|$$

Figure 3.2: Multiplication of a vector by a scalar (Sitters, 2014)

When the scalar is negative, the vectors $\vec{u}$ and $\vec{v}$ have opposite directions as shown in figure 3.2.

Dot product

The scalar product, dot product or in product is normally indicated by a dot ($\cdot$) between the two vector symbols, and is defined as the product of the lengths of the two vectors multiplied by the cosine of the enclosed angle θ (smallest angle $\leq 180^{\circ}$):

$$\vec{v} \cdot \vec{u} = \|\vec{u}\|\|\vec{v}\| \cos \theta$$
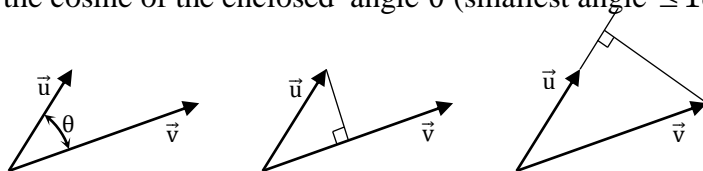
Figure 3.3: Dot product

The dot product can also be interpreted as the length of the projection of $\vec{u}$ on $\vec{v}$, times the length of $\vec{v}$, or vice versa figure 3.3.

The magnitude of a vector $\vec{u}$ can be obtained using a dot product, i.e. $\|\vec{u}\| = \sqrt{\vec{u} \cdot \vec{u}}$

Cross production

The vector product or cross product of two vectors $\vec{u}$ and $\vec{v}$ is indicated by an asterisk ($*$) between the two vector symbols. The result of this product is a new vector, the length of which is equal to the product of the lengths of the two original vectors $\vec{u}$ and $\vec{v}$ multiplied by the sine of the enclosed angle θ. The working line of the vector is perpendicular to the plane spanned by $\vec{u}$ and $\vec{v}$ as shown in figure 3.4. The direction of the vector $\vec{u} * \vec{v}$ can be found by using the "corkscrew rule". The first vector is rotated towards the second one over the enclosed angle. When a right-handed corkscrew aligned along the working line of $\vec{u} * \vec{v}$ is rotated in the same direction, the axial translation of the corkscrew determines the direction of $\vec{u} * \vec{v}$. It is handy to choose a unit normal $\vec{n}$ on the plane in the same direction as $\vec{u} * \vec{v}$. It then can be written:

$$\vec{u} * \vec{v} = \|\vec{u}\|\|\vec{v}\| \sin\theta \, \vec{n} \; ; \; \|\vec{u} * \vec{v}\| = \|\vec{u}\|\|\vec{v}\| \sin\theta$$

By definition, the vectors $\vec{u}$, $\vec{v}$ and $\vec{n}$ form a right-handed system.
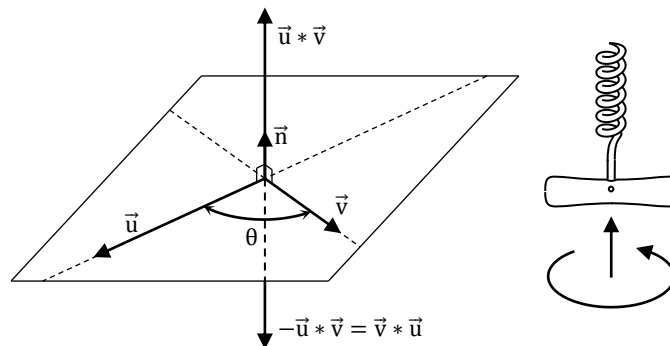
Figure 3.4: Vector product of two vectors (Sitters, 2014)

3.3.2.3 Cartesian right-handed coordinate system

In vector analysis a Cartesian right-handed coordinate system is indicated by three unit vectors $\vec{e}_x, \vec{e}_y, \vec{e}_z$ that are perpendicular and form a right-handed system (i.e. $\vec{e}_z =$

$\vec{e}_x * \vec{e}_y, \vec{e}_y = \vec{e}_z * \vec{e}_x, \vec{e}_x = \vec{e}_y * \vec{e}_z$) and (triple product is: $\vec{e}_x * \vec{e}_y \cdot \vec{e}_z = \vec{e}_z * \vec{e}_x \cdot \vec{e}_y = \vec{e}_y * \vec{e}_z \cdot \vec{e}_x = 1$). The directions of the base vectors of this base are fixed space, which means that the base vectors are independent of the position in space. The origin is indicated by **O** and the base itself is denoted by $\{\vec{e}_x, \vec{e}_y, \vec{e}_z\}$, as shown in figure 3.5.
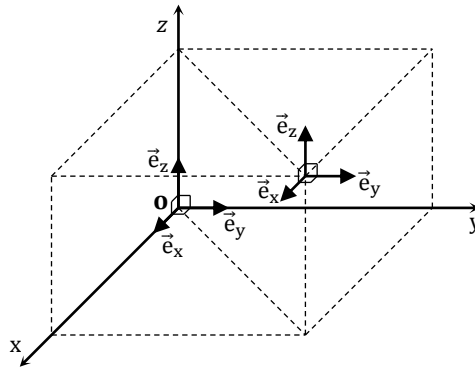
Figure 3.5: Cartesian right-handed orthonormal vector base (Sitters, 2014)

3.3.2.4 Representation of a vector with respect to a vector base

Considering the vector base $\{\vec{e}_x, \vec{e}_y, \vec{e}_z\}$ shown in figure 3.6, every arbitrary vector $\vec{P}$ can be written as a unique linear combination of the base vectors $\vec{e}_x, \vec{e}_y, \vec{e}_z$.

$$\vec{P} = P_x \vec{e}_x + P_y \vec{e}_y + P_z \vec{e}_z$$

It can also be seen that using the definition of the dot product $P_i = \vec{P} \cdot \vec{e}_i \ \forall i \epsilon (x, y, z)$
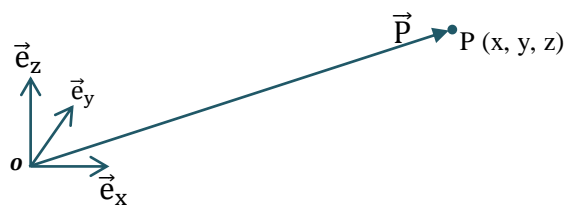
Figure 3.6: Vector base

In matrix notation, the following is the representation of $\vec{P}$ with respect to $\{\vec{e}_x, \vec{e}_y, \vec{e}_z\}$ can be made:

$$\vec{P} = \begin{bmatrix} P_x & P_y & P_z \end{bmatrix} \begin{bmatrix} \vec{e}_x \\ \vec{e}_y \\ \vec{e}_z \end{bmatrix}$$

The column $\begin{bmatrix} P_x & P_y & P_z \end{bmatrix}^T$ is called the matrix representation of the vector $\vec{P}$ with respect to the vector base $\{\vec{e}_x, \vec{e}_y, \vec{e}_z\}$.

3.3.3 Balance equations for moving control volume

Normally, the balance equations are formulated for a material volume which changes with time, generally denoted by $V_m(t)$. Such a volume always contains the same amount of material and therefore the formulation of the balance equations is relatively simple. A fluid dynamic system undergoes huge deformations, which makes the application of a material volume unsuited. For this type of systems a control volume $V_c(t)$ is used,

Which is an imaginary surface enclosing a volume of interest. As the denotation $V_c(t)$ already indicates, the control volume can be fixed or moving as a function of time, and it can be rigid or deformable (Hirsch C., 2007). In all cases, fluid is flowing into and out of the control volume through the control surface $A_c(t)$ together with the associated quantities such as mass, momentum, moment of momentum and energy. This type of transport is called advection.

In order to derive the balance equations for a moving control volume, a transport theorem is required that takes care of phenomenon of advection, so that mathematically a proper change is made from a material to a control volume.

3.3.3.1 Transport theorem formulation

In the derivation of the control-volume theorem, so-called extensive and intensive properties are of interest. The extensive properties are mass m, momentum $m\vec{v}$ and energy E. The corresponding intensive properties are mass per unit of mass, which is unity; momentum per unit of mass, which is $\vec{v}$; and energy per unit of mass, indicated by ϵ. So the extensive properties are proportional to mass, contrary to the intensive properties. Other intensive properties are: pressure p, temperature T, mass density ρ.

The symbol ϕ represents a general extensive quantity, while φ represents a general intensive quantity. ψ represents the intensive quantity per unit of volume. The relationship between the intensive and extensive quantities for a given system is denoted by:

$$\phi = \int_m \varphi\,dm = \int_V \rho\varphi\,dV = \int_V \psi\,dV$$

Therefore for a material volume $V_m(t)$ and a spatial/control volume $V_c(t)$, both as a function of time;

$$\phi_m(t) = \int_{V_m(t)} \psi(x,y,z)\,dV \quad ; \quad \phi_c(t) = \int_{V_c(t)} \psi(x,y,z)\,dV$$

Here dm and dV are differential mass and differential volume, respectively.

The integrand $\psi(x,y,z,t) = \rho(x,y,z,t)\varphi(x,y,z,t)$ is a function of the position (x,y,z) in a volume with respect to a Cartesian right-handed vector base, and the time t. If at time t volumes $V_m(t)$ and $V_c(t)$ coincide, the two integrals are equal: $\phi_m(t) = \phi_c(t)$.
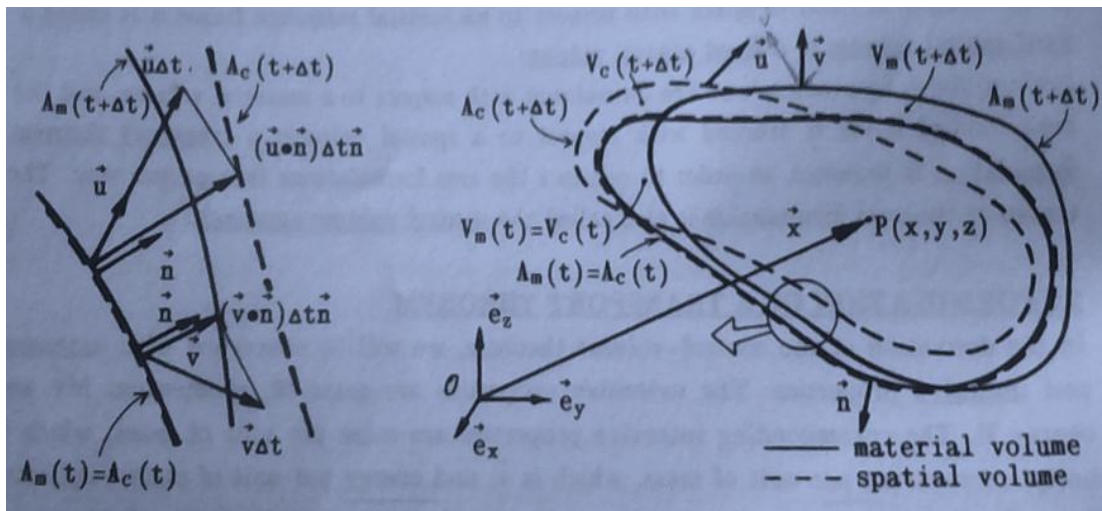
Figure 3.7: A time dependent material and control volume (Sitters, 1994)

Figure 3.7 shows a sketch of a time dependent material and spatial volume at the times t and $t + \Delta t$. At time t the two volumes coincide. $A_m(t)$ and $A_c(t)$ represents surfaces of the material volume and control volume respectively. The unit outward-pointing normal on the surface is indicated by $\vec{n}$. The velocity of the material particles is given by $\vec{v} = \vec{v}(x, y, z, t)$. The velocity of the surface $A_m(t)$ of the material bounded volume is equal to $\vec{v}$ of the particles at the surface as shown in figure 3.4, because the volume moves along with these (fluid) particles. The velocity of the surface of the non-material bounded spatial volume is indicated by $\vec{u}$. Inside the volume itself, the velocity $\vec{u}$ cannot be defined. In the general approach $\vec{u} \neq 0$ and $\vec{u} \neq \vec{v}$.

The normal displacement of the two surfaces after a small time step Δt as indicated in figure 3.7, are: $(\vec{v} \cdot \vec{n})\Delta t \vec{n}$ and $(\vec{u} \cdot \vec{n})\Delta t \vec{n}$, where $\vec{v}$, $\vec{u}$ and $\vec{n}$ are functions of the coordinates x, y, z and time t. $\vec{v}(\vec{x}, t)$ refers to the velocity of the material in the same spatial point at time t. $\{\vec{e}_y, \vec{e}_x, \vec{e}_z\}$ represents the fixed right-handed Cartesian coordinate system, actually it is the positioning and locating system.

The transport theorem provides a relation between the time derivatives of an extensive property expressed as integrals over a material volume and control (spatial) volume, respectively. In other words, it provides the relation between $d\phi_m(t)/dt$ and $d\phi_c(t)/dt$. Formulated as derivatives of the integrals over the intensive properties the theorem reads:

$$\frac{d}{dt}\left(\int_{V_m(t)} \rho(\vec{x},t)\varphi(\vec{x},t)dV \right) = \frac{d}{dt}\left(\int_{V_c(t)} \rho(\vec{x},t)\varphi(\vec{x},t)dV \right) + \int_{A_c(t)} \rho(\vec{x},t)\varphi(\vec{x},t)(\vec{v}-\vec{u}).\vec{n}dA \quad eqn\ 3.1\}$$

The integral over the control surface accounts for the advection of the intensive quantities across the control surface.

The complete derivation of equation 3.1 is found in appendix D.

When $\vec{u} = \vec{v}$, the control volume becomes a material volume, and the surface integral vanishes.

3.3.3.2 Continuity equation

Equation of continuity also referred to as the global equation for the conservation of mass, states that the mass in a material volume $V_m(t)$ does not change with time. In other words, the mass of a certain amount of material is constant unless of course there is a nuclear reaction within the volume. In formula form the continuity equation is:

$$\frac{d}{dt}\left(\int_{V_m(t)} \rho dV \right) = 0$$

As a short hand the indication $\vec{x}$ and t for position and time are omitted. Using the transport theorem equation 3.1, with $\varphi = 1$, it follows:

$$\frac{d}{dt}\left(\int_{V_c(t)} \rho dV \right) + \int_{A_c(t)} \rho(\vec{v}-\vec{u}).\vec{n}dA = 0 \qquad\qquad \{eqn\ 3.2\}$$

This equation can also be interpreted as follows: the change of mass as a function of time in the control volume plus the net outflow of mass (advection of mass) out of the control volume is equal to zero. In steady state flow equation 3.2 becomes:

$$\int_{A_c(t)} \rho(\vec{v} - \vec{u}).\vec{n}dA = 0 \quad \text{(steady state)}$$

3.3.3.3 Momentum equation

The global equation for the conservation of momentum states that the rate of change of momentum of a material volume V_m is equal to the resulting force of the applied external loads, and is represented as:

$$\frac{d}{dt}\left(\int_{V_m(t)} \rho\vec{v}dV\right) = \int_{V_m(t)} \rho\vec{f}dV + \int_{A_m(t)} \vec{t}dA$$

Where $\vec{v}$ is the material velocity, $\vec{f}$ is the specific external body force (N/kg), and $\vec{t}$ is the specific external surface load (N/m^2).

In most cases $\vec{f}$ is equal to the gravitational acceleration $\vec{g}$, and $\vec{t}$ is often a stress vector generated by the hydrostatic pressure $\left(\vec{t} = -p\vec{n} + \vec{\tau}\right)$. Applying the transport theorem equation 3.1 by omitting the $\vec{x}$ and t indicators and with $\varphi = \vec{v}$ it yields:

$$\frac{d}{dt}\left(\int_{V_c(t)} \rho\vec{v}dV\right) + \int_{A_c(t)} \rho\vec{v}(\vec{v} - \vec{u}).\vec{n}dA = \int_{V_c(t)} \rho\vec{g}dV + \int_{A_c(t)} \vec{t}dA \qquad \{eqn\ 3.3\}$$

3.3.3.4 Moment of momentum equation

The global equation for conservation of moment of momentum, or conservation of angular momentum, states that the rate of change of moment of momentum of a material volume is equal to the resulting moments of the applied external loads. Volume and surface torques are not taken into account, and therefore the balance equation can be written as:

$$\frac{d}{dt}\left(\int_{V_m(t)} \rho\vec{x}*\vec{v}dV \right) = \int_{V_m(t)} \rho\vec{x}*\vec{g}dV + \int_{A_m(t)} \vec{x}*\vec{t}dA$$

The position vectors of all the material points with respect to the specific point to which the moment of momentum is defined are indicated by $\vec{x}$. Application of the transport theorem 3.1 by omitting the $\vec{x}$ and t indicators and with $\varphi = (\vec{x}*\vec{v})$ it yields:

$$\frac{d}{dt}\left(\int_{V_c(t)} \rho\vec{x}*\vec{v}dV \right) + \int_{A_c(t)} \rho\vec{x}*\vec{v}(\vec{v}-\vec{u}).\vec{n}dA = \int_{V_c(t)} \rho\vec{x}*\vec{g}dV + \int_{A_c(t)} \vec{x}*\vec{t}dA \quad \{eqn\ 3.4\}$$

In the right-hand side of both equations the "material integral" has been replaced again by the "spatial integrals".

3.3.3.5 Energy equation

The global equation for conservation of energy for an isothermal system states that the rate of change of the kinetic and potential energy of a material volume is equal to the mechanical power performed by the external loads. In equation form this is expressed as:

$$\frac{d}{dt}\left(\int_{V_m(t)} \left(\rho\epsilon + \frac{1}{2}\rho\vec{v}\cdot\vec{v}\ dV \right) \right) = \int_{A_m(t)} \vec{t}\cdot\vec{v}dA$$

Where ϵ is the specific potential energy (i.e. $\epsilon = gz$), g is the magnitude of the acceleration by gravity and z is the height above the datum plane.

In the right-hand side of the equation no gravitational term appears, since the effect of gravity is already accounted for in the potential energy.

Again, application of the transport theorem equation 3.1 by omitting the $\vec{x}$ and t indicators and with $\varphi = \left(\epsilon + \frac{1}{2}\vec{v}\cdot\vec{v} \right)$ it yields:

$$\frac{d}{dt}\left(\int\limits_{V_c(t)} \left(\rho gz + \frac{1}{2}\rho\vec{v}\cdot\vec{v}\,dV\right)\right) + \int\limits_{A_c(t)} \left(\rho gz + \frac{1}{2}\rho\vec{v}\cdot\vec{v}\right)(\vec{v}-\vec{u}).\vec{n}dA = \int\limits_{A_c(t)} \vec{t}*\vec{v}dA \quad \{eqn\ 3.5\}$$

3.4 One Arm Reaction Turbine

Figure 3.8 shows the configuration of a rotating one arm reaction turbine. At the pivoting centre water is flowing into the turbine and at the exit nozzle the water leaves the turbine. The control volume coincides with the circular tube and the entry and exit areas and thus rotates with the same speed as the turbine. The various notations are explained below:

- Symbol $\vec{v}$ is used to indicate the absolute flow velocity with respect to fixed coordinate system $\{\vec{e}_y, \vec{e}_x, \vec{e}_z\}$. $\vec{v}_i$ represents the absolute flow velocity of water flowing into the "moving control volume" via the inlet pipe. While $\vec{v}_e$ represents the absolute flow velocity of water exiting the moving control volume via the nozzle.

- $\vec{n}_i$ is an outwardly directed unit normal to the inlet cross-sectional area. While $\vec{n}_p$ is an outwardly directed unit normal to the surface of the semicircular conduit. Furthermore $\vec{n}_e$ is an outwardly directed unit normal to the outlet cross-sectional area.

- The cross-sectional area at the inlet of the one arm reaction turbine is represented by A_i. A_p conversely represents the surface area along the semicircular conduit. While A_e represents the outlet cross-sectional area at the end of the semicircular conduit.

- V_c denotes the volume occupied by water within semicircular conduit of the one arm reaction turbine, also referred as a moving control volume. While capital V is used to represent volume in general.

- $\vec{x}$ is the distance of a fluid particle from the centre of rotation to a certain position in the control volume.

- $\vec{R}$ is the distance of nozzle from the centre of rotation.

- $\vec{u}_e$ is the linear velocity at the end of the turbine arm as the turbine rotate and is given by $\vec{u}_e = \vec{\omega} * \vec{R}$.

- Angle β is the angle between the vectors $\vec{u}_e$ and $\vec{v}_e$, usually referred as the angle of jet projection.

- The internal diameter of the semicircular conduit is denoted by $\emptyset$.
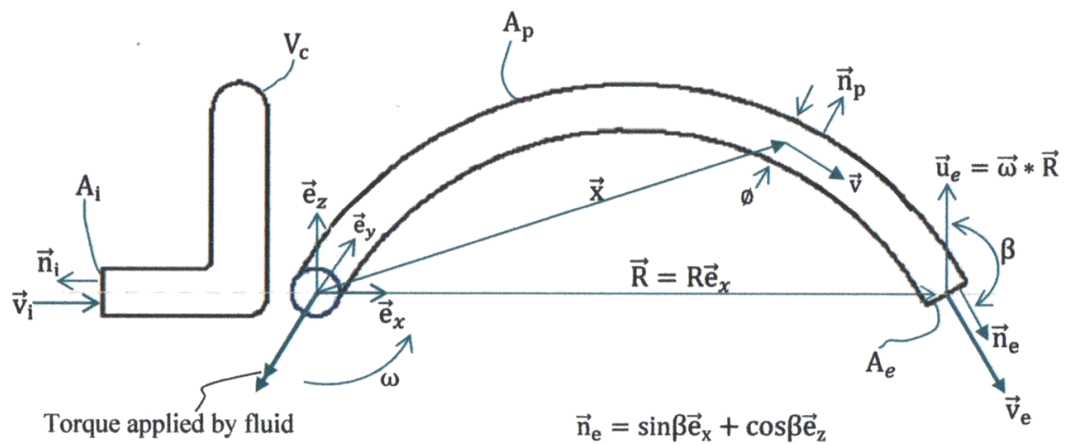
Figure 3.8: Flow in a one arm reaction turbine control volume

The velocity of the control volume V_c is equal to: $\vec{u} = \vec{\omega} * \vec{x}$

The angular velocity vector and the radial vector are given by:

$$\vec{\omega} = -\omega\vec{e}_y \text{ and } \vec{R} = R\vec{e}_x$$

Therefore;

$$\vec{u}_e = \vec{\omega} * \vec{R} = -\omega\vec{e}_y * R\vec{e}_x = -\omega R(\vec{e}_y * \vec{e}_x) = \omega R\vec{e}_z = u_e\vec{e}_z$$

The next step in the analysis is to formulate the balance equations for the moving control volume, in order to obtain the algebraic equations governing the problem.

3.4.1 Continuity Equation

From the explanations in section 3.3.3.2, the continuity equation for a one arm reaction turbine becomes:

$$\frac{d}{dt}\left(\int_{V_c} \rho dV\right) + \int_{A_c} \rho(\vec{v} - \vec{u}).\vec{n}dA = 0$$

First term is equal to zero: ρdV in control volume is constant since control volume moves at same speed as the conduit creating a steady-state situation. So:

$$\int_{A_c} \rho(\vec{v} - \vec{u}).\vec{n}dA = \int_{A_e} \rho(\vec{v}_e - \vec{u}_e).\vec{n}_e dA + \int_{A_p} \rho(\vec{v}_p - \vec{u}_p).\vec{n}_p dA + \int_{A_i} \rho(\vec{v}_i - \vec{u}_i).\vec{n}_i dA = 0$$

Bear in mind that the integral over A_p is equal to zero, since $\vec{v}_p = \vec{u}_p$ (assuming "no slip" condition).

The dot products of the first integral in the right-hand side can be worked out as follows:

$$\left.\begin{array}{l} \vec{v}_e.\vec{n}_e = v_e\vec{n}_e.\vec{n}_e = v_e \\ \vec{u}_e.\vec{n}_e = \|\vec{u}_e\|.\|\vec{n}_e\|\cos\beta = u_e\cos\beta \end{array}\right\} (\vec{v}_e - \vec{u}_e).\vec{n}_e = v_e - u_e\cos\beta$$

The term "$v_e - u_e\cos\beta$" is the relative velocity (v_r) of the water jet as it exits the turbine at nozzle. Therefore:

$$v_r = v_e - u_e\cos\beta .$$

Figure 3.9 shows the velocity diagram at the nozzle for $\vec{v}_r, \vec{v}_e$ and $\vec{u}_e$.
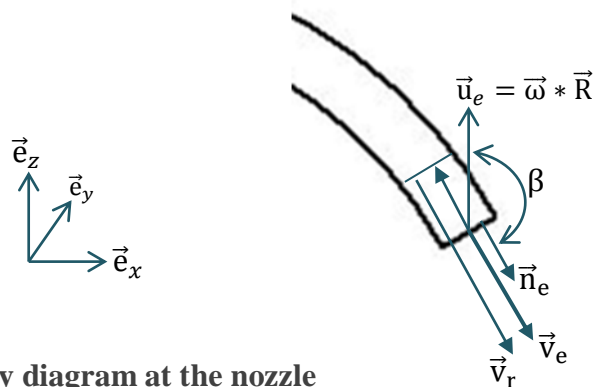
Figure 3.9: Velocity diagram at the nozzle

The dot products of the third integral in the Right-hand side can be solved out as follows:

$$\left.\begin{array}{l} \vec{v}_e.\vec{n}_i = -v_i\vec{n}_i.\vec{n}_i = -v_i \\ \vec{u}_i = \vec{0} \end{array}\right\} (\vec{v}_i - \vec{u}_i).\vec{n}_i = -v_i$$

Assuming velocities are constant over cross-section, the continuity equation becomes:

$$\int_{A_c} \rho(\vec{v} - \vec{u}).\vec{u}dA = \rho(v_e - u_e\cos\beta)A_e - \rho v_i A_i = 0$$

Using $Q = v_i A_i$ the continuity equation finally results into:

$$v_i A_i = (v_e - u_e\cos\beta)A_e = Q$$

$$\{eqn\ 3.6\}$$

3.4.2 Moment of momentum equation

From explanations and equation 3.4 in section 3.3.3.4 the moment of momentum equation for a one arm reaction turbine is given by:

$$\frac{d}{dt}\left(\int_{V_c} \rho\vec{x} * \vec{v}dV\right) + \int_{A_c} \rho\vec{x} * \vec{v}(\vec{v} - \vec{u}).\vec{n}dA = \int_{V_c} \rho\vec{x} * \vec{g}dV + \int_{A_c} \vec{x} * \vec{t}dA$$

Again the first term is equal to zero, since the integral is constant. Furthermore the effect of gravity within the turbine balances to approximately zero and can be neglected. Therefore:

$$\int_{A_c} \rho\vec{x} * \vec{v}(\vec{v} - \vec{u}).\vec{n}dA = \int_{A_c} \vec{x} * \vec{t}dA$$

The left hand side becomes:

$$\int_{A_c} \rho\,\vec{x} * \vec{v}(\vec{v} - \vec{u}).\vec{n}dA = \int_{A_e} \rho\,\vec{x}_e * \vec{v}_e(\vec{v}_e - \vec{u}_e).\vec{n}_e dA + \int_{A_i} \rho\,\vec{x}_i * \vec{v}_i(\vec{v}_i - \vec{u}_i).\vec{n}_i dA$$

Again the integral over A_i is zero and is therefore not included in the above equation.

Since from the centre of rotation $\vec{x}_i = \vec{0}$: it means that the integral over area (A_i) is equal to zero.

Conversely using $\vec{x}_e = R\vec{e}_x$ and $\vec{v}_e = v_e\vec{n}_e$, the dot product becomes $(\vec{v}_e - \vec{u}_e).\vec{n}_e = v_e - u_e\cos\beta$. This means that the integral over area (A_e) is equal to:

$$\rho R v_e (v_e - u_e\cos\beta)A_e\vec{e}_x * \vec{n}_e.$$

Again assuming that velocities are constant over cross-sections, moment of momentum of the control volume surface becomes:

$$\int\limits_{A_c} \rho\, \vec{x} * \vec{v}(\vec{v} - \vec{u}).\vec{n}dA = \rho R v_e(v_e - u_e\cos\beta)A_e\vec{e}_x * \vec{n}_e$$

With $\vec{e}_x * \vec{n}_e = \sin\beta\ \vec{e}_x * \vec{e}_x + \cos\beta\ \vec{e}_x * \vec{e}_z = -\cos\beta\ \vec{e}_y$ it is finally found:

$$\int\limits_{A_c} \rho\, \vec{x} * \vec{v}(\vec{v} - \vec{u}).\vec{n}\, dA = -\rho R v_e(v_e - u_e\cos\beta)A_e\cos\beta\ \vec{e}_y$$

The right-hand side of the moment of momentum equation becomes:

$$\int\limits_{A_c} \vec{x} * \vec{t}\, dA = \int\limits_{A_e} \vec{x}_e * \vec{t}_e dA + \int\limits_{A_i} \vec{x}_i * \vec{t}_i dA + \int\limits_{A_P} \vec{x} * \vec{t}\, dA$$

The resultant stress on the fluid $\left(\vec{t}_e\right)$ at the exit is given by $\vec{t}_e = \vec{\tau}_e - p_e\vec{n}_e$. The effects of shear stresses $(\vec{\tau}_e)$ on the fluid are minimal. Also the Atmospheric pressure on the fluid at the exit (p_e) is equal to zero. This means that $\vec{t}_e = 0$ and therefore zero contribution. On the other hand $\vec{x}_i = 0$, which also means that the contribution over area A_i is zero as well.

Therefore the right hand side of the equation can be written as:

$$\int\limits_{A_c} (\vec{x} * \vec{t})dA = \int\limits_{A_P} (\vec{x} * \vec{t})dA = +T\,\vec{e}_y$$

The integral over A_p is equal to the torque applied on the fluid and is denoted by $+T\vec{e}_y$ where $T > 0$. Consequently, the torque applied by the fluid on the arm is equal to $-T\vec{e}_y$.

Equating the left-hand side and right-hand side of the moment of momentum equation, delivers:

$$T \, \vec{e}_y = -\rho R v_e (v_e - u_e \cos\beta) A_e \cos\beta \, \vec{e}_y$$

With $u_e = \omega R$, and using the continuity equation (eqn 3.6) the following expressions for the moment of momentum equation can be derived:

$$T = -\rho R v_e (v_e - u_e \cos\beta) A_e \cos\beta$$
$$T = -\rho R v_e (v_e - \omega R \cos\beta) A_e \cos\beta$$
$$T = -\rho R v_e Q \cos\beta$$

$$\{eqn\ 3.7\}$$

Taking the angle of exit to be; $\beta = 180$, then $T = \rho R v_e Q$ which is similar to equation 2.3 by A. Akbarzadeh and Abhijit Date.

3.4.3 Energy equation

The energy equation 3.5 for the turbine reads;

$$\frac{d}{dt}\left(\int_{V_c} \left(\rho g z + \frac{1}{2}\rho v^2 \right) dV \right) + \int_{A_c} \left(\rho g z + \frac{1}{2}\rho v^2 \right) (\vec{v} - \vec{u}).\vec{n} dA = \int_{A_c} (\vec{t} * \vec{v}) dA$$

Again the time derivative is zero. Also since $\left(\vec{v}_p - \vec{u}_p\right) = 0$, the contribution of energy by surface A_P is equal to zero. Therefore the left-hand side becomes:

$$\int_{A_c} \left(\rho g z + \frac{1}{2}\rho v^2 \right) (\vec{v} - \vec{u}).\vec{n} dA$$

$$= \int_{A_e} \left(\rho g z_e + \frac{1}{2}\rho v_e{}^2 \right) (\vec{v}_e - \vec{u}_e).\vec{n}_e dA$$

$$+ \int_{A_i} \left(\rho g z_i + \frac{1}{2}\rho v_i{}^2 \right) (\vec{v}_i - \vec{u}_i).\vec{n}_i dA$$

Since the term $(\vec{v}_e - \vec{u}_e).\vec{n}_e$ is equal to $v_e - u_e\cos\beta$, while $(\vec{v}_i - \vec{u}_i).\vec{n}_i = (\vec{v}_i - o).\vec{n}_i = -v_i$ and knowing that $z_e = z_i = 0$, the left-hand side of the energy equation becomes:

$$\int_{A_c}\left(\rho gz + \frac{1}{2}\rho v^2\right)(\vec{v} - \vec{u}).\vec{n}dA = \frac{1}{2}\rho v_e{}^2(v_e - u_e\cos\beta)A_e - \frac{1}{2}\rho v_i{}^3 A_i$$

Working out the right-hand side:

$$\int_{A_c}(\vec{t}.\vec{v})dA = \int_{A_e}(\vec{t}_e.\vec{v}_e)dA + \int_{A_i}(\vec{t}_i.\vec{v}_i)dA + \int_{A_p}(\vec{t}.\vec{v})dA$$

The power (P) performed by the conduit on the fluid is given by:

$$\int_{A_p}(\vec{t} * \vec{v})dA = -T\omega$$

Further, substituting $\vec{t}_e = 0$, $\vec{t}_i = -p_i\vec{n}_i$ and that $\vec{v}_i = -v_i\vec{n}_i$ in the above equation and working out the integrals brings the following relation for the right-hand side:

$$\int_{A_c}(\vec{t}.\vec{v})dA = p_i v_i A_i - T\omega$$

Equating the left and right-hand sides, the energy equation then becomes

$$\frac{1}{2}\rho v_e{}^2(v_e - u_e\cos\beta)A_e = \left(p_i + \frac{1}{2}\rho v_i{}^2\right)v_i A_i - T\omega$$

$$\{eqn\ 3.8\}$$

3.4.4 Bernoulli equation for supply pipe

In this section the Bernoulli equation for the supply pipe is derived. This equation helps in determining $\vec{v}_i$ and p_i. Figure3.10 shows the modeling for both the penstock and the tank.
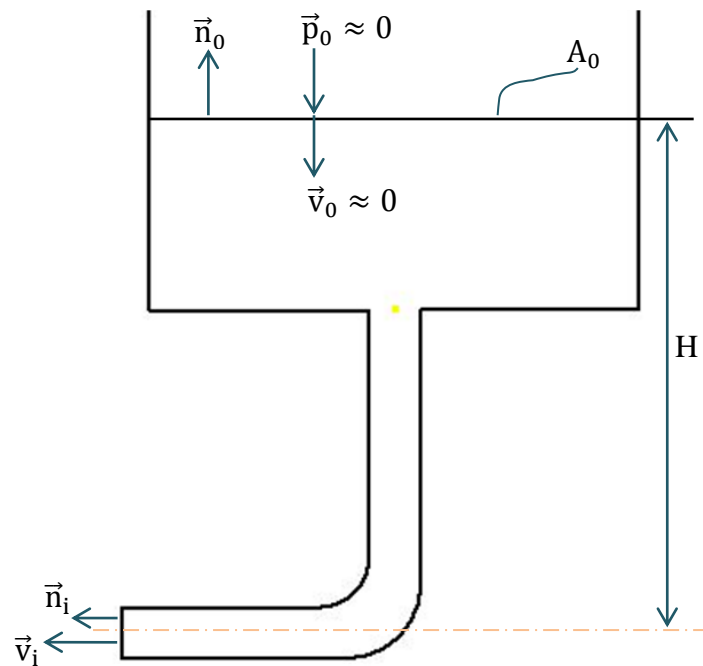
Figure 3.10: Velocity diagram of the penstock and the tank

Bernoulli's equation reads:

$$\frac{p_i}{\rho g} + z_i + \frac{v_i{}^2}{2g} = \frac{p_0}{\rho g} + z_0 + \frac{v_0{}^2}{2g} \quad \text{(Friction loss neglegted)}$$

Using the origin of the coordinate system as a datum then $z_i = 0$ and $z_0 = H$ .Further because of the large cross-sectional area of the tank $v_0 \approx 0$ the pressure level at the water surface in the tank is atmospherical so $p_0 = 0$ (Gauge pressure).

Therefore;

$$\frac{p_i}{\rho g} + 0 + \frac{v_i{}^2}{2g} = H \;\rightarrow\; p_i + \frac{1}{2}\rho v_i{}^2 = \rho g H \qquad\qquad \{eqn\ 3.9\}$$

Substituting this result into the energy equation and making use of the continuity equation and the moment of momentum equation, the following equation is arrived at;

$$\frac{1}{2}\rho v_e{}^2 Q = \rho g H Q + \rho R v_e Q \cos\beta\omega$$

Further simplification leads to;

$$v_e{}^2 - 2v_e\cos\beta\omega R = 2gH$$

Expansion of the above equation gives;

$$(v_e - \cos\beta\omega R)^2 = 2gH + \omega^2 R^2 \cos^2\beta$$

Relative velocity $v_r = (v_e - \cos\beta\omega R) = \sqrt{2gH + \omega^2 R^2 \cos^2\beta}$

{eqn 3.10}

Taking a condition where angle $\beta = 180$ then this equation becomes similar to equation 2.2 obtained using an ad-hoc analysis by A. Akbarzadeh and Abhijit Date.

It should be noted that an "ideal" turbine is considered in the above derivations, which means that friction and other losses in the nozzle are not taken into consideration. These losses will be accounted for in section 3.4.6.

3.4.5 Calculation of power and efficiency without nozzle losses

The power produced by the turbine (i.e. power performed by fluid on the tube) is calculated from the energy equation (3.8);

$$P = T\omega = \left(p_i - \frac{1}{2}\rho v_i^2\right)v_i A_i - \frac{1}{2}\rho v_e^2(v_e - u_e\cos\beta)A_e$$

Using the result of Bernoulli's equation 3.9 and the continuity equation 3.6, the power equation becomes;

$$P = \rho Q\left(gH - \frac{1}{2}v_e^2\right)$$

{eqn 3.11}

But according to equation 3.10; $v_e = \sqrt{2gH + \omega^2 R^2 \cos^2\beta} + \omega R\cos\beta$

Substitution into the power equation delivers the following;

$$P = -\rho Q\omega R\cos\beta\left(\sqrt{2gH + \omega^2 R^2 \cos^2\beta} + \omega R\cos\beta\right)$$

{eqn 3.12}

The power available is $P_H = \rho QgH$ so that the hydraulic efficiency is given by:

$$\eta = \frac{P}{P_H} = \frac{-(\omega R\cos\beta)(\sqrt{2gH + \omega^2 R^2 \cos^2\beta} + \omega R\cos\beta)}{gH}$$

Introduction of (centrifugal pumping effect) as discussed by A. Akbarzadeh in equation 2.1:

$$H_c = \frac{\omega^2 R^2 \cos^2 \beta}{2g} \qquad \{eqn\ 3.13\}$$

and taking into account that $\cos\beta < 0$, the efficiency becomes;

$$\eta = \frac{2\left(\sqrt{H. H_c + H_c^2} - H_c\right)}{H} \qquad \{eqn\ 3.14\}$$

Or:

$$\eta = 2\left(\sqrt{K + K^2} - K\right) \text{ with } K = \frac{H_c}{H} = \frac{\omega^2 R^2 \cos^2 \beta}{2g * H} \qquad \{eqn\ 3.15\}$$
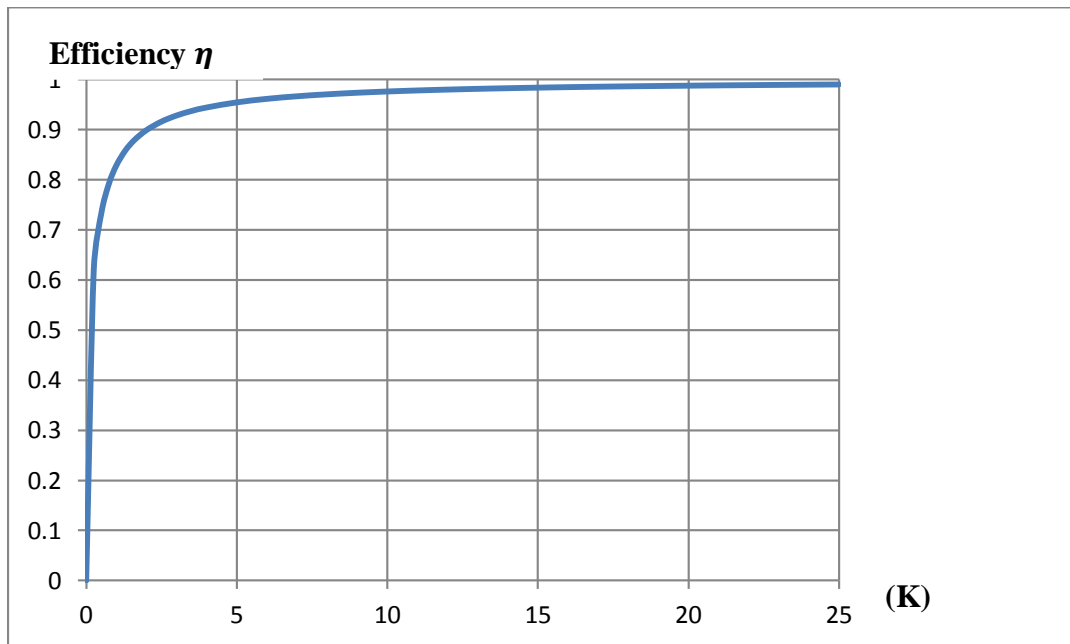
Figure 3.11: Efficiency η against K

Figure 3.11 shows the graph of efficiency against K. It can be seen that as K increases the efficiency approaches one.

3.4.6 Calculation of power and efficiency with nozzle losses

In the previous section it was assumed that we deal with an ideal fluid, without friction losses. However, at high rotational speeds the relative velocity between nozzle and fluid becomes very high introducing energy losses which are proportional to $v_r{}^2$.

To account for these losses the power equation 3.11 is adapted as follows:

$$P = \rho Q \left(gH - \frac{1}{2} v_e{}^2 - \frac{1}{2} k v_r{}^2 \right) \qquad \{eqn\ 3.16\}$$

Where k is a proportionality factor depending on the roughness and other losses in the nozzle.

The introduction of these losses will affect the exit velocity v_e. However, the moment of momentum equation remains unchanged.

From eqn 3.10, the relative velocity with respect to nozzle is; $v_r = v_e - \omega R\cos\beta$, so that eqn 3.16 transforms into:

$$P = \rho Q \left(gH - \frac{1}{2} v_e{}^2 - \frac{1}{2} k(v_e - \omega R\cos\beta)^2 \right) \qquad \{eqn\ 3.17\}$$

Since $P = T\omega$, with T equals to the third relation in eqn 3.7 it is found:

$$-\rho Q v_e(\omega R\cos\beta) = \rho Q (gH - \frac{1}{2} v_e{}^2 - \frac{1}{2} k(v_e - \omega R\cos\beta)^2)$$

Solving the above quadratic equation in v_e leads after some mathematical manipulation to:

$$v_e = \sqrt{\frac{2gH + \omega^2 R^2 \cos^2 \beta}{(1 + k)}} + \omega R\cos\beta$$

$$\{eqn\ 3.18\}$$

Equation 3.18 is therefore the equation of the water jet velocity (v_e) after introduction of the frictional losses at the nozzle.

Using equation 3.18 the power equation 3.17 can be rewritten to look like:

$$P = -\rho Q \omega R \cos\beta \left[\sqrt{\frac{2gH + \omega^2 R^2 \cos^2\beta}{(1 + k)}} + \omega R \cos\beta \right] \qquad \{eqn\ 3.19\}$$

Comparison of this power equation (i.e. including friction losses) with equation 3.12 (i.e. without friction losses) reveals that the only difference is the factor 1+k. However, as will be shown the factor k has a huge impact on the efficiency.

In this case the hydraulic efficiency becomes;

$$\eta = \frac{\sqrt{\dfrac{2gH(\omega R \cos\beta)^2 + (\omega R \cos\beta)^4}{(1 + k)}} - (\omega R \cos\beta)^2}{gH}$$

Introduction of the centrifugal pumping effect given by eqn 3.13 delivers for the efficiency:

$$\eta = \frac{2 \left[\sqrt{\dfrac{HH_c + H_c}{(1 + k)}} - H_c \right]}{H} \qquad \{eqn\ 3.20\}$$

Or:

$$\eta = 2 \left[\sqrt{\frac{K + K^2}{(1 + k)}} - K \right]; \qquad K = \frac{H_c}{H} \qquad \{eqn\ 3.21\}$$

Figure 3.12 (a) shows graphs of efficiency (η) against K and it also shows how efficiency varies with the factor k. Now the efficiency curves display a clear maximum.
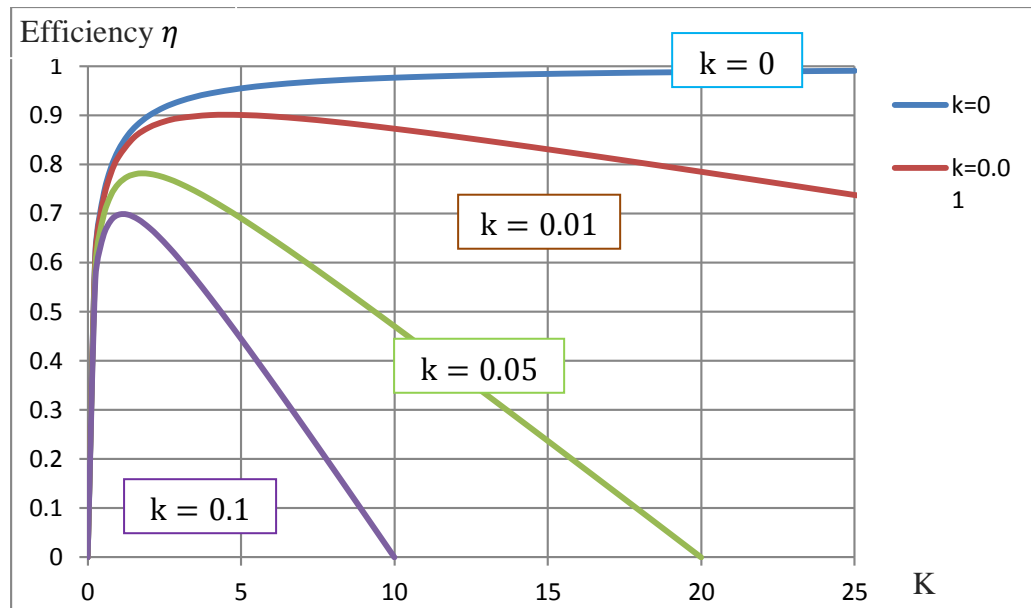
Figure 3.12 (a): Graph of efficiency against K with different k-factor values

It further can be seen that as k-factor increases maximum efficiency decreases. A similar graph of efficiency against RPM with different k-factor values shown in figure 3.12 (b) has been drawn and discussed by Abhijit Date in his Phd thesis (Date, 2009, page 32).
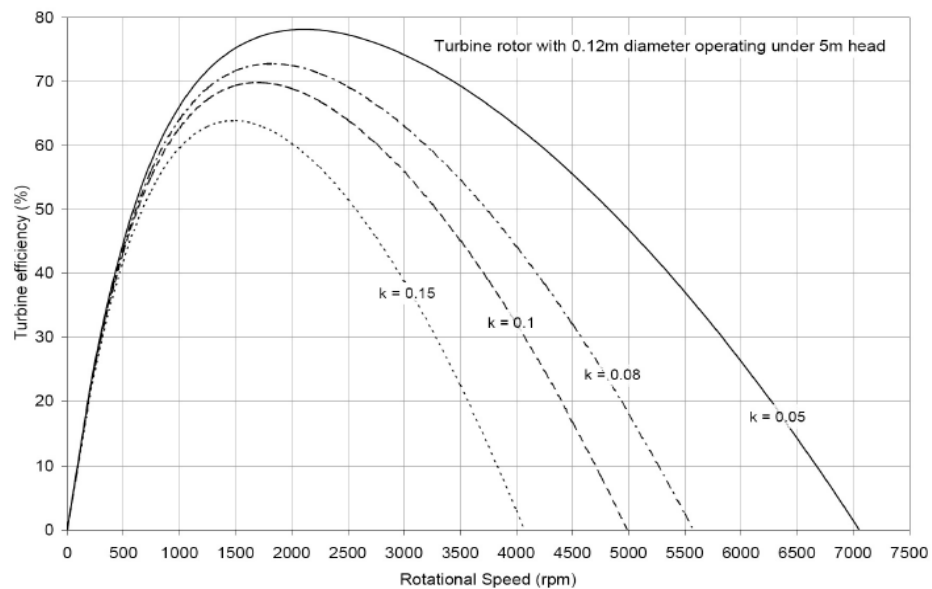
Figure 3.12 (b): Graph of efficiency against angular speed with different k values (Date, 2009)

3.4.7 Determination of k from experimental results

It should be noted that in an experiment certain variables can be easily measured. Therefore using the data from experimental results factor k can be determined;

For this purpose the continuity equation in eqn 3.6 is used:

$(v_e - u_e\cos\beta)A_e = Q$ or $\left(v_e - (\omega R\cos\beta)\right)A_e = Q$. Together with the relation for v_e (equation 3.18), the factor k can be written as:

$$k = (2gH + \omega^2R^2\cos^2\beta)\left(\frac{A_e}{Q}\right)^2 - 1 \qquad\qquad \{eqn\ 3.22\}$$

So k is a function of H, Q and ω which all are known during the experiments. A less general equation similar to eqn 3.22 has been derived by A. Akbarzadeh and Abhijit Date (Date A., 2009, p. 29).

3.5 Turbine design

Two similar centrifugal reaction turbines shown in figure 3.13(a) and 3.13(b) were fabricated and only the turbine in figure 3.13(b) was used for experiments. This is because the turbine in figure 3.13(a) had a lot of setbacks; first being the high frictional resistance due to the type of bearing used, second was that the plywood used to support the semicircular conduit absorbed the spilling water from the nozzle and got damaged.

| **Figure 3.13 (a): turbine 'A'** | **Figure 3.13 (b): turbine 'B'** |
| reinforced with plywood. | reinforced with metal strip. |

3.5.1 Turbine A design

The computer design of the turbine 'A' general outlook is shown in figure 3.14 (a), (b), (c) and (d). In this turbine the semicircular conduit is reinforced with plywood, which also acts as a flywheel. This type of turbine was not used for any performance analysis.
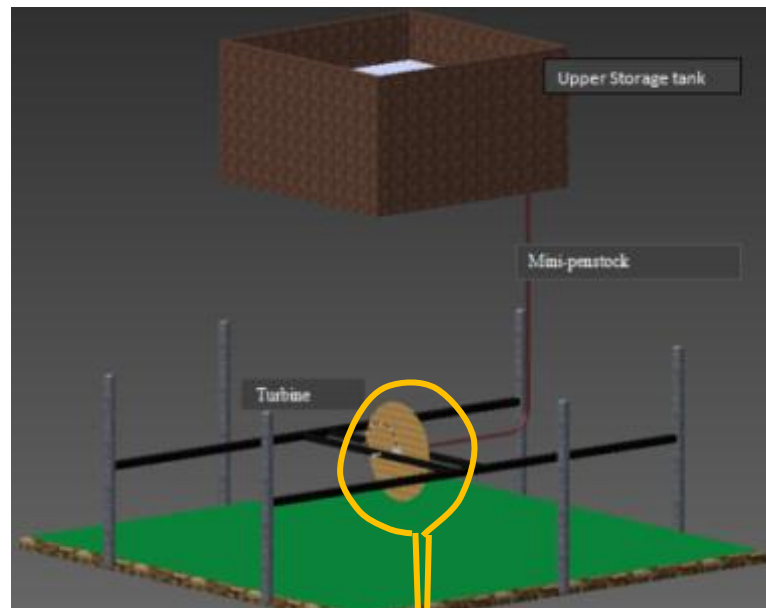
Figure 3.14 (a): Single Arm Centrifugal Reaction Water Turbine model
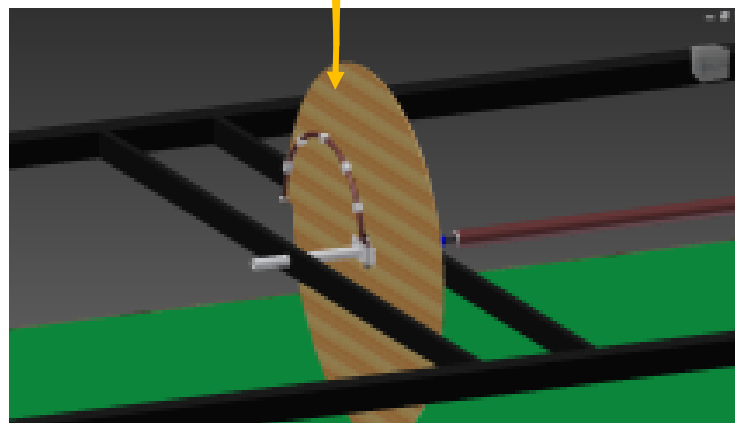
Figure 3.14 (b): close-up view of the actual
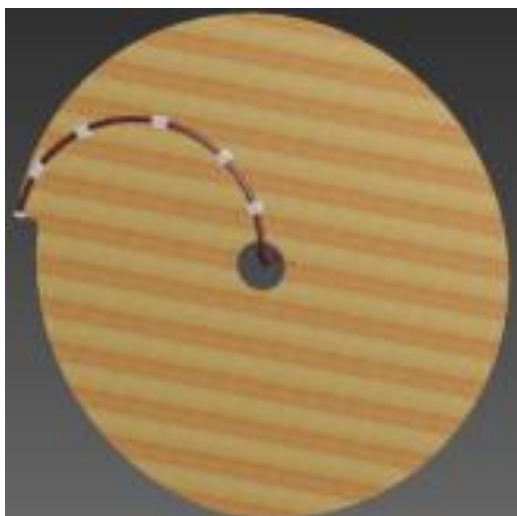
Figure 3.14(c): Turbine unit (without the central output shaft)

Figure 3.14(d): Complete turbine unit

3.5.2 Turbine B design

Figure 3.15 (a), (b), (c), and (d) shows the general design of the second type of turbine. This design uses a metal strip in place of plywood to reinforce the plastic semicircular conduit.
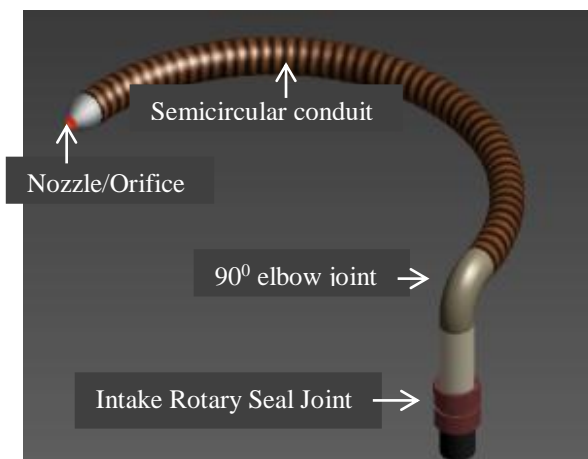
Figure 3.15 (a): semicircular conduit design
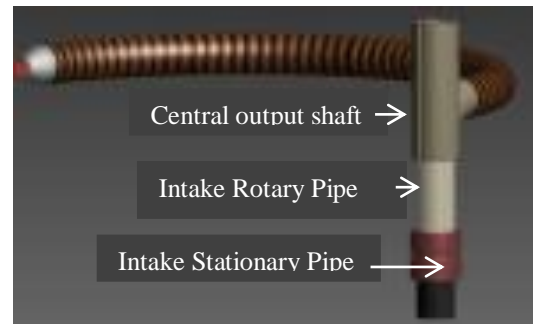
Figure 3.15 (b): extended output central shaft
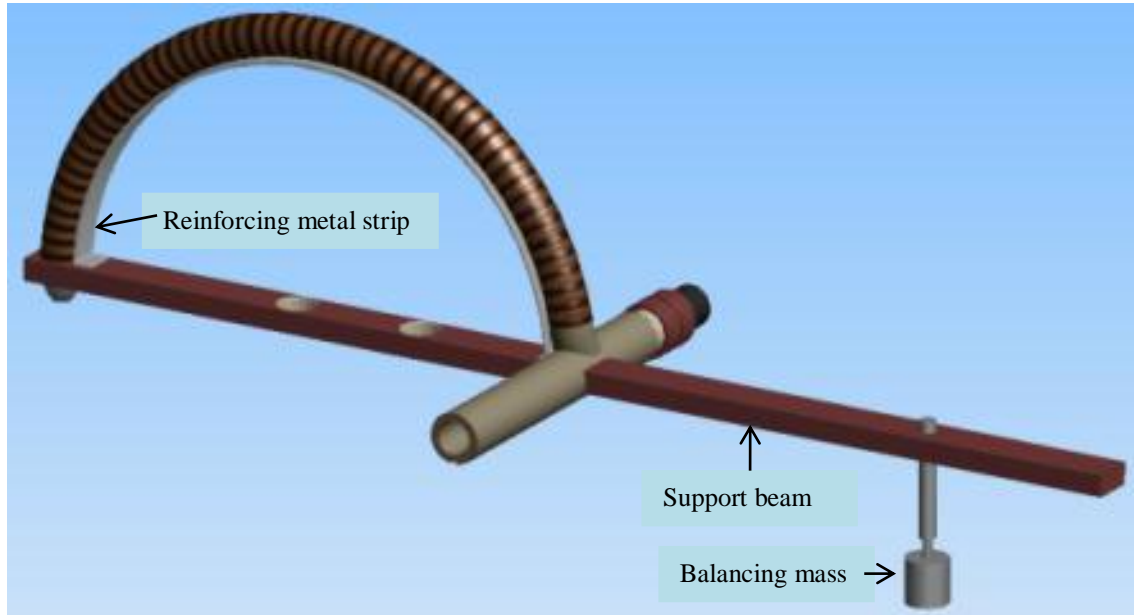
Figure 3.15 (c): turbine's 3D view
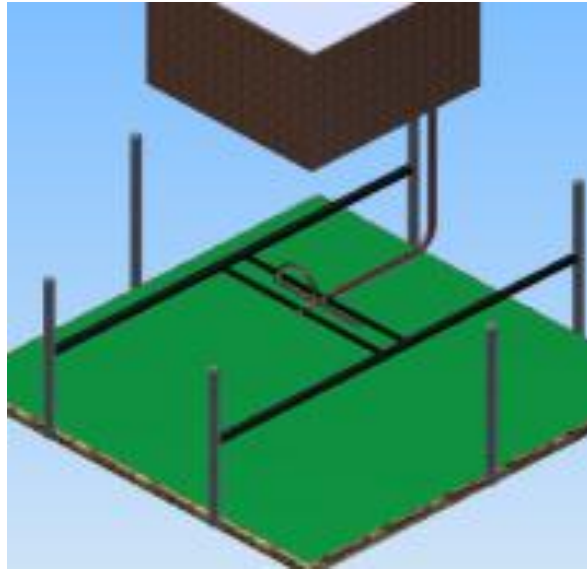
Figure 3.15(d): 3D view after installation of the

3.6 Turbine Fabrication

The turbine receives water from the raised tank or from the high pressure tap via the penstock and finally exits at the nozzle. All the components that build the turbine starting with the penstock all the way to the nozzle are discussed in this section.

3.6.1 Penstock

A plastic pipe is used as penstock as shown in figure 3.16 (a) and (b). Its internal diameter (ϕ_{in}) is equals to 20mm.

$\phi_{in}=20$ mm

Figure 3.16 (a): penstock
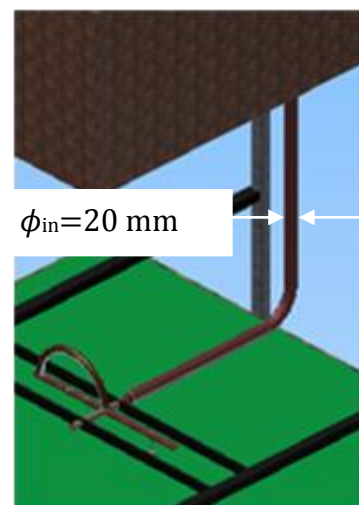
Figure 3.16(b): CAD view of penstock

3.6.2 Flow control valve

As the penstock joints the turbine a ball valve is used to control the flow as shown in figure 3.17. Its internal diameter (ϕ_{in}) is equals to 20 mm.

Figure 3.17: flow control valve

3.6.3 Mechanical rotary lip seal device

Mechanical rotary lip seal device is a mechanism that allows a rotation of one pipe at one end and a stationary pipe on the other end and still allows a continuous flow of water. Devices of this kind are rarely found in the market. For this reason the mechanical rotary lip seal mechanism used in this research was locally designed and fabricated. The components used to construct this device include; ball bearing (1/2" internal diameter) with a plastic cage seal, straight pipe fitting socket (3/4"), 70mm X 70mm rubber sheet obtained from a worn out motorbike tire tube and is drilled at centre. The arrangement of the various components to form a complete rotary lip seal mechanism is as shown in figure 3.18 (a). A picture of the actual mechanical rotary lip seal mechanism is shown in figure 3.18 (b).
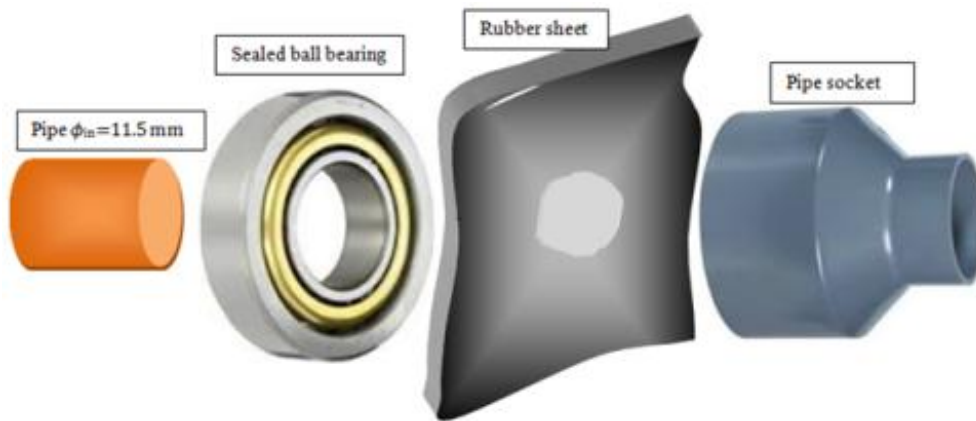
Figure 3.18 (a): mechanical rotary lip seal component arrangement

Figure 3.18 (b): a photograph of mechanical rotary lip seal mechanism

3.6.4 Axial, Central holed shaft

The axial, central holed shaft is made of a carbon steel pipe. It has an internal diameter of ϕ_{in}=13.0 mm. Figure 3.19 a photograph of a central holed shaft. Axial, central holed shaft serves two main functions which includes; providing a water passage through a ninety degrees turn and acting as main output shaft.
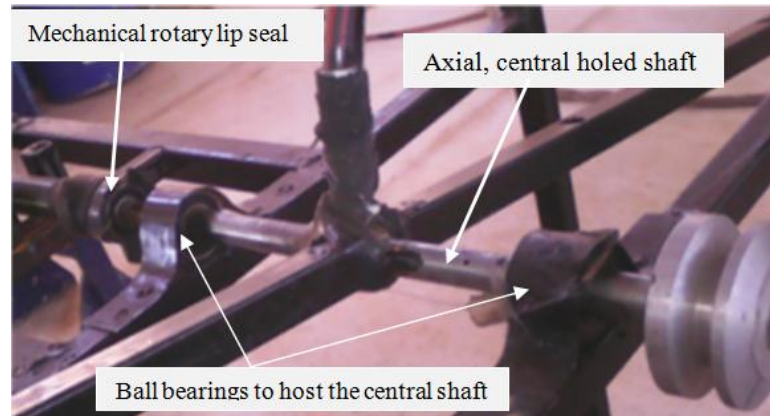
Figure 3.19: Axial, central holed shaft

3.6.5 Radial centre beam

The radial centre beam is made of a cast iron square pipe of width (W_{in}=1"), while the total length is L_{in}=2.06m. This type of square pipe is readily available in most of the hard-wares. The purpose of the radial centre beam is to support the semicircular conduit so that the conduit can be firm in its position and maintain its semicircular arrangement. Three holes of diameter (ϕ_{in}=12.0 mm) are drilled into the beam as shown in figure 3.20 (a) and (b). The nozzle of the semicircular conduit is inserted into the tight holes (each one at time) such that it appears on the other side where water can easily jet out and cause a reaction force.
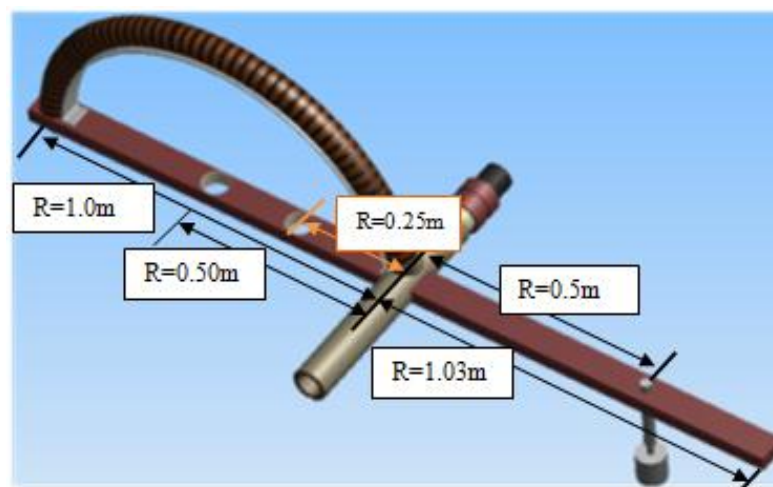
Figure 3.20 (a): Radial centre beam dimensions

Figure3.20 (b): Radial centre

3.6.6 Semicircular PVC conduit

Semicircular conduit is a PVC pipe that that joints the axial centre pipe and nozzle following a semicircular path as shown in figure 3.21 (a) and (b). The conduit has an internal diameter of (ϕ_{in}=11.50 mm).
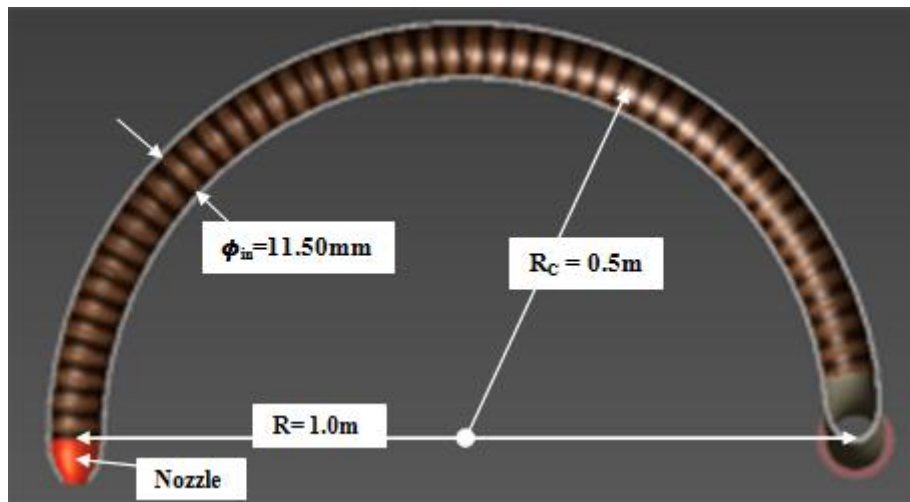
Figure 3.21 (a): Semicircular conduit and its dimensions

Figure 3.21 (b): A photograph of the semicircular conduit

3.6.7 Nozzle

The nozzle is meant to accelerate the speed of the water as they approach the exit. The nozzle used here is made of a plastic material and are found at most of the hardware shops. Five different sizes of nozzles are used as shown in figure 3.22. The diameters (ϕ_f) of the orifices are; 11.50 mm, 8.8mm, 6.0mm, 3.8mm, 2.5mm in the order shown in the figure 3.22.
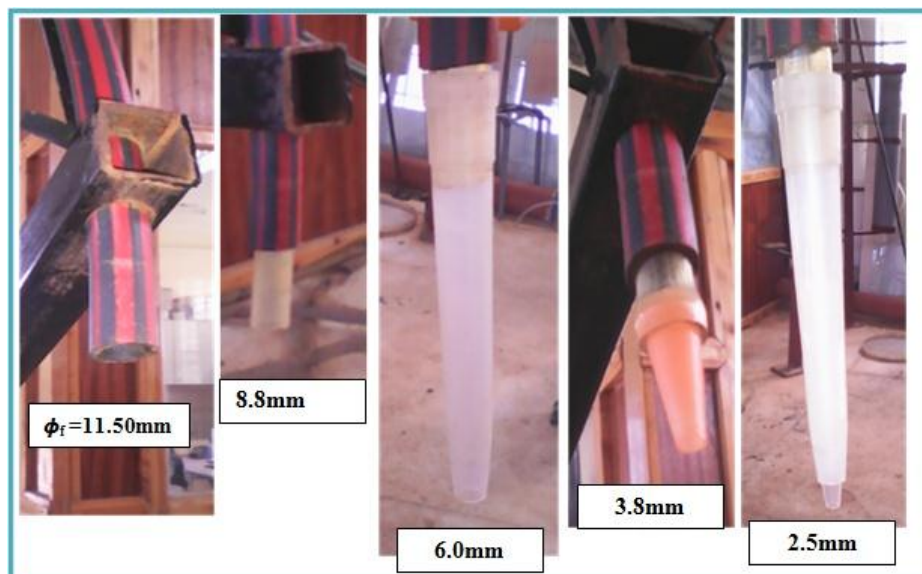
Figure 3.22: Five different sizes of turbine nozzles

3.7 Fabrication Cost analysis

The costs of the various components used in the construction of the turbine as well as the labour charges are shown in table 3.1

Table 3.1: Cost of fabricating the turbine

Type of component	Cost of component per unit in Ksh	No of units	Total coast in Ksh
Penstock	170	5	850
Flow control valve	750	1	750
Mechanical rotary lip seal device	(total= 400)	_	400
Axial, Central holed shaft	1870	0.5	935
Radial centre beam	200	2.5	500
Semicircular PVC conduit	90	4	360
Nozzle	80	4	320
Bearings	220	2	440
Turbine Frame materials	(Total= 2400)	_	2400
Labour	(Total= 2300)	_	2300
		TOTAL= KES 9255	

CHAPTER FOUR

EXPERIMENTAL SETUP AND MEASUREMENT SYSTEMS

4.1 Introduction

This chapter describes the procedure of how the set objectives were achieved. Further it provides the turbine test rig together with the measuring facilities and instrumentation. The experimental techniques used for performance study of the turbine are also described here. Furthermore all the data recording techniques for all the experiments carried out are illustrated in this chapter.

In this research a single arm, centrifugal reaction water turbine was built. The turbine was structured in such a way that the water from the supply pipe enters into the turbine from the centre. The water then leaves the turbine through a radial curved conduit and exiting at the nozzle. Up to three scientific analyses were carried out on the turbine, which includes; variation of nozzle ratio, variation of radial arm length and variation of the supply head. To determine the most efficient main pipe to nozzle ratio, a number of nozzles were randomly selected starting from the highest to the smallest. The ratios investigated, were between one and 0.0473. The internal diameter of the main radial conduit is 11.5mm, while the nozzle diameters are; 8.8mm, 6.0mm, 3.8mm, 2.5mm. In order to get the nozzle to main conduit cross-sectional area ratio, the cross-sectional area of the tip of the nozzle is divided by cross-sectional area of the main conduit. In the case where no nozzle is used the cross-sectional area ratio is taken to be one.

As for the relation between the arm length (arm radius) and the output power the arm radius was varied in three steps. Three radial lengths that were used includes; R=0.25m, R=0.5m, R=1m. By varying the radial arm length and keeping other

variables constant and measuring the variations in the angular speed, torque and flow rate, the effects of the radial arm length on the output power was determined.

In each experiment performed the efficiency of the turbine was calculated. Therefore to compare the efficiencies when the head H=1.85m and when H=11.5m the optimum efficiencies for each head were used. The lower head of H=1.85m was achieved by connecting the delivery pipe to the raised tank. The high head of H=11.5m was achieved by directly connecting the supply pipe to the high pressure tap source at Professor Huisman Laboratory.

4.2 Turbine Test Rig

4.2.1 Description of Test Rig Setup

Figure 4.1 shows a snap shot of the setup of the turbine test rig used for the performance analysis of the centrifugal reaction turbine prototype. The turbine test set up includes;

- ➢ Hydraulic power input components: This comprises the raised water storage tank (tank capacity 0.22m³), high pressure water tap, supply pipe, delivery pipe (penstock), and flow control valve.
- ➢ Power output components: This encompasses the turbine housing frame, single arm centrifugal reaction water turbine with the inlet rotary lip sill joint arrangement.
- ➢ A tachometer (for angular speed measurement) and a torque-meter

The torque of the turbine is measured using a rope brake dynamometer. Output power is calculated using the obtained data of torque and angular speed.

The housing frame in figure 4.1 is fabricated from rectangular hollow iron bars obtained from Moi university Mechanical engineering workshop store. A plastic

water tank (220L STAR) was purchased from a local hardware shop. Installation of the water tank and flow regulator along with the supply and delivery pipe plumbing on the housing frame and installation of the turbine prototype were done at Moi University Civil and Structural department Fluid Laboratory. During the experimental tests, a rope brake dynamometer and an electronic tachometer were utilized to collect the data. The digital tachometer was provided by Moi University Mechanical Engineering Department.
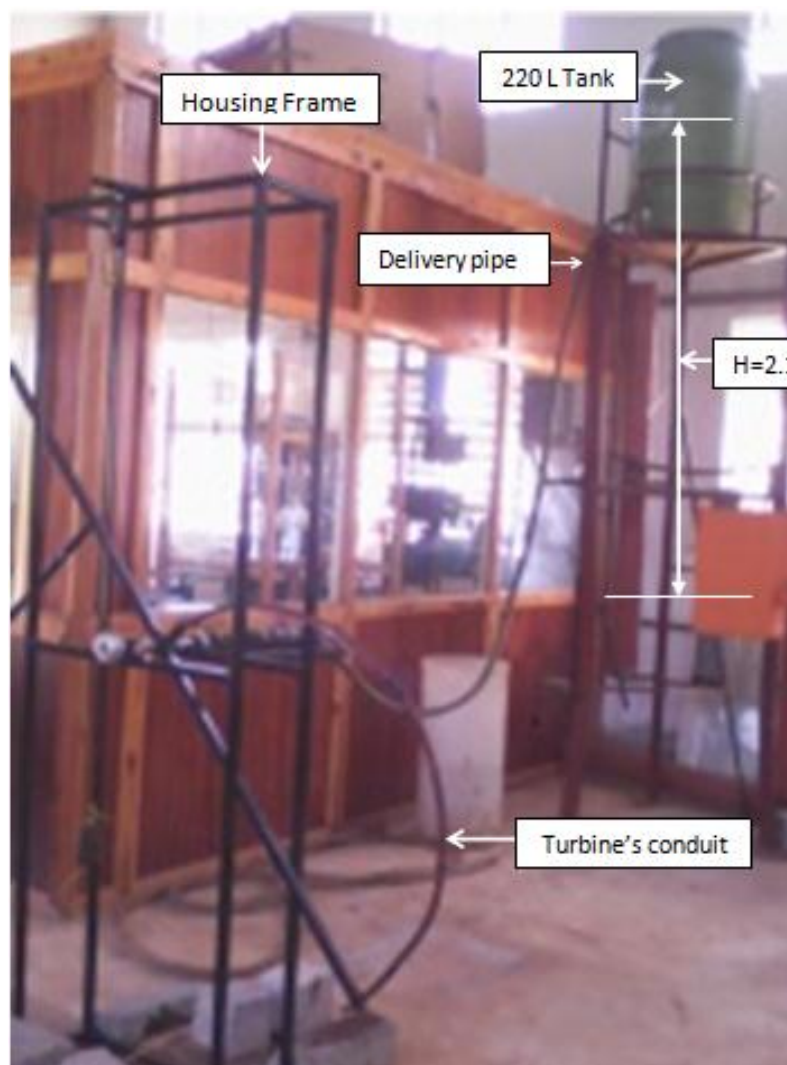
Figure 4.1: a picture of the turbine test rig

4.2.2 Hydraulic Power input Components

The selection of all the hydraulic input unit components is based on the maximum operating head and maximum flow rate available for turbine performance testing. In this research the estimated maximum delivery heads are (1.85m for the raised tank and 11.5m for the water source tap). Using the bucket method the maximum discharge by the delivery pipe is (Q=0.0003213m³/sec for the raised tank and Q=0.0004745m³/sec for the tap water). These flow rates are measured before installation of the turbine's semicircular conduit. Table 4.1 shows the time taken to achieve a water volume capacity of 0.005 m³.

Table 4.1: Raised tank water and tap water flow rate test data

	Tap Water ($H = 1.85m$)	Tap Water ($H = 11.5m$)
$t_1(s)$	15.40 sec	10.53 sec
$t_2(s)$	15.71 sec	10.55 sec
$t_{average}(s)$	15.56	10.54
$Q(m^3/s)$	0.0003213	0.0004745

The data for the raised tank water flow rate are obtained using the calibration in the tank. While for the tap water, since they are supplied by university main tank which could not actually be calibrated for this purpose a water flow meter was used.

The inner cross-sectional area of the delivery pipe is $A = 0.00031416 \, m^2$ for the raised tank and, $A = 0.000415475 \, m^2$ for the water source tap. Therefore the flow velocity is $v = 1.02273 \, m/sec$ for the raised tank delivery pipe and $v = 1.142066 \, m/sec$ for the tap water. The Reynolds number for this water flow is estimated using the Cengel equation (Cengel, 1996);

For the raised tank;

$$Re = \frac{4\rho.Q}{\pi D\mu} = 17942.704 \qquad \{eqn\ 4.1\}$$

For the Tap water, Reynolds number equals to;

$$Re = \frac{4\rho.Q}{\pi D\mu} = 23041.65385 \qquad \{eqn\ 4.2\}$$

Therefore the coefficient of friction can be estimated as follows (Cengel, 2006);

For the raised tank

$$f = 0.184 * (Re)^{-0.2} = 0.025944 \qquad \{eqn\ 4.3\}$$

For the tap water

$$f = 0.184 * (Re)^{-0.2} = 0.024678 \qquad \{eqn\ 4.4\}$$
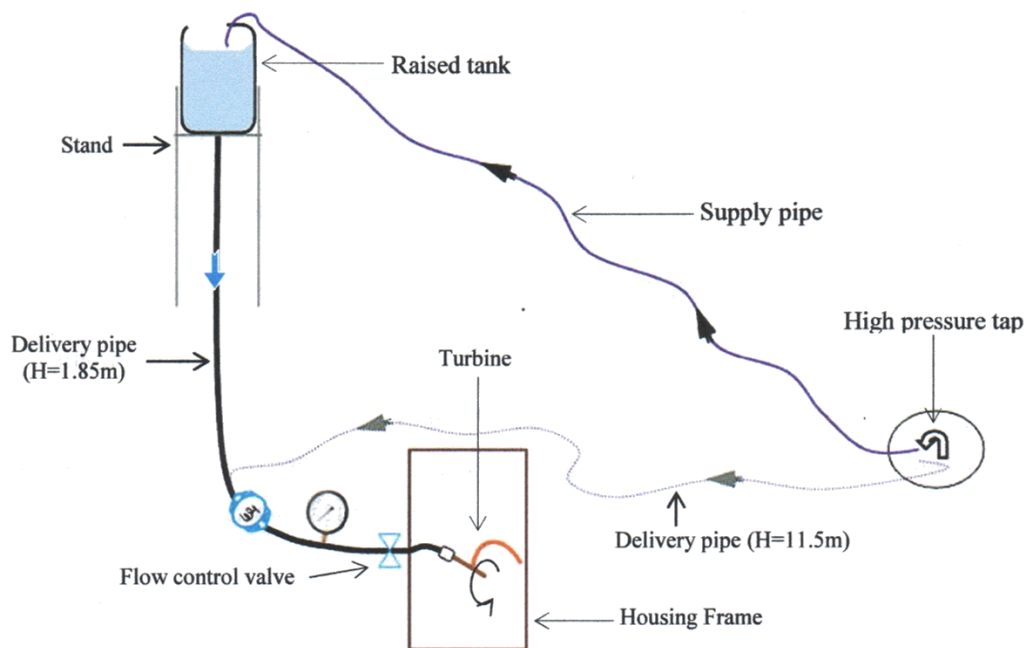
Figure 4.2: Schematic diagram of the test rig

Figure 4.2 is a schematic diagram of the turbine test rig which shows the position and arrangement of; raised water storage tank, high pressure water tap, supply pipe, delivery pipe (penstock), and flow control valve.

Figure 4.3 (a, b, c) shows the various input components and instruments of the turbine test rig.

Figure 4.3 (a): Flow control valve

**Figure 4.3 (b): Tap water pipe
and its source**

Figure 4.3 (c): Pressure gauge

The raised tank $(H = 1.85\ m)$ is filled by a supply pipe from the water tap. The supply pipe also acts as the delivery pipe when the tap water $(H = 11.5\ m)$ is used to drive the turbine. A valve is used to control the flow as it enters the turbine.

4.2.3 Power output components, torque-meter, tachometer

Power output components includes; housing frame, single arm centrifugal reaction water turbine and a central output shaft fitted with a pulleys. The pulley hosts the brake dynamometer rope as shown in Figure 4.4. Rope brake dynamometer is used as a torque-meter.

Figure 4.4: Picture of a pulley fitted to a turbine's output shaft

4.3 Summary of Test and Performance Proximate Procedure

The purpose of this section is to discuss the experimental procedures that are used to determine the performance of this turbine under different hydrostatic heads, different exit orifices and different turbine arm radius. These test procedures are divided into four distinct categories namely: Input power test, Output power test, Torque test and Power loss estimation.

The data achieved here are later used to estimate the dynamic coefficients and the general turbine performance.

4.3.1 Input power test

This test procedure measures the amount of input power at any instance by measuring the water flow rate into the turbine as well as the operating height. In this test a timed water volume measurement using the bucket method is used to estimate the water volume flow rate into the turbine. A calibrated bucket is placed at the end of the turbine's conduit and the valve is turned on. As the water fills the bucket they are being timed. The second method of measuring the volume flow involves taking the reading of the volume drop of water in the calibrated tank. The third method is by

using flow meter. In both cases volume flow rate is achieved by taking the volume flow over a certain period of time and dividing it by the time taken by the flow. For example;

$$Q = \frac{\left[\frac{(L_2 - L_1)}{1000}\right]}{\Delta t} = 0.0005128 \ m^3/sec \qquad \{eqn\ 4.5\}$$

Figure 4.5 is a schematic diagram of the arrangement of flow meter and pressure gauge. Figure 4.6 (a) shows a picture of a raised tank calibrated using a water level sight tube. Figure 4.6 (b) shows a calibrated container used in volume flow measurement by bucket method.
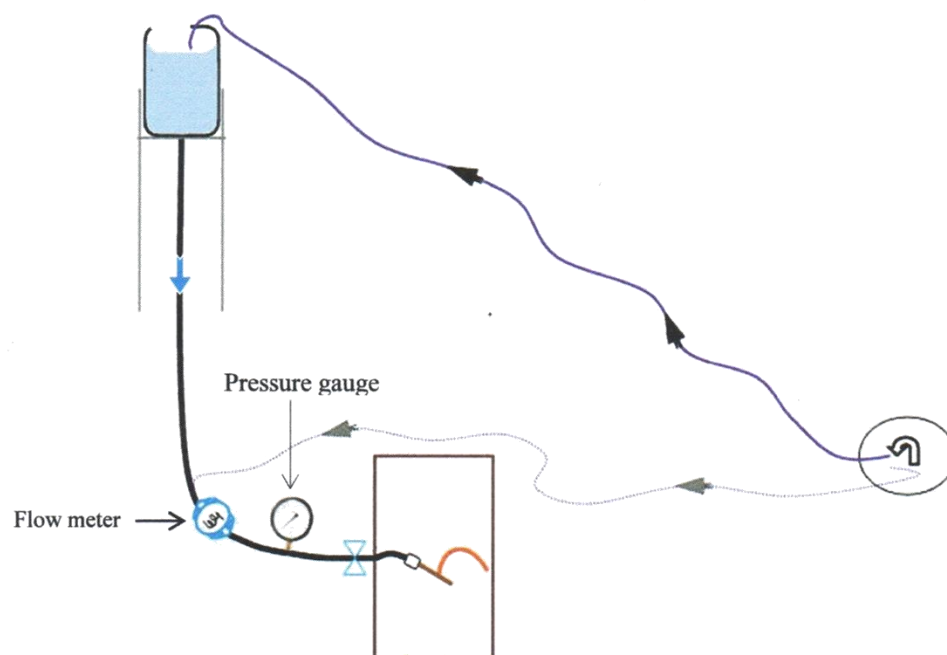
Figure 4.5: Flow meter and Pressure gauge arrangement

Figure 4.6 (a): Calibrated tank for measuring volume drop

Figure 4.6 (b): Bucket method of measuring volume flow

Moreover input power test involved measuring the operating head. This is achieved using a pressure gauge. The instrument is connected to the end of the turbine's conduit using an 11.5 mm diameter plastic pipe. The results of the two variables (i.e. volume flow rate Q and the operating head H) are inserted into the ($\rho g H Q$) formula. This gives an estimation of the input power. Note that just like most reaction turbine the flow rate increases with the increase in rotational speed due to centrifugal pumping effect as discussed in Chapter 3.

4.3.2 Output power test

This test procedure measures the output power usually referred as the turbine's shaft power. In this test estimation of the power produced by the rotating turbine's shaft is derived. This experiment is done at two different hydrostatic heads (i.e. low 1.85m, and high 11.5m), different nozzles as well as deferent turbine's arm radius. The head

of 11.5m was achieved by using the high pressure tap at Professor Huisman laboratories and was measured using a Pressure gauge. Output power test employs the formula $P = T * \omega$, where P is power and T is torque while ω is the angular speed. The test involves the use of a rope brake dynamometer to measure turbine's shaft torque at any given time. At the same time a digital tachometer is attached to the turbine's shaft so as to measure the angular speed.

4.3.3 Rope Brake Dynamometer for torque measurement

4.3.3.1 General working of a Rope Brake Dynamometer

In the case of a rope brake dynamometer; a rope is wrapped over the 'V' space of a pulley keyed to the shaft of the engine. The diametric size of the rope depends upon the power of the machine. The upper end of a rope is attached to the spring balance (weighing scale) whereas the lower end supports the weight of suspended mass. If the power is high, so will be the heat produced due to friction between the rope and the pulley, and a cooling arrangement is therefore necessary. For this case, the V space of the pulley usually has some water falling on it as the turbine rotates and sprinkle out water which falls on any nearby surface. None the less water or any coolant can be added manually onto the V space when need be. A rope brake dynamometer is frequently used to test the power of the engines. It is easy to manufacture, inexpensive, and requires no lubrication. Figure 4.7 shows a rope brake dynamometer diagram.
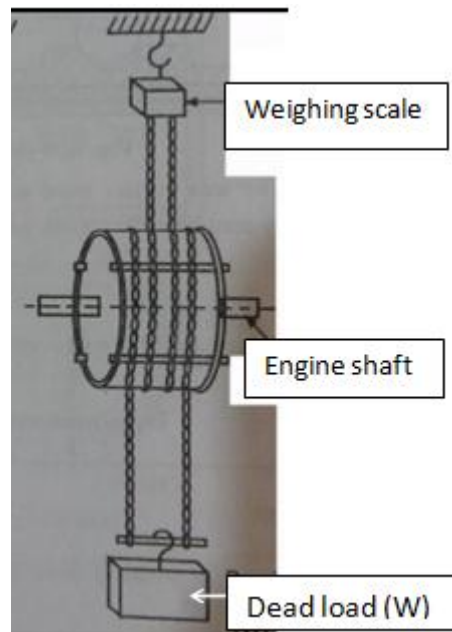
Figure 4.7: Rope Brake Dynamometer diagram

4.3.3.2 Rope Brake Dynamometer Test Rig

The rope brake dynamometer used in this research has a rope wrapped once (i.e. 360^0)

over the 'V' space of a pulley keyed to the turbine's output shaft. Figure 4.8 (a, b, c)

shows the various components that was used to set up a rope brake dynamometer.
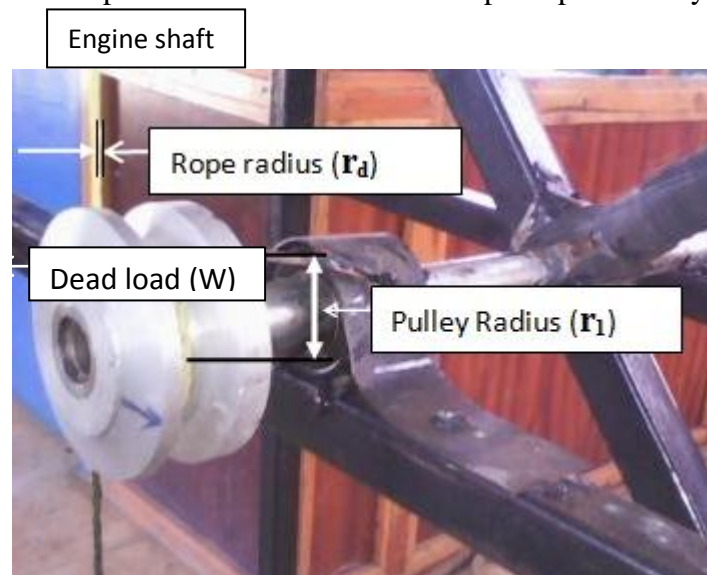
Figure 4.8 (a): A figure showing a Rope wounded once onto the 'V'

Figure 4.8 (c): Digital Weighing
Machine

**Figure 4.8 (b): Rope Brake Dynamometer test
rig**

Where;

W_0 = dead load shown in Figure 4.8 (b)

W= Weighing scale readings with the weight attached and R.p.m. is 0

S_{max}= Weighing scale readings with the weight attached and R.p.m. is maximum

$`r_p`$ = Effective radius = $(r_d + r_1)$ {*eqn* 4.6}

Where r_d = Rope radius, r_1= Pulley Radius

Also let N= r.p.m. of the engine

Therefore Braking Torque $(T_b) = (S - W) * g * r$ {*eqn* 4.7}

The power generated by the turbine $P = \omega * T = \omega[S - W]r$ {*eqn* 4.8}

With the type of digital weighing instrument used here one can directly read the value of $(W - S)$. This is achieved by resetting the weighing instrument when the weight is attached and just before the turbine start running. So that (W-S) is given as F and therefore torque will be (Garshelis, 2007);

$$T_b = F*r \qquad\qquad \{eqn\ 4.9\}$$

$$P = \omega * T = \omega[F]r \qquad\qquad \{eqn\ 4.10\}$$

Therefore the general output power is achieved by finding the product of the value measured torque and value of the measured angular speed. More explanations on how to find torque and angular speed in various conditions are discussed in appendix C.

4.4 Total power loss estimation

The estimation of total power loss between penstock and the turbine is required for accurate performance analysis and turbine efficiency estimation. The aim of the power loss test is to estimate the total power lost while converting potential energy in the water to mechanical output power in form of a rotating turbine shaft. The difference between the theoretical input power and the actual output gives the definite estimate of the total power loss. The major head losses identified here includes; penstock frictional losses, bearing frictional losses and head loss within the turbine's adjacent supply pipe. Head losses within the turbine are caused by the following; 90^0 bend at the central shaft junction, 180^0 bend at the semicircular conduit curve. These losses are discussed in detail in the following sections.

4.4.1 Head losses during the low head experiments

The delivery pipe (penstock) connecting the raised tank and the turbine has an internal diameter of $D = 0.02m$ hence a cross-sectional area $A.c = 0.00031416$ m^2. Water flow velocity within the delivery pipe is equivalent to;

$$v = \frac{Q}{A.c} = 1.16183 \frac{m}{s} \qquad \{eqn\ 4.11\}$$

The overall length of the delivery pipe is equals to $L = 4m$. The head loss due to friction is as follows;

Reynolds constant for the raised tank penstock

$$Re = \frac{4\rho * Q}{\pi D \mu} = 20383.0 \qquad \{eqn\ 4.12\}$$

For turbulent flow coefficient of friction is; $f = 0.184 * (Re)^{-0.2}$ (Incropera, 2002).

Therefore coefficient of friction is;
$$f = 0.184 * (Re)^{-0.2} = 0.0259087 \qquad \{eqn\ 4.13\}$$

Head loss in a flow duct is directly proportional to coefficient of friction, length and square of flow velocity, but inversely proportional to cross-sectional diameter and acceleration due to gravity (Cengel, 2006).

$$h_1 = f \frac{L * v^2}{D * 2g} = 0.356502\ m \qquad \{eqn\ 4.14\}$$

The average head loss due to frictional resistance within the turbine's adjacent supply pipe (h_2), given that the supply pipe overall length $L = 0.674\ m$. While internal diameter is $D = 0.0115m$. Therefore the Reynolds constant of the semicircular conduit is calculated as follows;

$$Re = \frac{4\rho * Q}{\pi D \mu} = 35{,}448.7$$

Therefore coefficient of friction is;
$$f = 0.184 * (Re)^{-0.25} = 0.0134097$$
$$h_2 = f \frac{L * V^2}{D * 2g} \approx 0.495\ m$$

The head loss (h_3) due to the 90^0 bend at the central shaft junction and the 180^0 bend at the semicircular conduit curve is calculated as follows. Given, the flow speed inside the turbine $v = 3.514\ m/s$. (h_3) is directly proportional to the bend coefficient K_L,

flow velocity V and inversely proportional to acceleration due to gravity (http://www.engineeringtoolbox.com/minor-loss-coefficients-pipes 18/02/2017).

$$h_3 = K_L \frac{V^2}{2g} = 0.12587 \ m$$

Therefore the absolute operating head;

$$(h_a) = H - (h_1 + h_2) = 1 \ m \hspace{4cm} \{eqn \ 4.15\}$$

It should be noted that 'h$_3$' is not included here since it is part of the turbine design.

Energy loss due to mechanical frictions at the central shaft bearing affects the output torque.

Having (F) to be the tangential force of the turbine the bearing frictional torque is given by the following equation (www.engineeringtoolbox.com/friction-coefficients 18/02/2017)

$$T_f = (F * \mu) * r \hspace{4cm} \{eqn \ 4.16\}$$

From the total torque expression in equation 3.7 the total tangential force can be expressed as follows;

$$F = \rho Q v_e \cos \beta$$

Given (r) is the operating radius of the bearing. The ball-bearings used in this research, has a radius of $r_b = 0.01 \ m$.

(μ) is the ball bearing coefficient of friction. Using the data given by the manufacturer $\mu = 0.0015$, (http://www.precisionrpm.com/pub/koyo/speed4, 17/2/2017).

Therefore the bearing frictional torque is given by;

$$T_f = \rho \ r_b Q v_e \cos \beta \hspace{4cm} \{eqn \ 4.17\}$$

Let T be the gross output torque

Therefore the absolute output torque (T_a) is equivalent to

$$T_a = T - T_f$$

4.4.2 Head losses during the high head experiments

In the case of the tap water the delivery pipe (penstock) connecting the high pressure water tap and the turbine has an internal diameter of $D = 20.023\ m$ hence a cross-sectional area $A.c\ = 0.000415475\ m^2$. Water flow velocity within the delivery pipe is equivalent to $v = 1.19863\ m/s$. The overall length of the delivery pipe is equals to $L = 11.5\ m$. The Reynolds's constant for the tap water penstock.

$$Re = \frac{4\rho * Q}{\pi D \mu} = 24182.81$$

Therefore coefficient of friction is;
$$f = 0.184 * (Re)^{-0.2} = 0.024441$$
$$h_1 = f \frac{L * v^2}{D * 2g} \approx 0.895\ m$$

Given $= 11.5\ m$, supply pipe overall length $L =\ 0.674\ m$, Internal diameter of $D = 0.0115\ m$, $A.c\ = 0.000103867\ m^2$ and Water flow velocity within the conduit $v = 4.00\ m/s$. The head loss due to frictional resistance within the turbine's adjacent supply pipe (h_2), is calculated as follows;

$$Re = \frac{4\rho * Q}{\pi D \mu} = 40353.244$$

Therefore coefficient of friction is;
$$f = 0.184 * (Re)^{-0.25} = 0.0145$$
$$h_2 = f \frac{L * v^2}{D * 2g} \approx 0.695m$$

The head loss (h_2) due to the 90^0 bend at the central shaft junction and the 180^0 bend at the semicircular conduit curve is calculated as follows. By varying the operating head the head loss also changes.

The flow speed inside the turbine

$$v = \left(\frac{Q}{A_c}\right) = 4.7945 \ m/s$$

$$h_3 = K_L \frac{v^2}{2g} \approx 0.234 \ m \qquad\qquad \{eqn \ 4.18\}$$

Absolute operating head

$$(h_a) = H - (h_2 + h_1) \approx 10.0 \ m \qquad\qquad \{eqn \ 4.19\}$$

Note: h_3 is not included here since it is part of the turbine design.

The procedure to find the bearing torque loss is shown in section 4.5.1 and applying equation 4.17.

4.5 Data Charts

In this section all the charts and tables used for data recording for any experiment carried out here are illustrated. Both the input and output power tests are done simultaneously. At the start of the tests, the turbine is allowed to rotate freely without any load, while the operating head is kept constant. Using the relevant equipments parameters like flow rate, rotational speed, operating torque are recorded simultaneously. Subsequently the mass load held by the rope brake dynamometer is gradually increased in steps, this leads to decrease in the rotational speed of the turbine. This decrease in rotational speed reduces the centrifugal pumping effect causing a reduction in the water flow rate. All the parameters like, flow rate, rotational speed, and operating torque are recorded for each step when load is increased. The increase in load is continued till the turbine slows down to a stop (zero rotational speed). This procedures is done for the two different operating heads in order to analyse the performance characteristics of the turbine for the low hydrostatic

head (tank water H=2m) and the medium hydrostatic head (Tap water H=11.5m). All
the generated data are recorded manually on data charts, which are later transferred to
the excel spreadsheet for further data analysis. Table 4.2 shows the arrangement of the
tests data charts used to record both the input and output power test data.

The arm radius used are as follows R=1.0m, 0.5m, 0.25m

Regarding the nozzle diameter (11.5 mm, 8.8 mm, 6.0 mm, 3.8 mm, and 2.5 mm), the
nozzle ratio (*n*) was found as follows;

$$\frac{11.5^2}{11.5^2} = 1, \qquad \frac{8.8^2}{11.5^2} = 0.586, \qquad \frac{6.0^2}{11.5^2} = 0.272, \qquad \frac{3.8^2}{11.5^2} = 0.109,$$

$$\frac{2.5^2}{11.5^2} = 0.047$$

Table 4.2: Arrangement of Power test data sheet

	Input Power $((\rho ghQ)$, **h=2m**		Output Power $(P= \omega * T)$	
Dead Load, placed on the rope brake dynamometer (Kg)	Time required for 0.01m³ of water to flow through the turbine (sec)	Q=V/T	Optimum Torque (*T*)	Optimum Angular Speed (*ω*)

The test was repeated for all the arm radius sizes and all the nozzle diameter sizes.

CHAPTER FIVE

DATA COLLECTION, ANALYSIS AND RESULTS

5.1 Introduction

The main aim of this chapter is to present the experimental results. The data presented are obtained from the results of various experiments done on the single arm centrifugal reaction water turbine. Experimental data are first presented in tables then converted to graphs for further discussion. The variables in these experiments are; $H = 1.85$m and 11.5m, $R = 1$m, 0.5m and 11.5m, $(1/n) = 1$, 0.5856, 0.2722, 0.1092 and 0.0473. The performance characteristics are discussed during the input power test, torque test, and the output power test.

5.2 Data Presentation and Analysis When Using The Low Head Of 1.85m

The actual operating height after subtracting all the major head losses is arrived at using the calculations in section 4.5.1, equation 4.15;

Absolute operating head $(\boldsymbol{h_a}) = H - (h_1 + h_2)$

$\boldsymbol{h_a} = 0.998998 \approx 1.0m$

5.2.1 Low head performance characteristics for nozzle diameter of 11.5mm

Here the main pipe to nozzle cross-section area ratio is $n = 1$. This means that the exit speed has not been accelerated. Therefore the nozzle to main pipe cross-section area ratio is the inverse of n, which is equals to $1/n = 1$. Moreover optimum Torque (T) is;

$T = [S - W] * g * r$ (From the equation of torque, equation 4.7)

Table 5.1 shows a data sheet table used to record input and output data for performance characteristics analysis, by varying the arm radius in the sequence of;

1m, 0.5m, 0.25m and keeping the nozzle to main pipe cross-sectional area ratio constant at 1.

Figure 5.1 (a) shows variation of efficiency with rotational speed for three different arm radiuses at constant nozzle to main pipe cross-sectional area ratio of 1.

Table 5.1: Low head experimental results using nozzle diameter of 11.5mm

Weighing scale readings (Kg)	Torque (Nm)	Angular speed		Power P_{out} (W)	Time required for 0.01m³ of water to flow (s)	Volume of flow (m²/s)	Power P_{in} (W)	Efficiency P_{out}/P_{in} (-)
		rpm	rad/s					
R=1.0 m								
0.980	0.21631	0	0	0	40	0.00025	2.4525	0
0.970	0.21410	3	0.3142	0.067263	40	0.00025	2.4525	0.02743
0.930	0.20527	5	0.5236	0.107481	40	0.00025	2.4525	0.04383
0.900	0.19865	8	0.8378	0.166423	40	0.00025	2.4525	0.06786
0.780	0.17216	11	1.1519	0.19832	40	0.00025	2.4525	0.08086
0.550	0.12139	14	1.4661	0.17798	40	0.00025	2.4525	0.07257
0.320	0.07063	17	1.7802	0.125742	40	0.00025	2.4525	0.05127
0.260	0.05738	18	1.885	0.108175	40	0.00025	2.4525	0.04411
0.130	0.02869	20	2.0944	0.060097	40	0.00025	2.4525	0.0245
0.000	0	22	2.3038	0	40	0.00025	2.4525	0
R= 0.5 m								
0.505	0.11102	0	0	0	40	0.00025	2.4525	0
0.470	0.10418	5	0.5236	0.05455	40	0.00025	2.4525	0.0222
0.445	0.09778	10	1.0472	0.102396	40	0.00025	2.4525	0.0418
0.425	0.09358	14	1.4661	0.137206	40	0.00025	2.4525	0.0559
0.370	0.08166	19	1.9897	0.162493	40	0.00025	2.4525	0.0663
0.280	0.06180	24.5	2.5656	0.158564	40	0.00025	2.4525	0.0647
0.210	0.04591	29	3.0369	0.139425	40	0.00025	2.4525	0.0569
0.120	0.02604	34.7	3.6338	0.094644	38.40	0.00026	2.5544	0.0371
0.050	0.01147	39	4.0841	0.046876	36.93	0.00027	2.6563	0.0176
0.000	0	42.1	4.4087	0	35.57	0.00028	2.7582	0
R= 0.25 m								
0.250	0.0554	0	0	0.0000	40	0.00025	2.4525	0.0000
0.235	0.0523	7.5	0.7854	0.0411	40	0.00025	2.4525	0.0168
0.220	0.0490	15	1.5708	0.0771	40	0.00025	2.4525	0.0315
0.215	0.0470	21	2.1991	0.1034	40	0.00025	2.4525	0.0422
0.185	0.0408	28.5	2.9845	0.1219	40	0.00025	2.4525	0.0497
0.145	0.0318	36.75	3.8485	0.1223	38.40	0.00026	2.5544	0.0479
0.105	0.0232	43.5	4.5553	0.1056	36.93	0.00027	2.6563	0.0397
0.060	0.0132	52.05	5.4507	0.0722	35.57	0.00028	2.7582	0.0262
0.025	0.0060	58.5	6.1261	0.0365	34.30	0.00029	2.8601	0.0128
0.000	0.0000	63.15	6.6131	0.0000	33.12	0.00030	2.9620	0.0000

Figure 5.1 (a): Graph of efficiency against angular speed (in rpm)
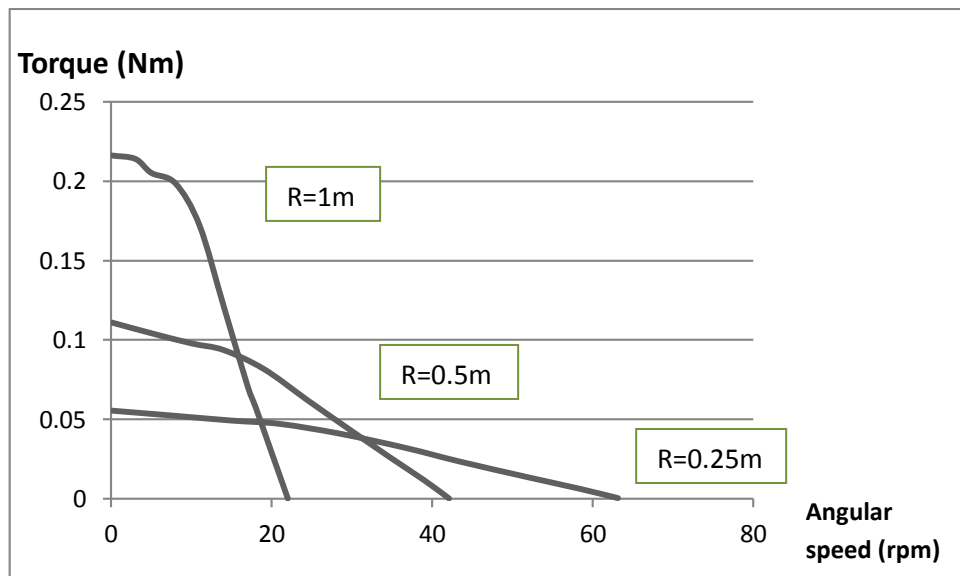
Figure 5.1 (b): Graph of torque against angular speed (in rpm)

As seen in the graph in figure 5.1 (a) optimum efficiency of the turbine reduces with decrease in the arm radius. Reduction in arm radius leads to reduction in the operating torque. Low operating torque accounts for low turbine efficiency. However with the decrease in the arm radius it means that there is a reduction in frictional head losses. Figure 5.1 (b) shows a graph of torque against rpm for each of the three different arm radiuses. This experiment where $'1/n = 1'$ produces the highest volume flow rate at zero angular speed as compared to all the other raised tank experiments. Furthermore

the flow rate in all the three arm radiuses appears to be constant at the beginning and starts increasing gradually, which is not the case with other nozzles. For these experiments the maximum working volume flow rate is low because the maximum angular speed is low. This scenario is in accordance with the explanations given by Calvert (2003) about the effects of low angular velocity on a lawn sprinkler.

5.2.2 Low head performance characteristics for nozzle diameter of 8.8 mm

Here the main pipe to nozzle cross-section area ratio is $n = 1.7078$. Therefore the inverse of n is equals to $1/n = 0.58556$. Table 5.2 shows the performance characteristics by varying the arm radius and keeping the nozzle to main pipe cross-section area ratio constant at 1.7078. Figure 5.2 (a) and (b) are graphs showing the efficiency and torque trends.

Table 5.2: Low head experimental results using nozzle diameter of 8.8 mm

Weighing scale readings (Kg)	Torque (Nm)	Angular speed		Power P_{out} (W)	Time required for 0.01m³ of water to flow (s)	Volume of flow (m²/s)	Power P_{in} (W)	Efficiency P_{out}/P_{in} (-)
		Output power			Input power			
		rpm	rad/s					
R=1.0 m								
1.050	0.2319	0	0.0000	0	50	0.00020	1.9620	0
0.970	0.2141	15	1.5708	0.3363	44.18	0.00023	2.2205	0.1515
0.950	0.2096	37	3.8746	0.8124	32.99	0.00030	2.9738	0.2732
0.920	0.2030	50	5.2360	1.0632	26.65	0.00038	3.6804	0.2889
0.870	0.1915	63	6.5973	1.2639	22.36	0.00045	4.3871	0.2881
0.750	0.1651	72	7.5398	1.2448	20.12	0.00050	4.8763	0.2552
0.555	0.1223	83	8.6917	1.0628	17.92	0.00056	5.4743	0.1942
0.365	0.0801	92	9.6342	0.7719	16.45	0.00061	5.9635	0.1294
0.190	0.0419	98	10.2625	0.4304	15.6	0.00064	6.2896	0.0684
0.000	0	104	10.8909	0	14.83	0.00067	6.6158	0
R= 0.5 m								
0.715	0.1573	0	0.0000	0	50	0.00020	1.9620	0
0.670	0.1481	17	1.7802	0.2637	42.27	0.00024	2.3210	0.11361
0.650	0.1435	35	3.6652	0.5258	34.24	0.00029	2.8651	0.1835
0.630	0.1391	51	5.3407	0.7427	26.27	0.00038	3.7348	0.1988
0.600	0.1324	64	6.7021	0.8876	22.09	0.00045	4.4415	0.1998
0.565	0.1247	77	8.0634	1.0056	19.06	0.00052	5.1481	0.1953
0.480	0.1059	88	9.2153	0.9763	16.82	0.00059	5.8331	0.1674
0.360	0.0795	97	10.1578	0.8072	15.49	0.00065	6.3336	0.1274
0.195	0.0430	108	11.3097	0.4868	14.12	0.00071	6.9452	0.0701
0.000	0	118	12.3569	0	13.08	0.00076	7.5013	0
R= 0.25 m								
0.715	0.1573	0	0.0000	0	50	0.00020	1.9620	0
0.670	0.1481	13	1.3614	0.16437	45.77	0.00017	2.1433	0.0767
0.650	0.1435	28	2.9322	0.33978	39.48	0.00025	2.4845	0.1835
0.630	0.1391	40	4.1888	0.46459	31.27	0.00032	3.1369	0.1988
0.600	0.1324	52	5.4454	0.58595	25.89	0.00039	3.7892	0.1998
0.565	0.1247	71	7.4351	0.77461	20.34	0.00049	4.8219	0.1953
0.480	0.1059	87	9.1106	0.90090	16.98	0.00059	5.7775	0.1674
0.360	0.0795	102	10.6814	0.79571	14.84	0.00067	6.6116	0.1274
0.195	0.0430	115	12.0428	0.53827	13.38	0.00075	7.3345	0.0701
0.000	0	127	13.2994	0	12.26	0.00082	8.0018	0
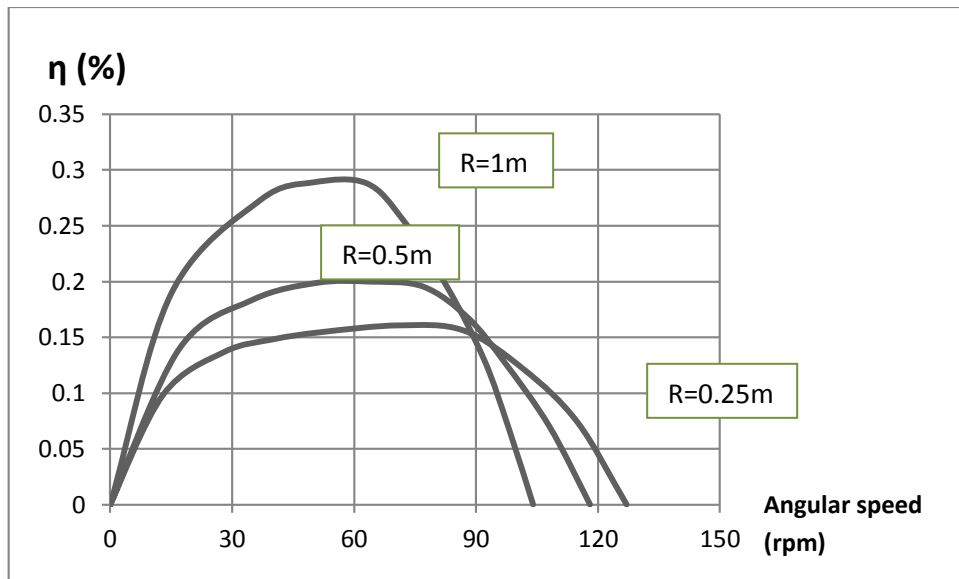
Figure 5.2(a): Graph of efficiency against angular speed (in rpm)
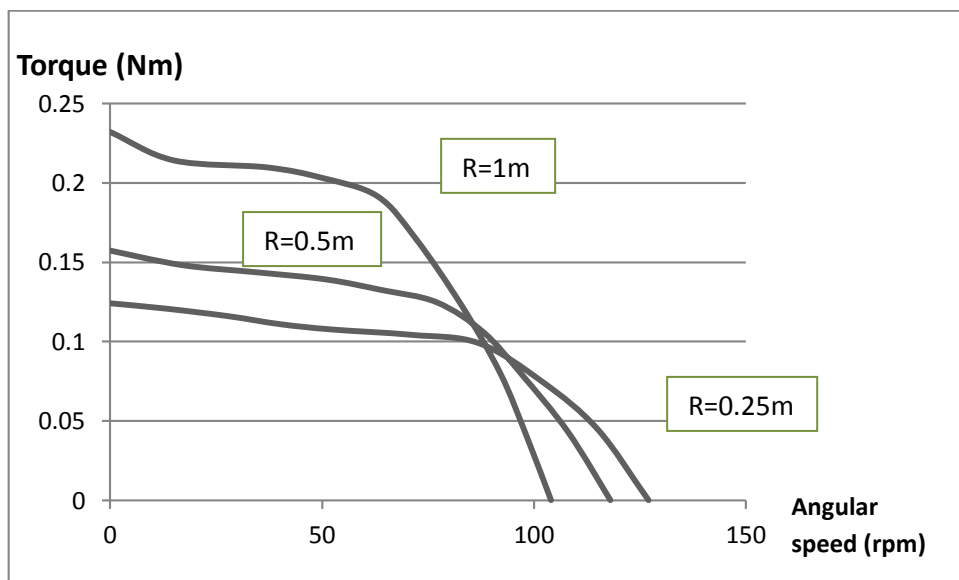
Figure 5.2 (b): Graph of torque against angular speed (in rpm)

The highest efficiency achieved in this experiment is 29%. This type of nozzle produces relatively second highest torque after that produced by the 6.0mm nozzle. Even so it operates with low angular speed which is as result of relatively low flow velocity (i.e. $\omega = V/R$). Moreover the nozzle allows for high volume flow rates this gives high power input. All this features accounts for the low efficiencies when using an 8.8mm nozzle in this experiment. Also as seen from the table the flow rate

increases with increase in angular velocity as explained by A. Akbarzadeh. Mass flow rate $\dot{m} = \rho Q = \rho.A.V_r = \rho.A.\sqrt{2gH + \omega^2 R^2}$, (Akbarzadeh, 2001).

5.2.3 Low head performance characteristics for nozzle diameter of 6.0 mm

Here the main pipe to nozzle cross-section area ratio is $n = 3.674$. Therefore the inverse of n is equals to $1/n = 0.27221$. Table 5.3 shows the performance characteristics by varying the arm radius and keeping the nozzle to main pipe cross-section area ratio constant at 0.27221.

Table 5.3: Low head experimental results using nozzle diameter of 6.0 mm

Output power				Input power			Efficiency
Weighing scale readings (Kg)	Torque (Nm)	Angular speed		Power P_{out} (W)	Time required for 0.01m³ of water to flow (s)	Volume of flow (m²/s)	Power P_{in} (W)	P_{out}/P_{in} (-)
		rpm	rad/s					
R=1.0 m								
1.400	0.30902	0	0	0	64.1	0.000156	1.5304	0.0000
1.315	0.29044	30	3.1416	0.7541	54.96	0.000182	1.7037	0.4426
1.300	0.28689	55	5.7596	1.6524	44.76	0.000223	2.1917	0.7539
1.205	0.26543	77	8.0634	2.1403	38.04	0.000263	2.5786	0.8282
1.190	0.26302	95	9.9484	2.6166	29.84	0.000335	3.2874	0.7959
1.025	0.22662	108	11.3100	2.5630	27.47	0.000364	3.5706	0.7178
0.765	0.16895	124	12.9852	2.1939	25.03	0.000400	3.9192	0.5598
0.485	0.10686	138	14.4513	1.5442	23.22	0.000431	4.2243	0.3656
0.255	0.05585	148	15.4985	0.8656	22.08	0.000453	4.4420	0.1949
0.000	≈ 0	157	16.4410	0	21.15	0.000473	4.6381	0.0000
R= 0.5 m								
0.950	0.20969	0	0	0.00000	64.1	0.000156	1.53036	0.00000
0.920	0.20307	26	2.7227	0.55289	52.78	0.000189	1.85879	0.29745
0.900	0.19865	53	5.5501	1.10255	43.4	0.00023	2.26021	0.48781
0.870	0.19203	76	7.9587	1.52832	38.45	0.00026	2.55117	0.59906
0.850	0.18762	96	10.053	1.88612	33.22	0.000301	2.95346	0.63862
0.800	0.17658	116	12.147	2.14500	27.96	0.000358	3.50870	0.61134
0.680	0.15009	132	13.823	2.07474	24.58	0.000407	3.99095	0.51986
0.480	0.10595	148	15.499	1.64204	22.28	0.000449	4.40321	0.37292
0.260	0.05739	162	16.966	0.97357	20.67	0.000484	4.74702	0.20509
0.000	0	176	18.431	0.00000	19.06	0.000525	5.14592	0.00000
R= 0.25 m								
0.750	0.16554	0	0	0	64.1	0.000156	1.53036	0
0.730	0.16113	20	2.0944	0.33746	58.06	0.000172	1.68974	0.1997
0.700	0.15451	45	4.7124	0.72809	46.51	0.000215	2.10917	0.3452
0.670	0.14789	55	5.7596	0.85176	44.52	0.000225	2.20349	0.3865
0.650	0.14347	78	8.1681	1.17189	37.16	0.000269	2.63976	0.4439
0.630	0.13906	107	11.205	1.55813	29.43	0.00034	3.33356	0.4674
0.600	0.13244	130	13.614	1.80291	24.84	0.000403	3.94913	0.4565
0.450	0.09933	153	16.022	1.59141	21.75	0.00046	4.51068	0.3528
0.270	0.05960	172	18.012	1.07342	19.4	0.000515	5.05645	0.2123
0.000	0	191	20.001	0	17.57	0.000569	5.58402	0

As seen from figure 5.3 (a), efficiency rises from zero to a maximum value then it starts falling to zero as angular speed rises from zero to a particular maximum. Also maximum efficiency for each individual arm radius tends to shift from left to right as the arm radius decreases. In all the experiments done in this research, this particular experiment (i.e. using 6.0mm nozzle and a arm radius of 1m) produced the highest efficiency of $\approx 83\%$.

On the other hand figure 5.3 (b) shows torque against angular speed for each individual arm radius all in one graph.

Figure 5.3 (c) shows a graph of efficiency against specific speed. Specific speeds are commonly used as a tool for comparison of the characteristics of similar hydraulic machines. In this case specific speed for this centrifugal reaction water turbine is calculated using the formulation provided by Turton (Turton, 1995) for the specific speed of turbines;
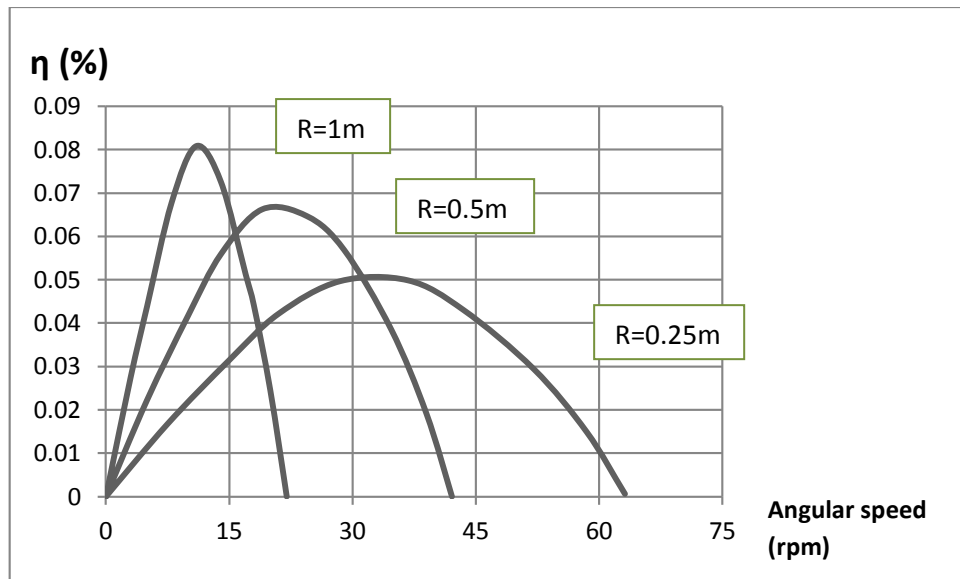
$$K_2 = \frac{\omega\sqrt{Q}}{(gH)^{3/4}} \qquad \{eqn\ 5.1\}$$

Figure 5.3(a): Graph of efficiency against angular speed (in rpm).
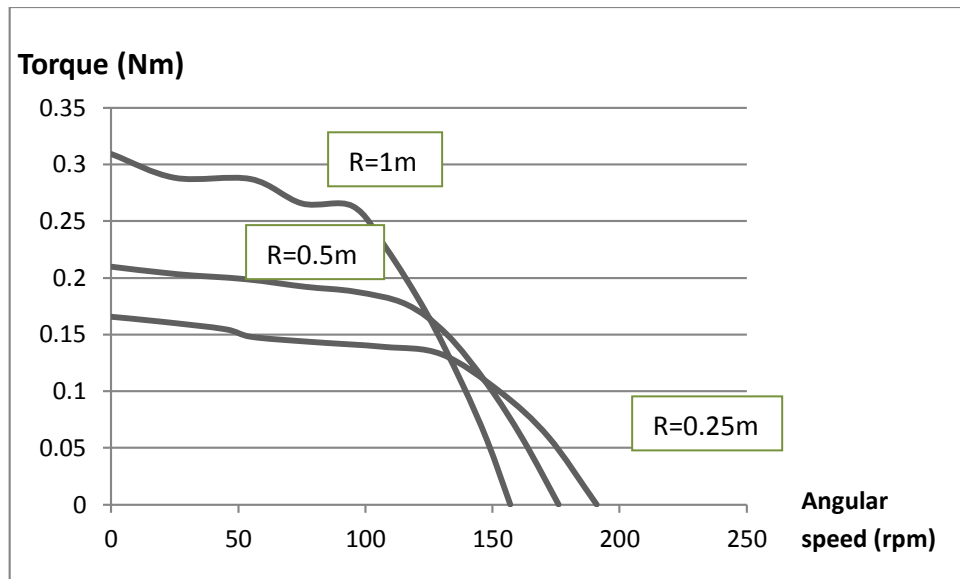
Figure 5.3 (b): Graph of torque against angular speed (in rpm)
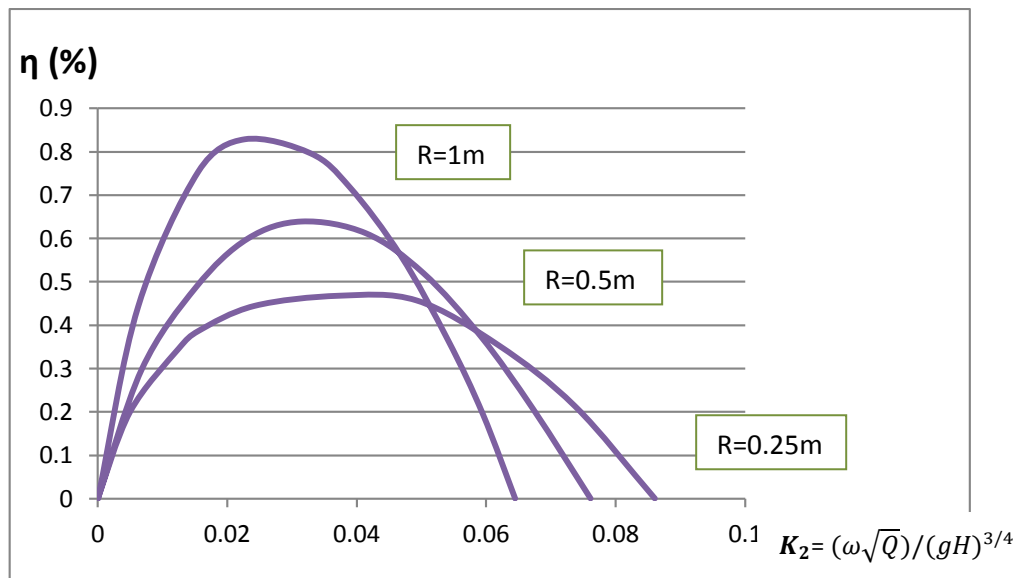
Figure 5.3 (c): Graph of efficiency against specific speed (in rpm)

Here also there is an increase in flow rate in relation to increase in angular speed as seen in table 5.3.

5.2.4 Low head performance characteristics for nozzle diameter of 3.8 mm

Here the main pipe to nozzle cross-section area ratio is $n = 9.159$. Therefore the inverse of n is equals to $1/n = 0.109187$. Table 5.4 shows the performance characteristics by varying the arm radius and keeping the main pipe to nozzle cross-

section area ratio constant at 9.159. Figure 5.4 (a) and (b) are graphs showing the course of efficiency and torque against rpm.

Table 5.4: Low head experimental results using nozzle diameter of 3.8 mm

Output power				Input power			Efficiency
Weighing scale readings (Kg)	Torque (Nm)	Angular speed		Power P_{out} (W)	Time required for $0.01m^3$ of water to flow (s)	Volume of flow (m^2/s)	Power P_{in} (W)	P_{out}/P_{in} (-)
		rpm	rad/s					
R=1.0 m								
0.600	0.13243	0	0.0000	0	147.9	0.0000676	0.663156	0
0.570	0.12581	18	1.8850	0.23715	135.6	7.374E-05	0.72337	0.3278
0.560	0.12360	37	3.8746	0.47893	115.2	8.683E-05	0.851761	0.5623
0.530	0.11698	54	5.6549	0.66153	101.5	9.854E-05	0.966638	0.6844
0.520	0.11477	67	7.0162	0.80530	93.03	0.0001075	1.054485	0.7637
0.460	0.10153	78	8.1681	0.82934	86.91	0.0001151	1.128817	0.7347
0.365	0.08056	89	9.3201	0.75087	81.54	0.0001226	1.203148	0.6241
0.250	0.05518	100	10.4720	0.57786	76.79	0.0001302	1.27748	0.4523
0.130	0.02869	108	11.3097	0.32452	73.67	0.0001357	1.33154	0.2437
0.000	0	114	11.9380	0	71.5	0.0001399	1.372085	0
R= 0.5 m								
0.475	0.10429	0	0.0000	0.00000	147.9	0.0000676	0.66316	0.00000
0.440	0.09684	22	2.3038	0.22311	126	7.936E-05	0.77855	0.28657
0.420	0.09213	46	4.8171	0.44378	98.79	0.0001012	0.99302	0.44690
0.400	0.08815	67	7.0162	0.61849	83.09	0.0001204	1.18068	0.52385
0.385	0.08468	84	8.7965	0.74485	73.62	0.0001358	1.33259	0.55895
0.360	0.07971	102	10.6814	0.85141	65.69	0.0001522	1.49344	0.57010
0.315	0.06953	115	12.0428	0.83731	60.95	0.0001641	1.60961	0.52020
0.235	0.05165	129	13.5088	0.69773	56.55	0.0001768	1.73472	0.40221
0.130	0.02905	142	14.8702	0.43202	56.15	0.0001781	1.74713	0.24728
0.000	0.00000	154	16.1268	0.00000	53.17	0.0001881	1.84499	0.00000
R= 0.25 m								
0.300	0.06622	0	0.0000	0.00000	147.9	0.0000676	0.66316	0.00000
0.290	0.06445	18	1.8850	0.12149	143.6	6.963E-05	0.68311	0.17785
0.280	0.06180	39	4.0841	0.25241	122.5	8.161E-05	0.80057	0.31528
0.270	0.05915	48	5.0265	0.29734	117.2	8.536E-05	0.83736	0.35510
0.260	0.05739	68	7.1209	0.40866	99.2	0.0001008	0.98893	0.41323
0.250	0.05562	97	10.1578	0.56501	77.91	0.0001283	1.25907	0.44875
0.240	0.05297	113	11.8333	0.62686	68.06	0.0001469	1.44143	0.43489
0.180	0.03973	134	14.0324	0.55752	59.62	0.0001677	1.64548	0.33882
0.110	0.02384	151	15.8127	0.37695	53.32	0.0001875	1.83981	0.20488
0.000	0.00000	167	17.4882	0.00000	48.59	0.0002058	2.01892	0.00000

η (%)
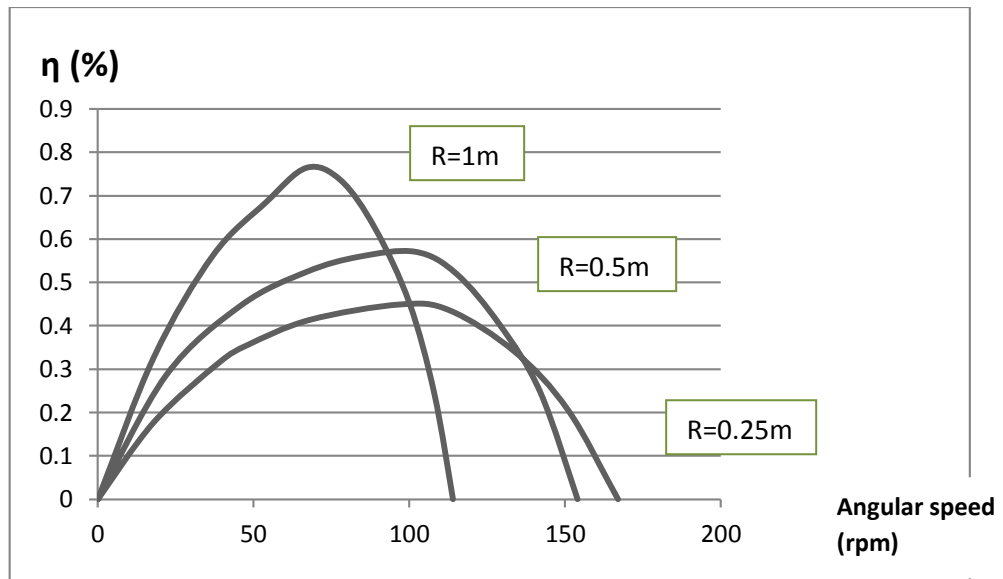
Figure 5.4 (a): Graph of efficiency against angular speed (rpm)
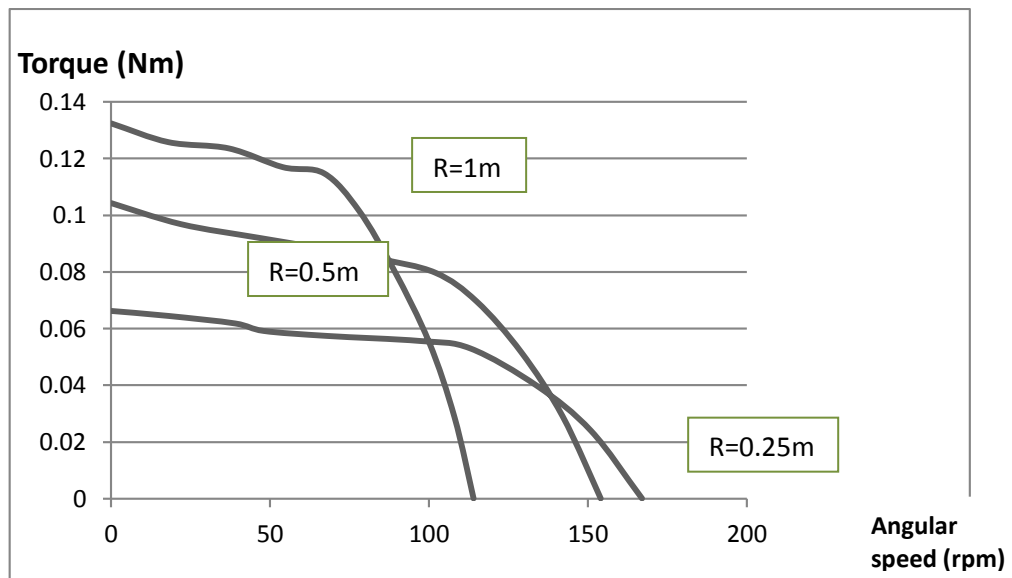
Torque (Nm)

Figure 5.4 (b): Graph of torque against angular speed (in rpm)

In this experiment using a nozzle of diameter (d=3.8mm) and arm radius of 1m, the highest efficiency achieved is 76.4%. Nevertheless, with high efficiency the power produced is relatively low compared to using a nozzle of (d=6.0mm). Moreover as the arm radius decreases the efficiency also decreases. Also as seen in table 5.2.4 the flow rate increase with increase in angular speed.

5.2.5 Low head performance characteristics for nozzle diameter of 2.5 mm

Here the main pipe to nozzle cross-section area ratio is $n = 21.16$. Therefore the inverse of n is equals to $1/n = 0.04726$. Table 5.5 shows the performance characteristics by varying the arm radius while keeping the main pipe to nozzle cross-section area ratio at 21.16. Figure 5.5 (a) and (b) are graphs showing the efficiency and torque drift respectively.

Table 5.5: Low head experimental results using nozzle diameter of 2.5 mm

Output power				Input power			Efficiency
Weighing scale readings (Kg)	Torque (Nm)	Angular speed		Power P_{out} (W)	Time required for 0.01m³ of water to flow (s)	Volume of flow (m²/s)	Power P_{in} (W)	P_{out}/P_{in} (-)
		rpm	rad/s					
R=1.0 m								
0.225	0.04966	0	0.0000	0.00000	235.3	0.0000425	0.41693	0.00000
0.200	0.04415	6	0.6283	0.02774	245.6	4.072E-05	0.39950	0.06943
0.185	0.04120	12	1.2566	0.05321	239.8	4.17E-05	0.40908	0.13008
0.175	0.03907	18	1.8850	0.07364	234.9	4.257E-05	0.41765	0.17632
0.170	0.03708	22	2.3038	0.08672	231.3	4.324E-05	0.42421	0.20444
0.150	0.03311	26	2.7227	0.09015	228.3	4.381E-05	0.42975	0.20976
0.120	0.02693	29	3.0369	0.08366	225.4	4.437E-05	0.43530	0.19219
0.085	0.01832	33	3.4558	0.06395	222.5	4.494E-05	0.44085	0.14506
0.045	0.00949	36	3.7699	0.03578	220.5	4.535E-05	0.44488	0.08043
0.000	0.00000	38	3.9793	0.00000	219	4.566E-05	0.44791	0.00000
R= 0.5 m								
0.160	0.03487	0	0.0000	0.00000	235.3	0.0000425	0.41693	0.00000
0.145	0.03223	7	0.7330	0.02362	244.6	4.088E-05	0.40101	0.05891
0.140	0.03046	15	1.5708	0.04785	237.5	4.211E-05	0.41311	0.11582
0.130	0.02891	24	2.5133	0.07267	225.6	4.432E-05	0.43482	0.16713
0.120	0.02693	30	3.1416	0.08460	221.9	4.506E-05	0.44207	0.19137
0.110	0.02428	34	3.5605	0.08645	217.9	4.589E-05	0.45013	0.19205
0.090	0.01987	38	3.9793	0.07905	214.1	4.671E-05	0.45820	0.17252
0.060	0.01324	43	4.5029	0.05963	209.5	4.774E-05	0.46829	0.12735
0.035	0.00728	47	4.9218	0.03585	205.9	4.856E-05	0.47636	0.07526
0.000	0.00000	51	5.3407	0.00000	202.3	4.944E-05	0.48503	0.00000
R= 0.25 m								
0.105	0.02207	0	0.0000	0.00000	235.3	0.0000425	0.41693	0.00000
0.100	0.02148	6	0.6283	0.01350	259.6	3.852E-05	0.37786	0.03572
0.095	0.02060	13	1.3614	0.02805	244.3	4.093E-05	0.40151	0.06985
0.090	0.01987	16	1.6755	0.03328	238.8	4.188E-05	0.41085	0.08101
0.085	0.01920	22	2.3038	0.04558	224.6	4.452E-05	0.43673	0.10437
0.085	0.01854	32	3.3510	0.06278	206.8	4.835E-05	0.47427	0.13237
0.080	0.01700	38	3.9793	0.06704	202.3	4.942E-05	0.48485	0.13827
0.060	0.01280	45	4.7124	0.05988	192.9	5.184E-05	0.50850	0.11776
0.035	0.00795	50	5.2360	0.04188	185.9	5.379E-05	0.52765	0.07938
0.000	0.00000	56	5.8643	0.00000	179.8	5.562E-05	0.54567	0.00000

η (%)
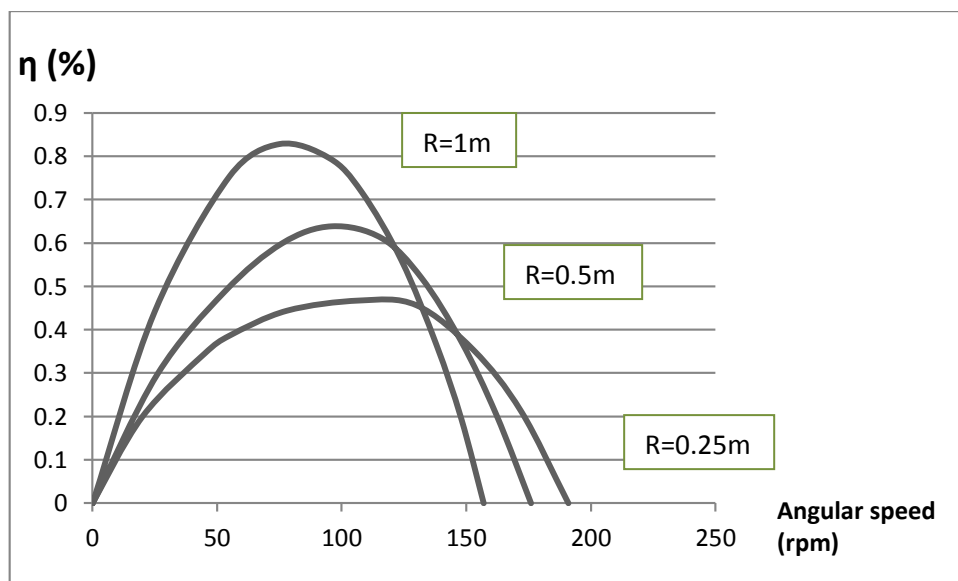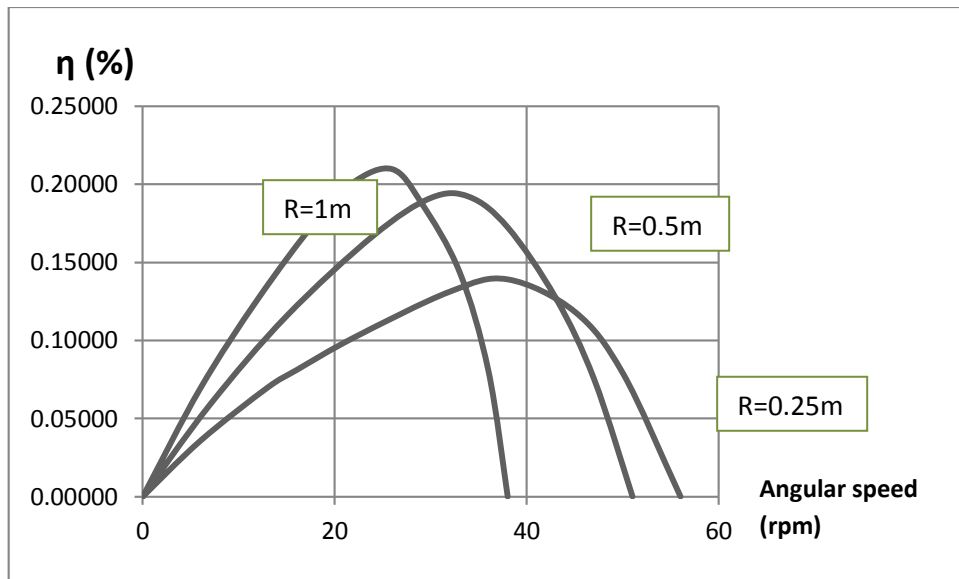
Figure 5.5 (a): Graph of efficiency against angular speed (in rpm)
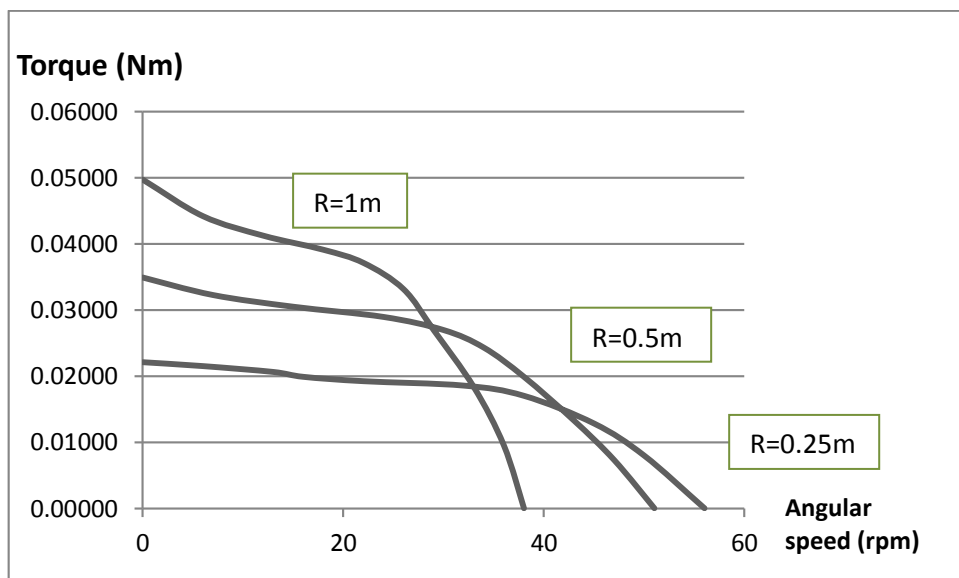
Figure 5.5 (b): Graph of torque against angular speed (in rpm)

The highest efficiency achieved with this type of nozzle used in this section (i.e. d =2.5mm) is approximately equals to 21%. The reasons for this relatively low efficiency are things to do with high resistance at the nozzle area. The other reason is that the ratio of the resistive bearing frictional torque to the driving torque is high. This mean there is relatively low resultant torque. Resultant absolute torque T_a = driving torque (T_d) – Bearing frictional torque (T_d).

Moreover, there is an increase in the flow rate owing to the increase in angular speed. This increase in flow rate is smaller relative to the low operating angular speeds.

5.2.6 Nozzle and arm length performance characteristics for low head of 1.85m

To find the optimum 'main pipe to nozzle cross-sectional area ratio' as well as the optimum arm length, which will produce the highest efficiency; a graph of efficiency against 'nozzle to main pipe nozzle cross-sectional area ratio' for each of the three arm radius is drawn. The graph picks the highest efficiency for each of the five nozzles used in the raised tank experiments. The procedure is replicated for each of the three arm lengths.

Table 5.6: Data table for optimum efficiencies against (1/n) operating under low head.

(1/n)	Efficiency (%)
Arm radius **R = 1m**	
1	0.081
0.585558	0.289
0.272212	0.828
0.109187	0.764
0.047259	0.210
0	0.000
Arm radius **R = 0.5m**	
1	0.066
0.585558	0.200
0.272212	0.611
0.109187	0.570
0.047259	0.192
0	0.000
Arm radius **R = 0.25m**	
1	0.050
0.585558	0.161
0.272212	0.467
0.109187	0.449
0.047259	0.139
0	0.00000
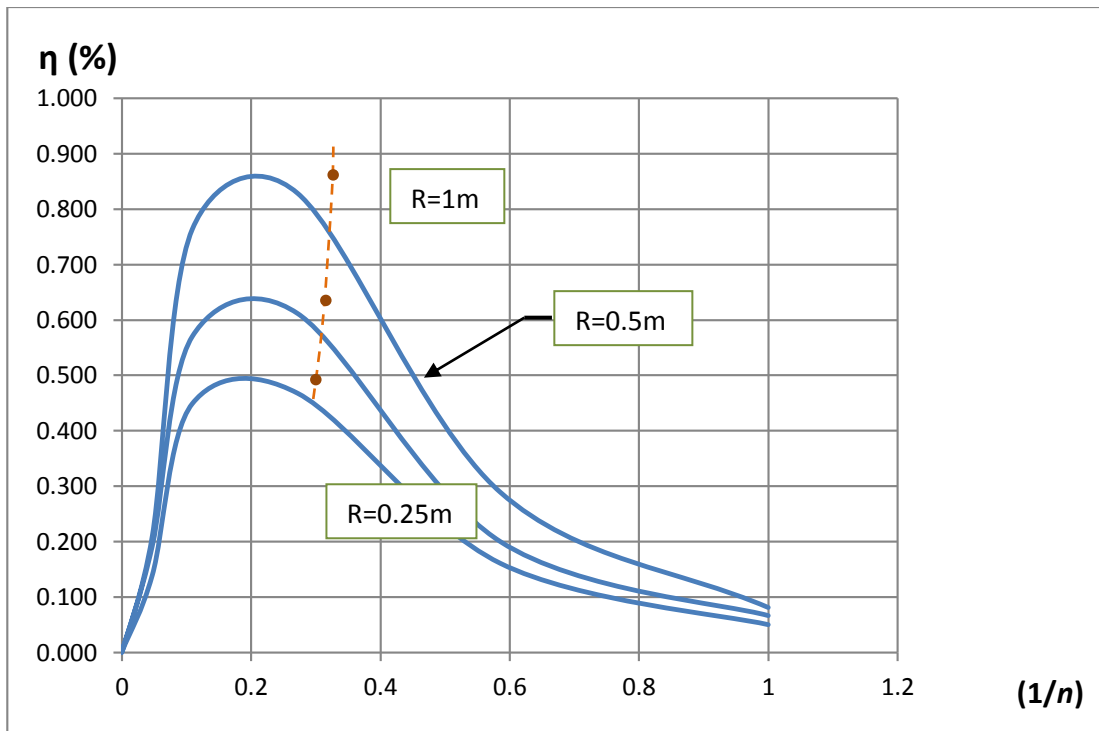
Figure 5.6: Graph of optimum efficiencies against (1/n) operating under low head

At optimum 'nozzle to main pipe cross-sectional area ratio' the highest efficiency for a particular set-up is achieved. This means that not all nozzles give the same torque given relatively equal potential energy. The data given in table 5.6 has taken into account the all the head losses due to any resistance at the nozzle.

The optimum 'nozzle to main pipe cross-sectional area ratio' as seen in the graph is approximately; $(1/n) = 0.22$ for arm radius $R = 1$m. In the case of arm radius $R = 0.5$m, optimum 'nozzle to main pipe cross-sectional area ratio' occurs at $(1/n) = 0.2$. Whereas in the case of arm radius $R = 0.25$m, optimum 'nozzle to main pipe cross-sectional area ratio' occurs at $(1/n) = 0.18$.

5.2.7 Coefficient of Discharge (C_d)

Using the most efficient nozzle, whose cross-sectional diameter is 0.006m, the coefficient of discharge (C_d) is calculated as follows:

Nozzle cross-sectional area $A_N = 0.0000282743 \text{ m}^2$

Water exit velocity

$$V_e = \frac{Q}{A_N} = 9.3017\text{m/s}$$

Therefore the coefficient of discharge

$$C_d = \frac{V_a}{\sqrt{2gH}} = 1.544$$

Notice that the coefficient of discharge C_d in relation to height only, is greater than one which is not usually the case with the conventional turbines. This is because of the centrifugal pumping effect of the radial conduit as it rotates (Akbarzadeh, 2001) and (Date, 2009). This effect adds more pressure to the water as they travel radialy through the arm conduit.

5.3 Data presentation and analysis while operating under high head of 11.5m

Keeping H at 11.5m, all the experiments in section 5.2 are repeated. Using the calculations in section 4.5.2 and equation 4.19. The actual operating height after subtracting all the major head losses is as follows.

Absolute operating head (h_a) = $H - (h_1 + h_2)$
$h_a \approx 10.0m$

5.3.1 High head performance characteristics for nozzle diameter of 11.5mm

Here the main pipe to nozzle cross-section area ratio is $n = 1$. This means that the exit speed has not been accelerated. Therefore the inverse of n is equals to $1/n = 1$. While specific Optimum Torque (*T*) is equals to;

$$T = [S - W] * g * r$$

Table 5.7 shows the performance characteristics by varying the arm radius and keeping the main pipe to nozzle cross-section area ratio constant at 1. Figure 5.7 (a) and (b) are graphs that shows the efficiency trends and torque trends respectively.

Table 5.7: High head experimental results using nozzle diameter of 11.5mm

| Output power				Input power			Efficiency
Weighing scale readings (Kg)	Torque (Nm)	Angular speed		Power P_{out} (W)	Time required for 0.01m³ of water to flow (s)	Volume of flow (m²/s)	Power P_{in} (W)	P_{out}/P_{in} (-)
		rpm	rad/s					
R=1.0 m								
3.920	0.86524	0	0.0000	0.00000	29.41	0.00034	33.354	0.0000
3.880	0.85641	4	0.4320	0.36994	29.41	0.00034	33.354	0.0111
3.720	0.82110	7	0.7199	0.59115	29.41	0.00034	33.354	0.0177
3.600	0.79461	11	1.1519	0.91533	29.41	0.00034	33.354	0.0274
3.200	0.70632	15	1.5839	1.11873	29.41	0.00034	33.354	0.0335
2.200	0.48560	19	2.0159	0.97889	29.41	0.00034	33.354	0.0293
1.280	0.28253	23	2.4478	0.69158	29.41	0.00034	33.354	0.0207
1.040	0.22955	25	2.5918	0.59496	29.41	0.00034	33.354	0.0178
0.520	0.11478	28	2.8798	0.33053	29.41	0.00034	33.354	0.0099
0.000	0.00000	30	3.1678	0.00000	28.54	0.00035	34.373	0.0000
R= 0.5 m								
2.010	0.44410	0	0.0000	0.00000	29.41	0.00034	33.354	0.0000
1.890	0.41673	7	0.7199	0.30002	29.41	0.00034	33.354	0.0090
1.770	0.39112	14	1.4399	0.56318	29.41	0.00034	33.354	0.0169
1.695	0.37435	19	2.0159	0.75463	29.41	0.00034	33.354	0.0226
1.480	0.32667	26	2.7358	0.89371	29.41	0.00034	33.354	0.0268
1.120	0.87210	34	3.5277	0.87210	28.54	0.00035	33.354	0.0254
0.830	0.76684	40	4.1757	0.76684	27.72	0.00036	33.354	0.0217
0.470	0.52054	48	4.9964	0.52054	26.94	0.00037	33.354	0.0143
0.210	0.25782	54	5.6156	0.25782	26.21	0.00038	33.354	0.0069
0.000	0.00000	58	6.0620	0.00000	25.51	0.00039	33.354	0.0000
R= 0.25 m								
1.005	0.22161	0	0.0000	0.00000	29.41	0.00034	33.354	0.0000
0.950	0.20925	10	1.0799	0.22597	29.41	0.00034	33.354	0.0068
0.890	0.19645	21	2.1598	0.42429	29.41	0.00034	33.354	0.0127
0.850	0.18806	29	3.0238	0.56865	29.41	0.00034	33.354	0.0170
0.740	0.16334	39	4.1037	0.67028	28.54	0.00035	34.373	0.0195
0.575	0.12714	51	5.2916	0.67276	27.72	0.00036	35.392	0.0190
0.420	0.09270	60	6.2636	0.58066	26.94	0.00037	36.411	0.0159
0.240	0.05297	72	7.4947	0.39702	26.21	0.00038	37.430	0.0106
0.110	0.02384	80	8.4234	0.20080	25.51	0.00039	38.449	0.0052
0.000	0.00000	87	9.0929	0.00000	24.86	0.00040	39.468	0.000

Figure 5.7 (a): Graph of efficiency against angular speed (in rpm)
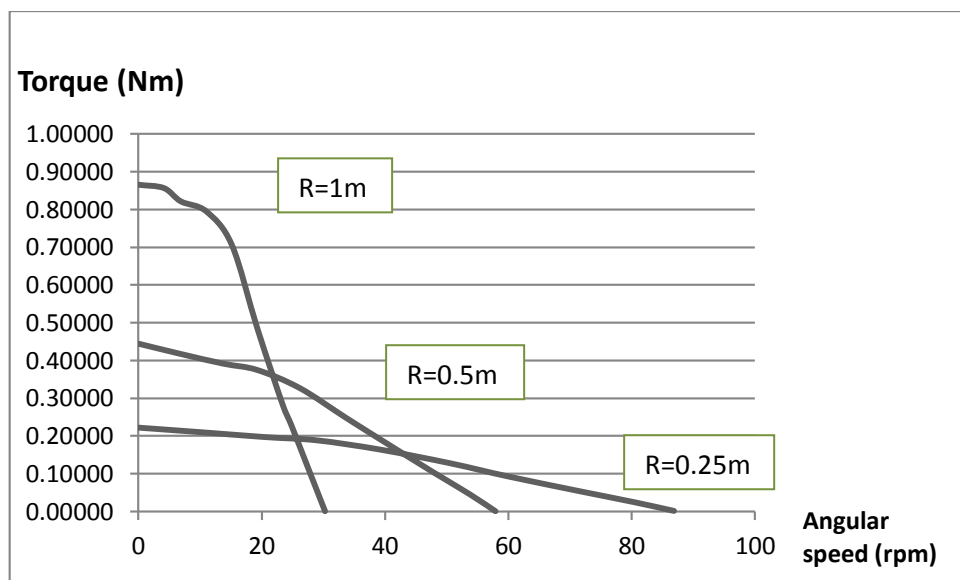
Figure 5.7 (b): Graph of torque against angular speed (in rpm)

Both efficiency and torque trends are similar to those in section 5.2.1. Nevertheless the highest efficiency achieved in this experiment is much lower than that in section 5.2.1. On the other hand the optimum torque here is relatively higher than the similar experiment in section 5.2.1. The other parameter is the flow rate which is appears to be constant at the beginning and starts increasing gradually. The maximum flow rate for these experiments is higher than that of 5.2.1 this is because of a higher head. The relation of Q to H is given by: $Q = A_e * \sqrt{2gh + \omega^2 R^2}$, (Date et al, 2009).This is not

the case with the other types of nozzles whose nozzle to main pipe cross-section area ratio is less than one (i.e. $1/n < 1$).

5.3.2 High head performance characteristics for nozzle diameter of 8.8 mm

Here the main pipe to nozzle cross-section area ratio is $n = 1.7078$. Therefore the inverse of n is equals to $1/n = 0.58556$. Table 5.8 shows the performance characteristics by varying the arm radius as shown and keeping the nozzle to main pipe cross-section area ratio constant at 1.7078.

Table 5.8: Low head experimental results using nozzle diameter of 8.8 mm

Output power				Input power			Efficiency
Weighing scale readings (Kg)	Torque (Nm)	Angular speed		Power P_{out} (W)	Time required for 0.01m³ of water to flow (s)	Volume of flow (m²/s)	Power P_{in} (W)	P_{out}/P_{in} (-)
		rpm	rad/s					
R=1.0 m								
4.205	0.92793	0	0.0000	0.00000	36.76	0.00027	26.68320	0.0000
3.880	0.85641	21	2.1991	1.88335	33.03	0.00029	28.44910	0.0769
3.800	0.83876	51	5.3407	4.47954	24.04	0.00042	40.81216	0.1098
3.680	0.81227	69	7.2257	5.86917	19.39	0.00052	50.59679	0.1160
3.470	0.76636	87	9.1106	6.98199	16.25	0.00062	60.38143	0.1156
2.990	0.66041	99	10.3673	6.84663	14.66	0.00068	66.90451	0.1023
2.310	0.50987	114	11.9380	6.08691	13.07	0.00077	75.05837	0.0811
1.450	0.32049	127	13.2994	4.26236	11.95	0.00084	82.12505	0.0519
0.760	0.16775	135	14.1372	2.37152	11.34	0.00088	86.47378	0.0274
0.000	0.00000	142	14.8702	0.00000	10.87	0.00092	90.27891	0.0000
R= 0.5 m								
2.850	0.62907	0	0.0000	0.00000	36.76	0.00027	26.68320	0.0000
2.685	0.59243	23	2.4478	1.45015	32.06	0.00030	29.77508	0.0563
2.600	0.57389	48	5.0396	2.89217	24.81	0.00040	39.53823	0.0731
2.520	0.55623	70	7.3435	4.08464	18.95	0.00053	51.77215	0.0789
2.460	0.54298	88	9.2153	5.00378	15.9	0.00063	61.71220	0.0811
2.260	0.49884	106	11.0872	5.53072	13.69	0.00073	71.65226	0.0772
1.920	0.42379	121	12.6711	5.36991	12.25	0.00082	80.06307	0.0671
1.440	0.31784	133	13.9670	4.43933	11.28	0.00089	86.94465	0.0511
0.780	0.17217	149	15.5509	2.67733	10.29	0.00097	95.35547	0.0281
0.000	0.00000	162	16.9908	0.00000	9.524	0.00105	103.00166	0.0000
R= 0.25 m								
2.250	0.49663	0	0.0000	0.00000	36.76	0.00027	26.68320	0.0000
2.190	0.48339	18	1.8719	0.90484	43.25	0.00023	22.68095	0.0399
2.070	0.45690	41	4.3197	1.97367	27.41	0.00036	35.79632	0.0551
2.010	0.44366	55	5.7596	2.55528	22.55	0.00044	43.51125	0.0587
1.950	0.43041	72	7.4875	3.22271	18.59	0.00054	52.76916	0.0611
1.890	0.41717	98	10.2233	4.26484	14.55	0.00069	67.42752	0.0633
1.740	0.38406	120	12.5271	4.81118	12.3	0.00081	79.77141	0.0603
1.350	0.29798	140	14.6869	4.37640	10.74	0.00093	91.34380	0.0479
0.810	0.17879	158	16.5588	2.96050	9.677	0.00103	101.37320	0.0292
0.000	0.00000	175	18.2867	0.00000	8.867	0.00113	110.63111	0.0000

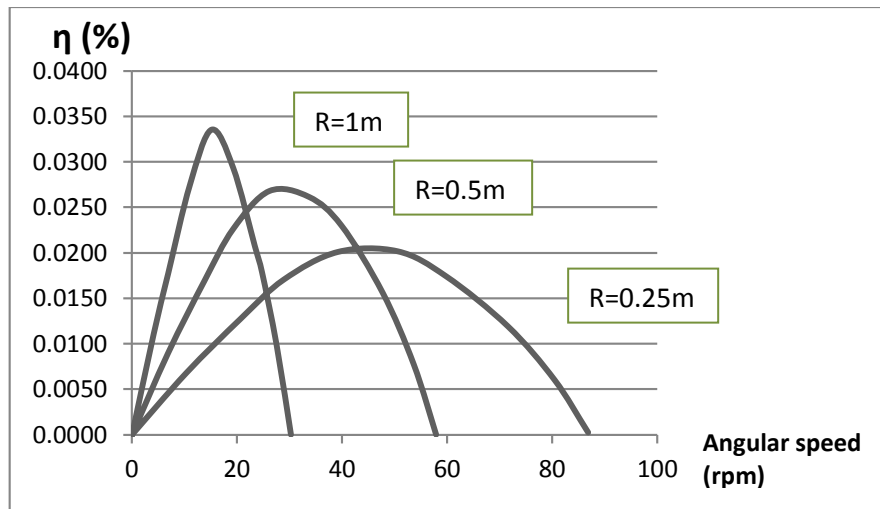Figure 5.8 (a) and (b) are graphs showing the efficiency and torque trends in relation to rpm.
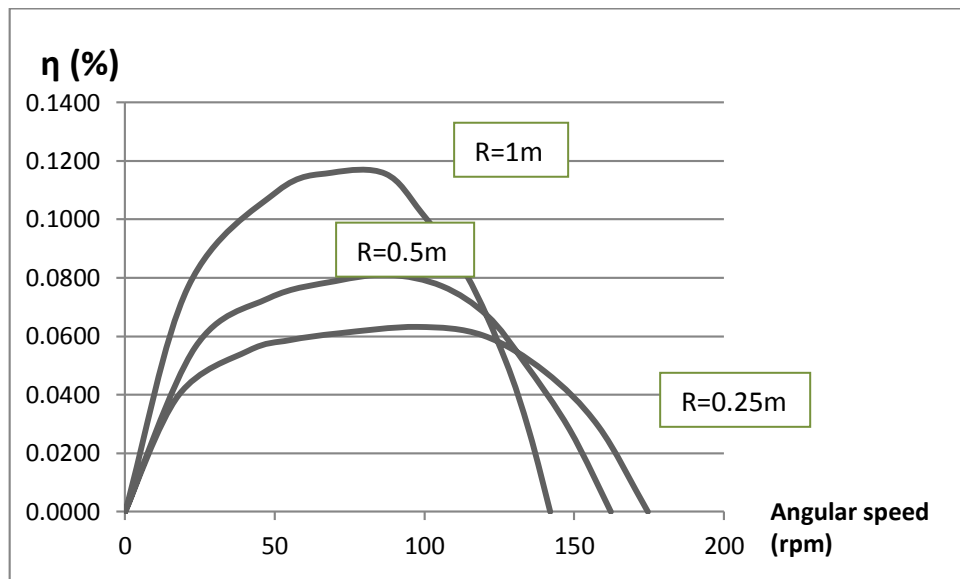
Figure 5.8 (a): Graph of efficiency against angular speed (in rpm)
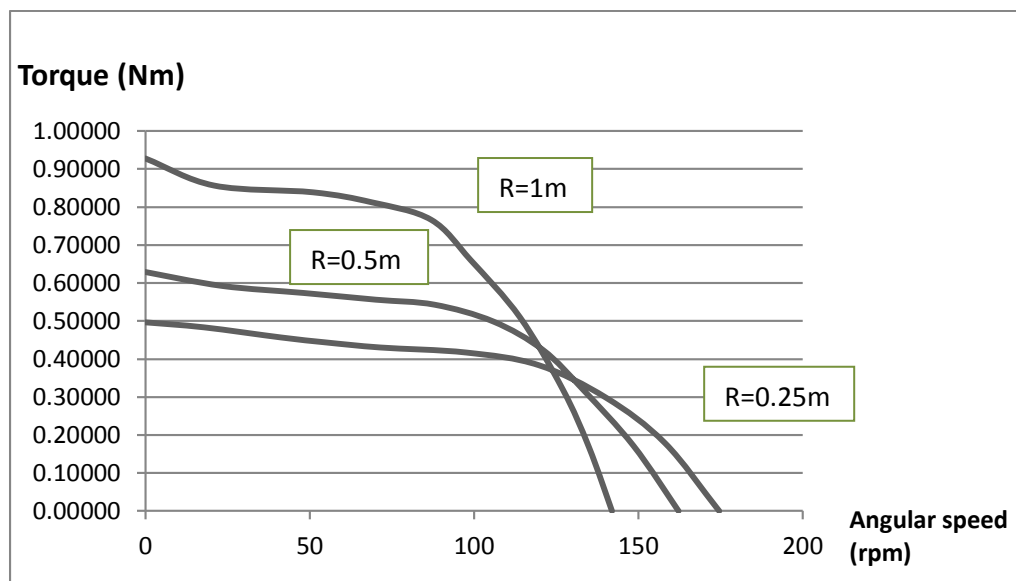
Figure 5.8 (b): Graph of torque against angular speed (in rpm)

The highest efficiency achieved in this experiment is about 11.60%, which is much less than the maximum efficiency of a similar experiment in section 5.2.2.This type of nozzle produces relatively second highest torque after that produced by the 6.0mm nozzle. All the parameters including efficiency, torque, angular speed and volume flow rate follow a similar trend as the experiments in section 5.2.2. The highest

maximum mass flow rate is witnessed in this section as compared to all the other experiments done in this research. This is because of high head and a fairly high angular speed of the turbine. The effects of head and angular speed on mass flow rate is given by $\dot{m} = \rho Q = \rho.A.V_R = \rho.A.\left(\sqrt{2gH + \omega^2 R^2}\right)$, (Date, 2009) and (Akbarzadeh, 2001). The other reason for high mass flow rate is that the nozzle used in this section has a relatively high nozzle to main-conduit cross-sectional area ratio of about $1/n = 0.586$. This means that the nozzle offers a relatively lower resistance to flow.

5.3.3 High head performance characteristics for nozzle diameter of 6.0 mm

Here the main pipe to nozzle cross-section area ratio is $n = 3.674$. Therefore the inverse of n is equals to $1/n = 0.27221$. Table 5.9 shows the performance characteristics by varying the arm radius and keeping the nozzle to main pipe cross-section area ratio constant at 3.674.

Table 5.9; High head experimental results using nozzle diameter of 6.0 mm

Weighing scale readings (Kg)	Torque (Nm)	Angular speed		Power P_out (W)	Time required for 0.01m³ of water to flow (s)	Volume of flow (m²/s)	Power P_in (W)	Efficiency P_out/P_in (-)
		rpm	rad/s					
R=1.0 m								
7.000	1.54508	0	0.0000	0.0000	47.13	0.00021	20.8129	0.0000
6.525	1.44024	38	3.9793	5.7312	39.34	0.000254	24.9384	0.2298
6.500	1.43447	83	8.6917	12.4680	28.03	0.000357	35.0029	0.3562
6.030	1.33097	113	11.8333	15.7498	24.98	0.0004	39.2686	0.4011
5.900	1.30228	143	14.9749	19.5015	19.82	0.000505	49.4984	0.3940
5.135	1.13309	162	16.9646	19.2224	18.62	0.000537	52.6718	0.3649
3.825	0.84477	186	19.4779	16.4543	16.9	0.000592	58.0395	0.2835
2.420	0.53428	207	21.6770	11.5817	15.64	0.00064	62.7363	0.1846
1.265	0.27925	222	23.2478	6.4919	14.84	0.000674	66.0911	0.0982
0.000	0.00000	236	24.7139	0.0000	14.17	0.000706	69.2223	0.0000
R= 0.5 m								
4.275	0.94360	0	0.0000	0.0000	47.13	0.00021	20.8129	0.0000
4.140	0.91380	39	4.0841	3.7320	37.3	0.000268	26.3024	0.1419
4.050	0.89394	79	8.3252	7.4422	28.23	0.000354	34.7496	0.2142
3.915	0.86414	114	11.9380	10.3161	23.39	0.000428	41.9427	0.2460
3.825	0.84427	150	15.7080	13.2618	19.19	0.000521	51.1316	0.2594
3.600	0.79461	174	18.2212	14.4788	17.3	0.000578	56.7085	0.2553
3.060	0.67542	198	20.7345	14.0045	15.75	0.000635	62.2854	0.2248
2.160	0.47677	222	23.2478	11.0838	14.46	0.000692	67.8623	0.1633
1.170	0.25825	243	25.4469	6.5716	13.49	0.000742	72.7420	0.0903
0.000	0.00000	264	27.6460	0.0000	12.64	0.000791	77.6218	0.0000
R= 0.25 m								
3.000	0.66218	0	0.0000	0.0000	47.13	0.00021	20.8129	0.0000
2.700	0.59596	30	3.1416	1.8723	41.92	0.000239	23.4000	0.0800
2.565	0.56616	62	6.4926	3.6759	31.34	0.000319	31.3006	0.1174
2.490	0.54961	83	8.6394	4.7482	26.98	0.000371	36.3619	0.1306
2.430	0.53636	117	12.2522	6.5716	21.86	0.000457	44.8797	0.1464
2.370	0.52312	161	16.8075	8.7923	17.64	0.000567	55.6196	0.1581
2.310	0.50987	195	20.4203	10.4118	15.3	0.000654	64.1374	0.1623
2.025	0.44697	229	23.9808	10.7187	13.53	0.000739	72.5317	0.1478
1.215	0.26818	262	27.4366	7.3580	12.16	0.000822	80.6792	0.0912
0.000	0.00000	287	30.0546	0.0000	11.3	0.000885	86.8515	0.0000

The data used to calculate the specific speed (K_2) to be used in figure 5.9 (c) are found in table 5.9.
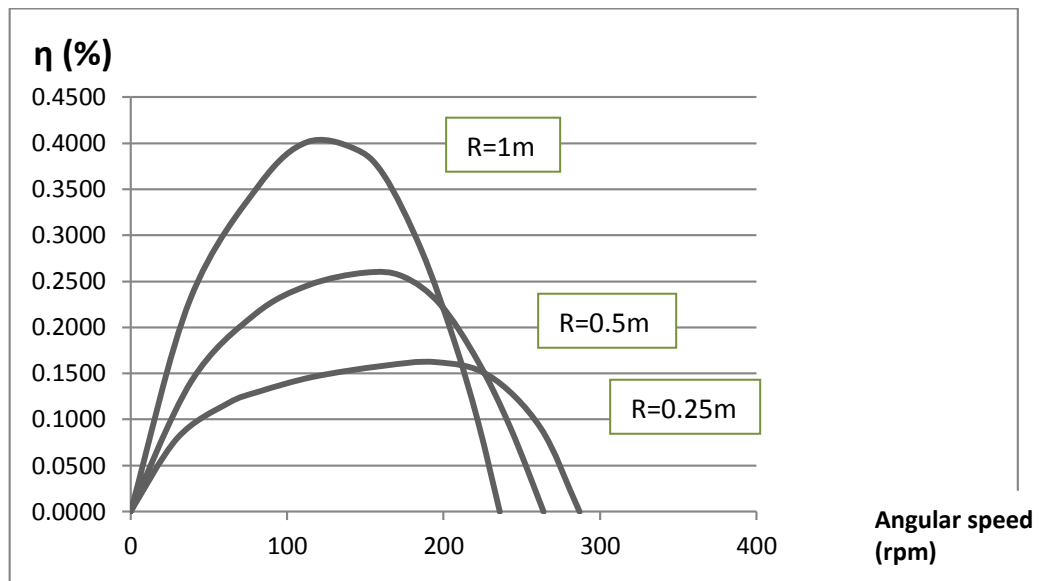
Figure 5.9 (a): Graph of efficiency against angular speed (in rpm)
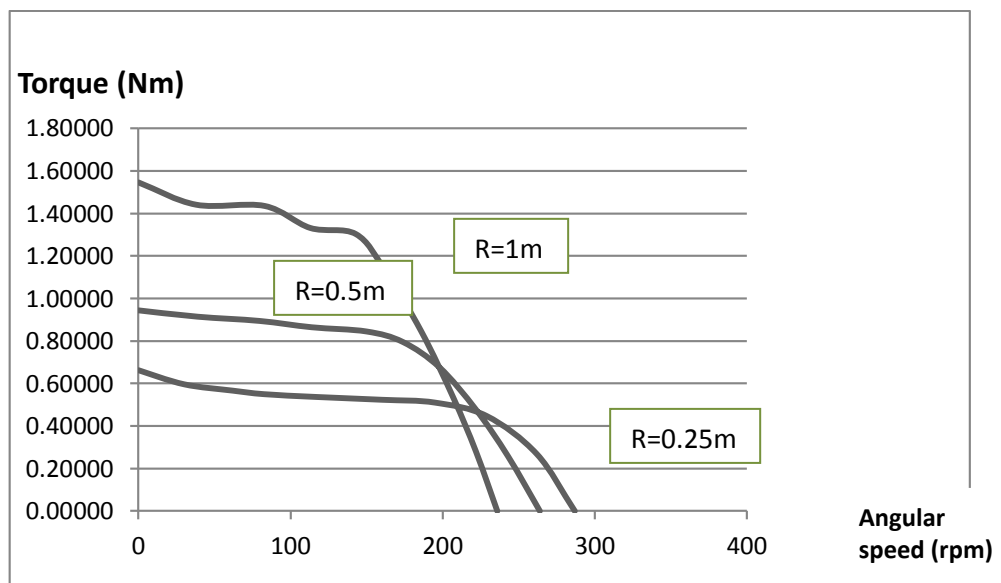
Figure 5.9 (b): Graph of torque against angular speed (in rpm)
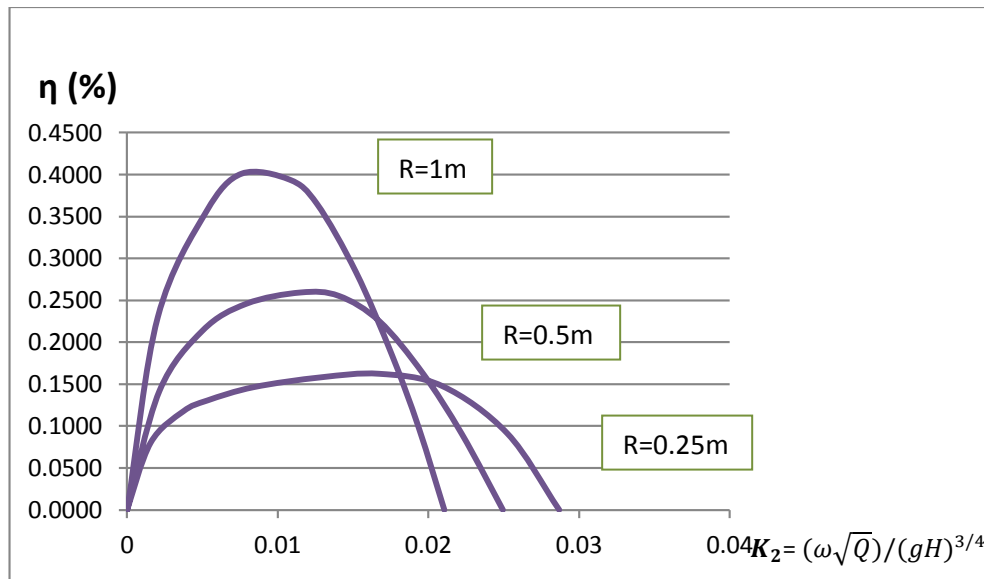
Figure 5.9 (c): Graph of efficiency against specific speed (K_2)

Figure 5.9 (a), (b), (c) are graphs showing efficiency against rpm, torque against rpm as well as a graph of efficiency against specific speed. The highest efficiency in this experiment is 40.11% which is also the highest efficiency in the high pressure tap experiments. Even so, this efficiency is much lower than the highest efficiency in the raised tank experiments. The highest maximum mass flow rate is witnessed in this section as compared to all the other experiments done in this research. The highest maximum flow velocity is witnessed in this section as compared to all the other experiments done in this research. This is because of the high head and a highest angular speed experienced in this section. The effects of head and angular speed on flow velocity is given by $V_R = \sqrt{(2gH + \omega^2 R^2)}$, (Date, 2009) and (Akbarzadeh, 2001). None the less the high flow velocity dose not translates to high mass flow rate. The reason for this scenario is that the nozzle used in this section has a relatively low nozzle to main-conduit cross-sectional area ratio of about $1/n = 0.272$. This means that the nozzle offers a relatively high resistance to flow.

5.3.4 High head performance characteristics for nozzle diameter of 3.8 mm

In this case the main pipe to nozzle cross-section area ratio is $n = 9.159$. Therefore

the inverse of n is equals to $1/n = 0.109187$. Table 5.10 shows the performance

characteristics by varying the arm radius and keeping the nozzle to main pipe cross-

section area ratio constant at 9.159. Figure 5.10 (a) and (b) are graphs showing the

course of efficiency and torque against rpm.

Table 5.10; High head experimental results using nozzle diameter of 3.8 mm

| Output power					Input power			Efficiency
Weighing scale readings (Kg)	Torque (Nm)	Angular speed		Power P_{out} (W)	Time required for 0.01m³ of water to flow (s)	Volume of flow (m²/s)	Power P_{in} (W)	P_{out}/P_{in} (-)
		rpm	rad/s					
R=1.0 m								
2.400	0.52974	0	0.0000	0.0000	102.8	0.000097	9.5451	0.0000
2.280	0.50325	25	2.5918	1.3043	95.29	0.0001049	10.2946	0.1267
2.240	0.49398	51	5.3276	2.6317	81.55	0.0001226	12.0296	0.2188
2.155	0.47610	74	7.7754	3.7019	72.23	0.0001384	13.5819	0.2726
2.085	0.46021	92	9.6473	4.4398	66.42	0.0001505	14.7690	0.3006
1.830	0.40393	107	11.2312	4.5366	62.19	0.0001608	15.7734	0.2876
1.470	0.32447	122	12.8151	4.1581	58.47	0.000171	16.7778	0.2478
1.050	0.23176	138	14.3990	3.3371	55.17	0.0001813	17.7823	0.1877
0.540	0.11919	149	15.5509	1.8535	52.99	0.0001887	18.5128	0.1001
0.000	0.00000	157	16.4148	0.0000	51.47	0.0001943	19.0607	0.0000
R= 0.5 m								
1.890	0.41717	0	0.0000	0.0000	102.8	0.000097	9.5451	0.0000
1.755	0.38737	30	3.1678	1.2271	88.81	0.0001126	11.0458	0.1111
1.670	0.36883	63	6.6235	2.4430	70.1	0.0001427	13.9947	0.1746
1.600	0.35294	92	9.6473	3.4049	59.19	0.000169	16.5750	0.2054
1.535	0.33870	116	12.0951	4.0967	52.56	0.0001903	18.6639	0.2195
1.425	0.31453	140	14.6869	4.6195	46.99	0.0002128	20.8756	0.2213
1.260	0.27811	158	16.5588	4.6052	43.65	0.0002291	22.4729	0.2049
0.935	0.20660	177	18.5747	3.8375	42.81	0.0002336	22.9136	0.1675
0.525	0.11621	195	20.4465	2.3761	40.25	0.0002484	24.3714	0.0975
0.000	0.00000	212	22.1744	0.0000	38.15	0.0002622	25.7171	0.0000
R= 0.25 m								
1.200	0.26487	0	0.0000	0.0000	102.8	0.000097	9.5451	0.0000
1.165	0.25759	25	2.5970	0.2230	93.11	0.0001074	10.5363	0.0635
1.100	0.24302	54	5.6156	0.4549	75.14	0.0001331	13.0551	0.1045
1.070	0.23640	66	6.9115	0.5446	69.4	0.0001441	14.1364	0.1156
1.040	0.22977	94	9.7913	0.7499	59.31	0.0001686	16.5394	0.1360
0.975	0.21521	133	13.9670	1.0019	48.99	0.0002041	20.0237	0.1501
0.900	0.19865	160	16.7552	1.1095	43.89	0.0002278	22.3502	0.1489
0.720	0.15892	184	19.2946	1.0221	40.09	0.0002494	24.4692	0.1253
0.430	0.09535	208	21.7424	0.6911	37	0.0002703	26.5117	0.0782
0.000	0.00000	230	24.0463	0.0000	34.5	0.0002898	28.4341	0.0000

Figure 5.10 (a): Graph of efficiency against angular speed (rpm)
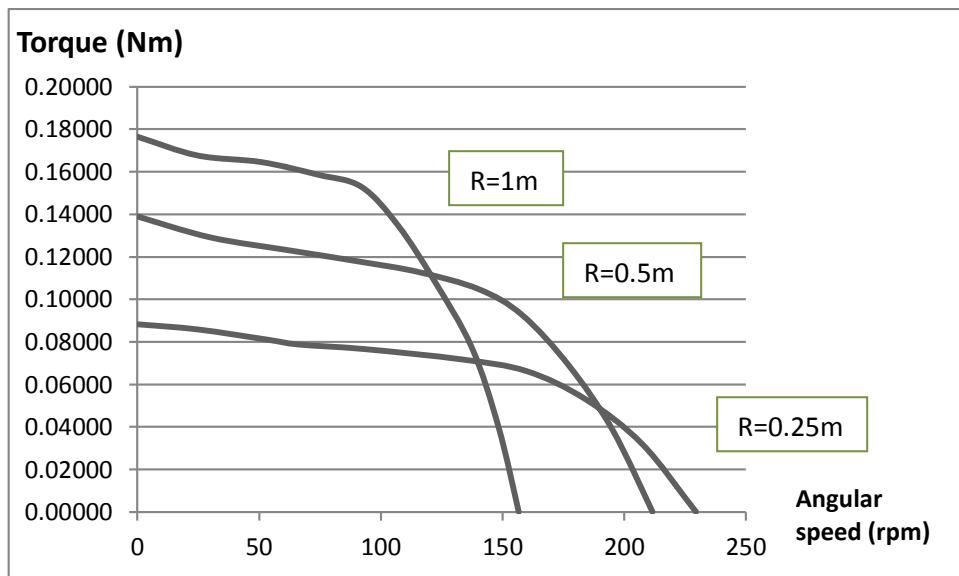
**Figure 5.10 (b): Graph of torque against angular speed (in rpm)**

Here the highest efficiency is 30.06%, which is much lower than a similar experiment in section 5.3.4. None the less all the parameters here follow a similar trend as the experiments in section 5.3.4.

5.3.5 High head performance characteristics for nozzle diameter of 2.5 mm

In this case the main pipe to nozzle cross-section area ratio is $n = 21.16$. Therefore the inverse of n is equals to $1/n = 0.04726$. Table 5.11 shows the performance

characteristics by varying the arm radius and keeping the nozzle to main pipe cross-section area ratio constant at 21.16.

Table 5.11; Low head experimental results using nozzle diameter of 2.5 mm

Output power				Input power			Efficiency
Weighing scale readings (Kg)	Torque (Nm)	Angular speed		Power P_{out} (W)	Time required for 0.01m³ of water to flow (s)	Volume of flow (m²/s)	Power P_{in} (W)	P_{out}/P_{in} (-)
		rpm	rad/s					
R=1.0 m								
0.900	0.19865	0	0.0000	0.000000	167	0.00005987	5.8732	0.0000
0.810	0.17879	8	0.8639	0.154461	163.5	6.116E-05	5.9997	0.0257
0.750	0.16554	17	1.7759	0.293985	160	6.25E-05	6.1314	0.0479
0.710	0.15627	25	2.5918	0.405031	157	6.37E-05	6.2493	0.0648
0.670	0.14833	31	3.2158	0.476986	154.7	6.462E-05	6.3394	0.0752
0.600	0.13244	36	3.7437	0.495801	152.9	6.54E-05	6.4157	0.0773
0.490	0.10793	41	4.2717	0.461063	151.1	6.618E-05	6.4920	0.0710
0.335	0.07350	46	4.7997	0.352781	149.4	6.695E-05	6.5683	0.0537
0.170	0.03774	50	5.1836	0.195651	148.1	6.752E-05	6.6237	0.0295
0.000	0.00000	52	5.4716	0.000000	147.2	6.794E-05	6.6653	0.0000
R= 0.5 m								
0.635	0.13972	0	0.0000	0.00000	167	0.00005987	5.8732	0.0000
0.585	0.12912	10	1.0085	0.13022	162.9	6.137E-05	6.0206	0.0216
0.550	0.12184	21	2.1572	0.26284	158.6	6.306E-05	6.1865	0.0425
0.525	0.11588	33	3.4558	0.40045	153.9	6.498E-05	6.3741	0.0628
0.485	0.10661	41	4.3197	0.46052	150.9	6.625E-05	6.4989	0.0709
0.430	0.09535	47	4.8956	0.46682	149	6.71E-05	6.5821	0.0709
0.360	0.07946	52	5.4716	0.43478	147.2	6.794E-05	6.6653	0.0652
0.240	0.05297	59	6.1785	0.32730	145	6.899E-05	6.7674	0.0484
0.130	0.02914	65	6.7649	0.19710	143.2	6.985E-05	6.8522	0.0288
0.000	0.00000	71	7.3827	0.00000	141.3	7.076E-05	6.9414	0.0000
R= 0.25 m								
0.400	0.08807	0	0.0000	0.00000	167	0.00005987	5.8732	0.0000
0.390	0.08608	8	0.8639	0.07437	163.5	6.116E-05	5.9997	0.0124
0.370	0.08211	18	1.8719	0.15370	159.6	6.264E-05	6.1453	0.0250
0.360	0.07946	22	2.3038	0.18306	158	6.328E-05	6.2077	0.0295
0.350	0.07681	31	3.2638	0.25070	154.6	6.469E-05	6.3464	0.0395
0.320	0.07085	43	4.4637	0.31626	150.5	6.646E-05	6.5197	0.0485
0.290	0.06423	52	5.4716	0.35145	147.2	6.794E-05	6.6653	0.0527
0.230	0.05099	61	6.4315	0.32793	144.2	6.936E-05	6.8040	0.0482
0.145	0.03178	69	7.2475	0.23036	141.7	7.056E-05	6.9219	0.0333
0.000	0.00000	77	8.0154	0.00000	139.5	7.169E-05	7.0328	0.0000

Figure 5.10 (a) and (b) are graphs showing the course of efficiency and torque against rpm.
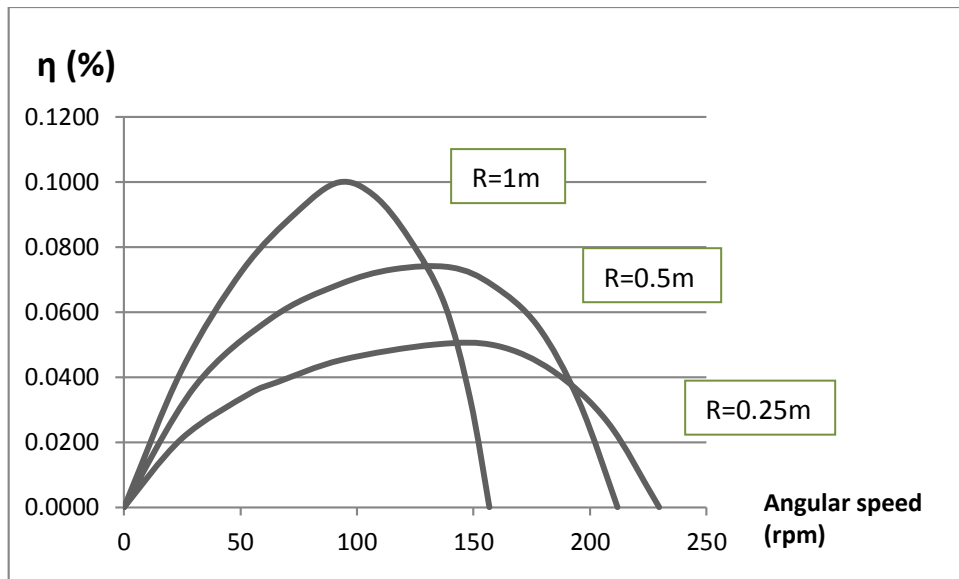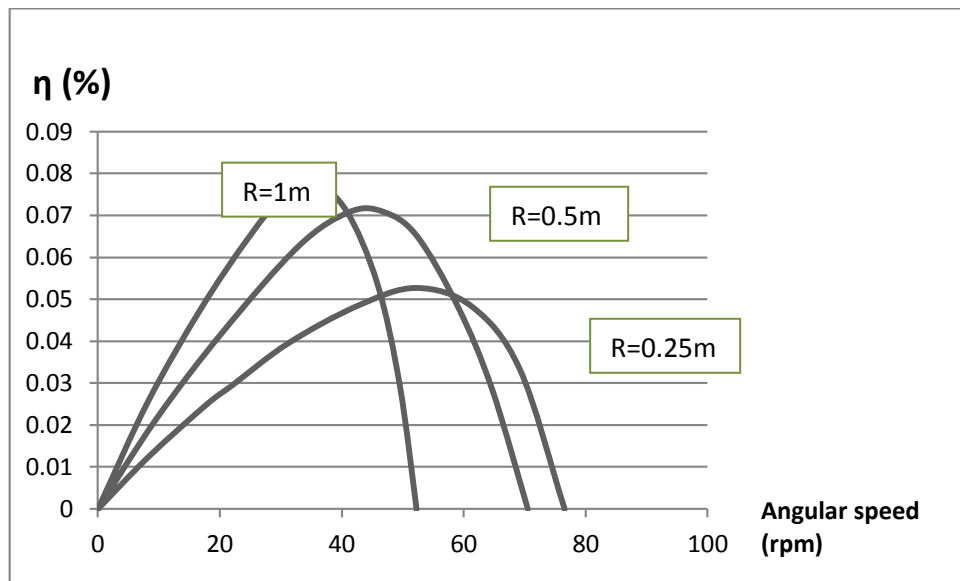

Figure 5.11 (a): Graph of efficiency against angular speed (in rpm)
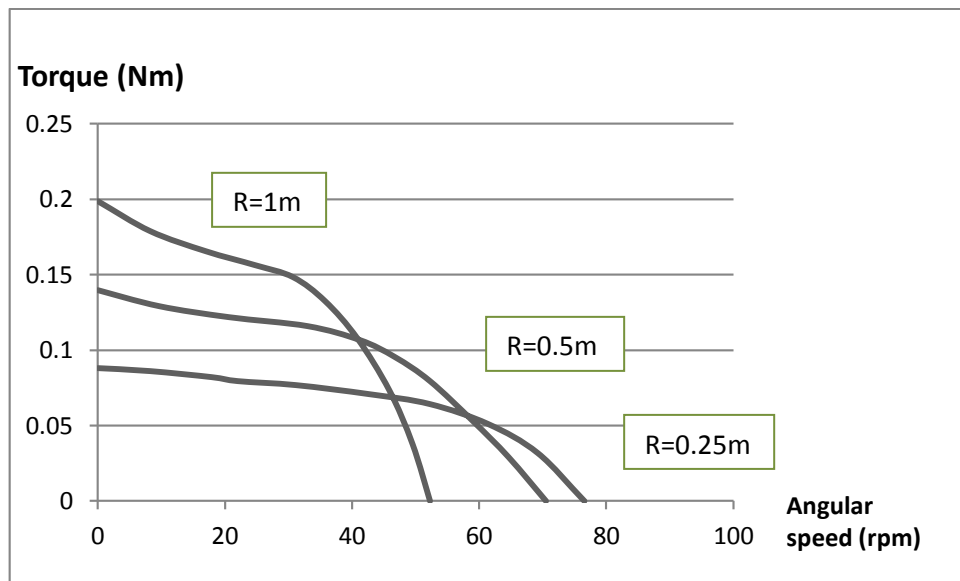
Figure 5.11 (b): Graph of torque against angular speed (in rpm)

The highest efficiency achieved with this type of nozzle is approximately equals to 7.73%. The reason for this low efficiency is the same as the reason given in section 5.2.5. Again all the parameters here follow a similar trend as the experiments in section 5.3.5.

5.3.6 Nozzle and arm length performance characteristics under high head

The procedure of finding the optimum 'main pipe to nozzle cross-sectional area ratio', which will produce the highest efficiency is similar to that in section 5.2.6. The graph picks the highest efficiency for each of the five nozzles used in the high pressure tap experiments. The procedure is replicated for each of the three arm lengths. This data are taken from the experiments done under high head of 11.5m.

Table 5.12: Data table for optimum efficiencies against 1/n for each of the three different arm radiuses.

(1/n)	Efficiency (%)
Arm radii **R = 1m**	
1	0.034
0.5856	0.116
0.2722	0.401
0.1092	0.304
0.0473	0.077
0	0.000
Arm radii **R = 0.5m**	
1	0.027
0.5856	0.081
0.2722	0.259
0.1092	0.221
0.0473	0.071
0	0.000
Arm radii **R = 0.25m**	
1	0.020
0.5856	0.063
0.2722	0.162
0.1092	0.150
0.0473	0.053
0	0.000
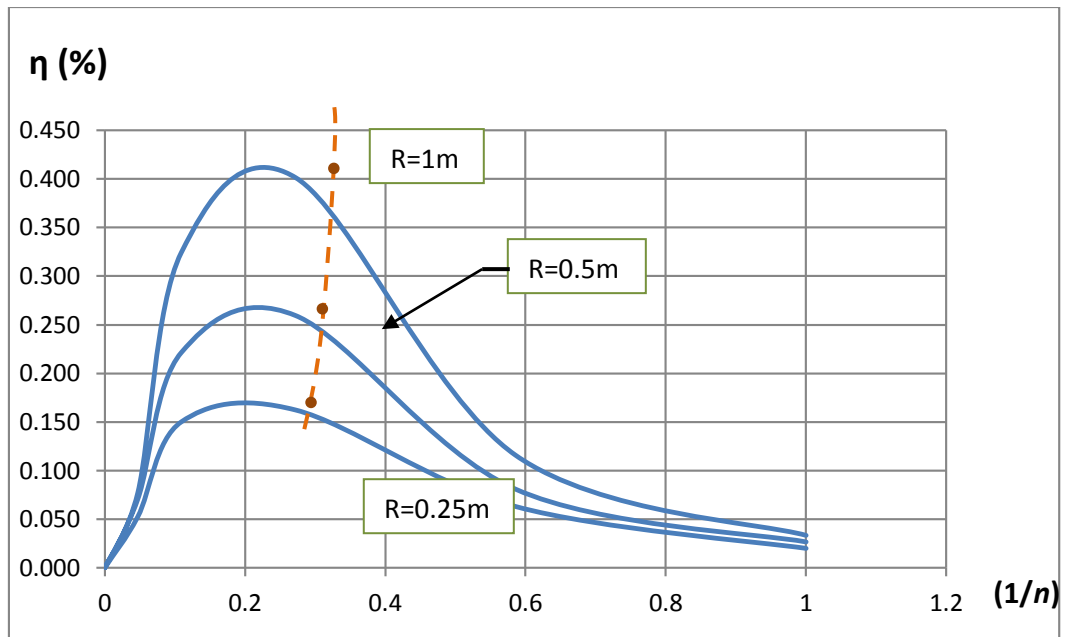
Figure 5.12: Graph of optimum efficiencies against (1/n) operating under high head

Here the optimum 'nozzle to main pipe cross-sectional area ratio' as seen in the graph is approximately; $(1/n)$ =0.24, for arm radius R = 1m. In the case of arm radius R = 0.5m, optimum 'nozzle to main pipe cross-sectional area ratio' occurs at $(1/n)$ =0.22. While in the case of arm radius R = 0.25m, optimum 'nozzle to main pipe cross-sectional area ratio' occurs at $(1/n)$ =0.2.

5.4 Combined Efficiency graph

The data used to prepare the graph in figure 5.13 was obtained from the data in table 5.6 and 5.12. The data were combined and used to draw a one overall efficiency graph for both heads.
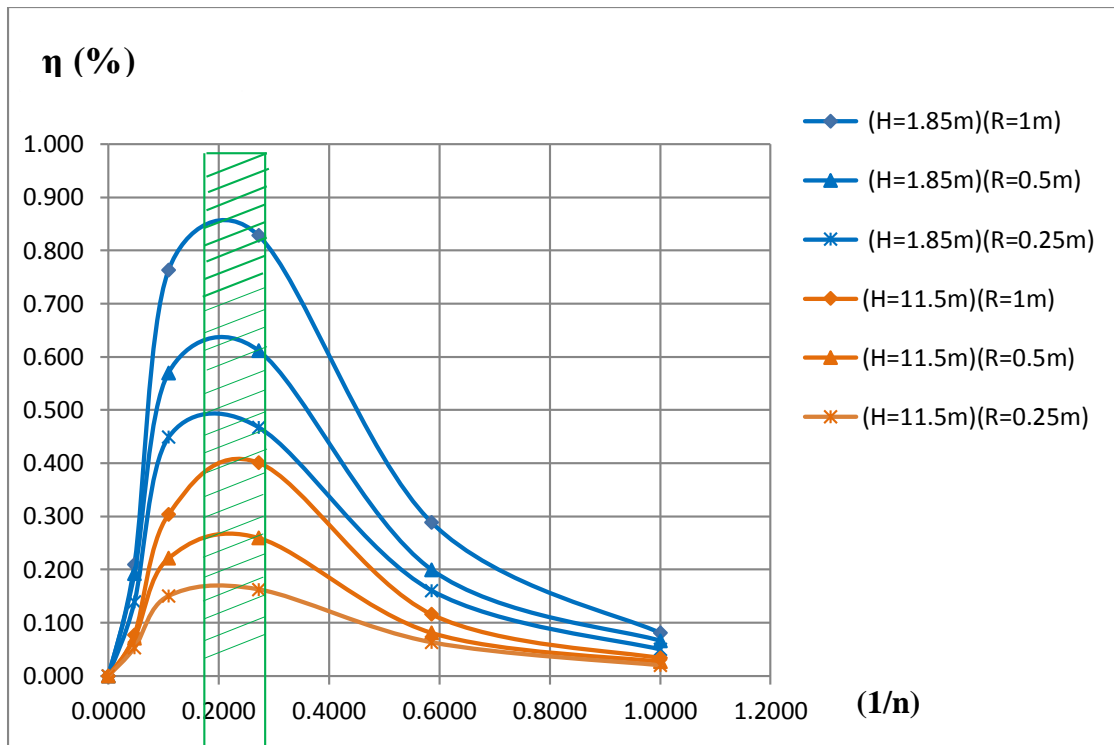
Figure 5.13: Combined efficiency graph

It can be seen from the graph in figure 5.13 that, efficiency is high when operating with a relatively lower head than when operating with high head. This is because from the equation 3.20, at particular optimum angular velocity and radius, efficiency is given by;

$$\eta = \frac{2\left[\sqrt{\dfrac{HH_c + H_c}{(1 + k)}} - H_c\right]}{H}$$

Where; H_c is head due centrifugal acceleration and k is a friction factor at the nozzle while H is head due to gravitational acceleration.

This means that keeping other variables constant; the lower the head the higher the value of η, which is higher operating efficiency.

5.5 Optimum theoretical efficiency

From the data in table 5.3 which produces the highest efficiency at H=1.85m;

Table 6.1: Optimum efficiency when, nozzle diameter =6.0mm and R=1m

Output power					Input power			Efficiency
Weighing scale readings (Kg)	Torque (Nm)	Angular speed		Power P_{out} (W)	Time required for 0.01m³ of water to flow (s)	Volume of flow (m²/s)	Power P_{in} (W)	P_{out}/P_{in} (-)
		rpm	rad/s					
R=1.0 m								
1.400	0.30902	0	0	0	64.1	0.000156	1.5304	0.0000
1.315	0.29044	30	3.1416	0.7541	54.96	0.000182	1.7037	0.4426
1.300	0.28689	55	5.7596	1.6524	44.76	0.000223	2.1917	0.7539
1.205	0.26543	77	8.0634	2.1403	38.04	0.000263	2.5786	0.8282
1.190	0.26302	95	9.9484	2.6166	29.84	0.000335	3.2874	0.7959

$Q = 0.000263 \; m^3/s$ $\omega = 8.0634$ $P_{out} = 2.1404W$ $P_{in} = 2.5786W$ $\eta = 0.83 = 83\%$

Again from the equation of power and efficiency in section 3.5.5

$$P = -\rho Q(\omega R\cos\beta)(\sqrt{2gH + \omega^2 R^2 \cos^2\beta} + \omega R\cos\beta)$$

Power available is $P_H = \rho Q gH$

$$\eta = \frac{(\omega R\cos\beta)(\sqrt{2gH + \omega^2 R^2 \cos^2\beta} + \omega R\cos\beta)}{gH}$$

Since the turbine in this research has a semicircular arm conduit then $\beta = 180^0$, so that

$$cos\beta = -1$$

Calculated output power $P_{out} = \rho Q(\omega R)(\sqrt{2gH + \omega^2 R^2} - \omega R)$

$$P_{out} = 2.4102W$$

Power available is $P_H = \rho Q gH = 2.5786W$

Therefore theoretical efficiency;

$$\eta = \frac{\text{P}_{\text{out}}}{\text{P}_H} = 93.4\% \qquad \qquad \{eqn\ 5.2\}$$

5.6 Determination of the optimum 'K' and 'k' values

Using the calculated theoretical efficiency $\eta = 93.4\%$ in section 6.2, as well as the actual efficiency $\eta = 83\%$ from the experimental results in table 5.3, 'K' and 'k − factor' values can be optioned.

5.6.1 Optimum K value

From the equation of theoretical efficiency (η) and 'K' in section 3.5.5;

$$\eta = 2\left(\sqrt{K + K^2} - K\right)$$

But theoretical efficiency $\eta = \frac{P}{P_H} = 0.934$ in section 6.1

Therefore 'K' is equals to;

$$0.934 = 2\left(\sqrt{K + K^2} - K\right)$$

Solving the above equation and making 'K' the subject;

$$K \approx 3.30438 \qquad \qquad \{eqn\ 5.3\}$$

5.6.2 Optimum k value

From the equation 3.21 of actual efficiency (η) and 'k' efficiency is given by;

$$\eta = 2\left[\sqrt{\frac{K + K^2}{(1 + k)}} - K\right] \qquad \qquad \{eqn\ 5.4\}$$

But optimum experimental efficiency, $\eta = \frac{P}{P_H} = 0.83$, from table 5.3.

While $K \approx 3.3044$, from equation 5.3

By replacing η and K in equation 5.4 the value of k is found to be;

$$k \approx 0.028157$$

CHAPTER SIX

CONCLUSIONS AND RECOMMENDATIONS

6.1 Introduction

This chapter gives the conclusion of this research. This is in relation to the objectives set at chapter one. It further gives relevant recommendation concerning the reaction turbine that was designed, fabricated and finally tasted in this research.

6.2 Conclusions

To begin with single arm centrifugal reaction water turbine is a simple turbine in design that can easily be fabricated in most local workshops. It is fabricated using locally available plumbing materials. It is important to note that continuum mechanics approach was successful in the mathematical modelling of the turbine. Using the approach the main governing equations were effectively developed in section 3.4.

One of the objectives of the research was to study the effects conduit to nozzle cross-sectional area ratio. From the experimental results in chapter 5 the optimum nozzle to main conduit cross-sectional area ratio is in the range of; $0.18 < \left(\frac{1}{n}\right) < 0.24$. This means that using a large nozzle or a relatively smaller nozzle reduces the efficiency of the turbine. Therefore the size of the nozzle in relation to the main conduit affects efficiency of the turbine.

The other important parameter in these experiments is the radial arm length. As seen from the data in chapter five, the arm radius affects the output power in a direct proportion. Moreover the arm length affects the angular speed of the turbine in an inverse proportion. This means that the lower the arm radius the higher the angular velocity. On the other hand the arm radius affects the operating torque in such a manner that torque $T = \rho R V_e Q \cos\beta$, this conforms to equation 3.7. The research

found out that (in a non-ideal situation where external forces e.g. bearing frictional torque etc play a role), the shorter the radial arm length the lower the efficiency. This is because the available torque is barely enough to overcome the frictional torque. From the experimental results it is found that, as the arm radius increases from 0.25m to 1m the efficiency also increase up to a maximum of 83%. The research could not go beyond a radius of 1m and find out the very optimum arm radius which gives the highest efficiency.

In conclusion the optimum efficiency of the turbine when H=1.85m is 83% while the optimum efficiency of the turbine when H=11.5m is 40.11%. This variation in efficiency means that a lot of potential energy is wasted when operating at relatively higher heights. This therefore renders the turbine mostly suitable for low heads when efficiency is the key factor.

6.3 Recommendation for future work

It is observed that the semicircular centrifugal reaction water turbine is a fairly suitable type of turbine for Low head and low flow application. As analysed in this research this type of turbine has proven to operate with a remarkably higher efficiency as compared to the rest of the turbine under similar condition. Moreover the research recommended that an arm conduit with a larger and varying cross-sectional area could be used so as to allow higher discharge and scaling up of the turbine.

Research is still needed on the study about the very optimum radial arm length, while incorporating the negative effects of friction along the radial arm conduit. This is because from the results in chapter 5; as the arm radius increases from 0.25m to 1.0m the efficiency also increase up to a maximum of 83% but then, the research could not

go beyond a radius of 1m and find out the very optimum arm radius which gives the highest efficiency.

One of the limitations in this research is that it does not pay attention to the process by which the water reaches the turbine from the river (reservoir, penstock design, housing for turbine). Furthermore the research does not pay attention to the process by which the water flows back to the river. Therefore there is need for further research on the same.

The research recommended that an arm conduit with a larger and varying cross-sectional area could be used so as to allow higher discharge and scaling up of the turbine.

REFERENCES

3Helix power. (n.d.). Selection of hydro-turbines. Retrieved August, 08, 2015, from http://www.3helixpower.com/hydropower/types-of-turbines.

Akbarzadeh, A. (2001) Parametric Analysis of a Simple Reaction Water Turbine and its Application for Power Production from Low Head Reservoirs. *Fluids Engineering Division Summer Meeting*. New Orleans, Louisiana, USA, ASME.

An Introduction to Nuclear Energy. Retrieved January, 6, 2017, from https://www.azocleantech.com/article.aspx?ArticleID=60 .

Barr, J. (2013). *Improving Maintenance of Micro Hydropower Systems in Rural Nepal*. Uppsala University, Sweden.

Basar, M. F., Ahmad, A., Hasim, N., & Sopian, K. (2011). Introduction to the pico-hydro power and the status of implementation in Malaysia. In *Research and Development (SCOReD), 2011 IEEE Student Conference on* (pp. 283-288). IEEE.

Bearing coefficient of friction. (n.d.). Retrieved February 17, 2017, from http://www.amroll.com/friction-frequency-factors.html.

Bearing coefficient of friction. (n.d.). Retrieved February 17, 2017, from http://www.precisionrpm.com/pub/koyo/speed4.

Calvert, J. B. (2003). Turbines. Retrieved September 12, 2015, from https://mysite.du.edu/~jcalvert/tech/fluids/turbine.htm History and Modeling of turbines.

Çengel, Y. A., & Cimbala, J. M. (1996). Introduction to Computational Fluid Dynamics.

Cengel, Y., & Cimbala, J. (2006). *Fundamentals and Application*. McGraw-Hill, USA.

Coefficient of friction. (n.d.). Retrieved February 17, 2016, from http://www.engineershandbook.com/Tables/frictioncoefficients.

Coefficient of friction. (n.d.). Retrieved February 18, 2017, from http://www.engineeringtoolbox.com/minor-loss-coefficients-pipes.

Date, A. (2009). Low head simple reaction water turbine. *School of Aerospace Mechanical and Manufacturing Engineering*, 251.

Date, A., & Akbarzadeh, A. (2009). Design and cost analysis of low head simple reaction hydro turbine for remote area power supply. *Renewable Energy*, *34*(2), 409-415.

Daugherty, R. L., & Ingersoll, A. C. (1954). *Fluid mechanics: with engineering applications*. Tata McGraw-Hill Education.

Derry, T. K., & Williams, T. I. (1993). A short history of technology from the earliest times to AD 1900 (rist. anast.). Mineola.

Development of Kenya power sector. Retrieved February, 11, 2017, from https://www.usaid.gov/sites/default/files/documents/1860/Kenya_Power_Sect or_report.

Duncan, W. J., & Thom, A. S. (1970). *Mechanics of fluids* (No. 532 D8 1970).

Energy regulatory commission of Kenya. Retrieved August, 5, 2015, from https://www.erc.go.ke/.

Garshelis, I. J. (2007). 20.4 Torque and Power Measurement. *Mechatronic Systems, Sensors, and   Actuators: Fundamentals and Modeling*, *20*, 48.

Gorlov, A. (1998). Development of the helical reaction hydraulic turbine. *NASA*, (19990036780).

Government Publications Office (Ed.). (2016). *International Energy Outlook 2016: With Projections to 2040*. Government Printing Office.

Harvey, A. (1993). *Micro-Hydro Design Manual: a guide to small-scale water power schemes* (No. 621.24/H341). Intermediate Technology Publications.

Helix power. (n.d.). Types of hydropower turbines. Retrieved January, 09, 2017, from http://www.ritchiewiki.com/wiki/index.php/Hydraulic_Turbine.

Hirsch, C. (2007). *Numerical computation of internal and external flows: The fundamentals of computational fluid dynamics*. Butterworth-Heinemann.

Husain, Z., Mohd. Zulkifly Abdullah, & Alimuddin, Z. (2008). *Basic fluid mechanics and hydraulic machines*. Hyderabad, India: BS publications.

Hydro power. (n.d.). Retrieved March 02, 2016, from http://edugen.wiley.com/edugen/courses/crs2436/crowe9771/crowe9771...1.

Incropera, F. P. deWitt DP (2002): Fundamentals of Heat and Mass Transfer.

Kaunda, C. S., Kimambo, C. Z., & Nielsen, T. K. (2012). Potential of small-scale hydropower for electricity generation in Sub-Saharan Africa. *ISRN Renewable Energy*, *2012*.

Kothandaraman, C.P., & Rudramoorthy R. (2007). *Fluid Mechanic and Machinery 2nd ed*.

Kothari, D. P., Ranjan, R., & Singhal, K. C. (2011). Renewable energy sources and technology.

Maher, P., Smith, N. P. A., & Williams, A. A. (2003). Assessment of pico hydro as an option for off-grid electrification in Kenya. *Renewable Energy*, *28*(9), 1357-1369.

Mango, L. M., Melesse, A. M., McClain, M. E., Gann, D., & Setegn, S. G. (2011). Land use and climate change impacts on the hydrology of the upper Mara River Basin, Kenya: results of a modeling study to support better resource management. *Hydrology and Earth System Sciences*, *15*(7), 2245-2258.

McCulloch, M. (2011). *Studies into the technical feasibility of the transverse horizontal axis water turbine* (Doctoral dissertation, University of Oxford).

Najafi, M. R., Zwiers, F. W., & Gillett, N. P. (2015). Attribution of Arctic temperature change to greenhouse-gas and aerosol influences. *Nature Climate Change*, *5*(3), 246.

Nuclear Fusion Power. Retrieved January, 6, 2017, from http://www.world-nuclear.org/information-library/current-and-future-generation/nuclear-fusion-power.aspx.

Rigden, J. S., & Rigden, J. S. (2005). *Einstein 1905*. Harvard University Press.

Secretariat, R. (2014). Renewables 2014 global status report. *REN21, Paris, Tech. Rep*.

Shepherd, D. G. (1956). *Principles of turbomachinery*. Macmillan.

Sieminski, A. (2014). International energy outlook. *Energy Information Administration (EIA)*, *18*.

Sitters, C. W. M. (1994). Class notes. *Continuum analysis of control vole*.

Sitters, C. W. M. (2014). Class notes. *Introduction to continuum mechanics*.

Sternberg, R. (2008). Hydropower: dimensions of social and environmental coexistence. *Renewable and Sustainable Energy Reviews*, *12*(6), 1588-1621.

Strandh S., (1979). *A History of the Machine.* New York: A&W Publishers.

Taylor, R. (2004) Hydropower. In J Trinnaman, A. C. (Ed.) *2004 Survey of Energy Resources (Twentieth Edition).* 20 ed. Oxford, Elsevier Science.

Toshiba Corporation Power Systems and Services Company, (2010). *Hydraulic Turbines*.

Twidell, J., & Weir, T. (2006). Renewable Energy Resources. by Taylor and Francis. *Newyork, USA*.

Twidell, J., & Weir, T. (2015). *Renewable energy resources*. Routledge.

Waddell, R., Bryce, P. (1999) Micro-hydro systems for small communities. *Renewable Energy,* 16**,** 1257-1261.

Wilson, P. N. (1974). *Water turbines*. HM Stationery Off.

APPENDICES

Appendix A

Relative uncertainty in measurement of supply pressure with Aijkelkamp-Agrisearch Equipment pressure gauge is ± 1.8%. Relative uncertainty in measurement of the flow through turbine using Omega flow meter is ± 2.5%. Relative uncertainty in measurement of time using a standard stop watch is +/-3.4% up to 10sec, there after ±1.6%. Relative uncertainty in measuring turbine force using the electronic weighing scale is ±0.5%. Based on this information the relative uncertainty of torque can be calculated.

Appendix B

Bearing Friction by American Roller Bearing Company

Rolling element bearings, such as ball bearings and roller bearings, are used in equipment primarily because they support the loads inherent to the machine's function at a much lower friction level than any oil film bearing, such as bronze or Babbitt. This reduces the power required to drive the equipment, lowering the initial cost of the prime mover and the energy to operate it. While sometimes generically referred to as "Anti-Friction" bearings*, there is a small amount of friction or resistance to rotation in every ball and roller bearing. The sources of this friction are: slight deformation of the rolling elements and raceways under load, sliding friction of the rolling elements against the cage and guiding surfaces. Different bearing types, because of their internal designs, result in slightly different amounts of internal friction.

Table A1: Friction coefficient of bearings (http://www.amroll.com/friction-frequency-factors.html)

Bearing Type	Coefficient of friction – µ
Deep Groove Ball Bearing	0.0015
Angular Contact Bearing	0.0020
Cylindrical Roller Bearing, Cage	0.0010
Cylindrical Roller Bearing, Full Comp.	0.0020
Tapered Roller Bearing	0.0020
Spherical Roller Bearing	0.0020
Ball Thrust Bearing	0.0015
Cylindrical Roller Thrust Bearing	0.0050
Tapered Roller Thrust Brg. Cage	0.0020
Tapered Roller Thrust Brg. Full Comp	0.0050

Frictional force would simply be: Force = P x μ

Another contributor to bearing internal friction is the lubricant, grease or oil, that is continually being pushed aside as the rolling elements circulate around the raceways. Coefficients of friction for the various types of bearings are based on a reference value of lubricant viscosity of 20 cSt/100SUS at the bearing's operating temperature. Coefficients of friction for different bearing types are shown in Table III.

More important to the equipment designer than frictional force is the amount of frictional torque that must be overcome. This parameter can easily be calculated using the formula below:

where:

P = Equivalent Load on the bearing

μ = Coefficient of friction

dm = Pitch diameter of bearing

Lastly, the amount of power consumed by bearing friction can be easily calculated using the appropriate SI or Imperial formula knowing the resistance Torque and RPM.

Table A2: Coefficient of friction for a range of material combinations

Coefficient of friction for a range of material combinations				
Combination	**Static**		**Dynamic**	
	Dry	**Lubricated**	**Dry**	**lubricated**
steel-steel	0.5...0.6	0.15	0.4...0.6	0.15
copper-steel	-	-	0.5...0.8	0.15
steel-cast iron	0.2	0.1	0.2	0.05
cast iron - cast iron	0.25	0.15	0.2	0.15
friction material - steel	-	-	0.5-0.6	-
steel-ice	0.03	-	0.015	-
steel-wood	0.5-0.6	0.1	0.2-0.5	0.05
wood-wood	0.4-0.6	0.15...0.2	0.2...0.4	0.15
leather-metal	0.6	0.2	0.2...0.25	0.12
rubber-metal	1	-	0.5	
plastic-metal	0.25...0.4	-	0.1...0.3	0.04...0.1
plastic-plastic	0.3-0.4	-	0.2...0.4	0.04...0.1

The coefficient of friction between two materials in relative sliding may depend on contact pressure, surface roughness of the relative harder contact surface, temperature, sliding velocity and the type of lubricant whether the level of contamination. It's the reason that the data found in the many reference tables available may show a large

variation.   The   reference   of   table   A2   found   at;
http://www.engineershandbook.com/Tables/frictioncoefficients.htm.

The table A3 retrieved from; www.engineeringtoolbox.com/friction-coefficients-
d_778.html

Table A3: Coefficient of friction in bearings

Coefficient of friction in bearings	
	Coefficient of friction [-]
Slide bearing, hydrodynamic	0.003...0.04
Slide bearing, sinter bronze, oil lubricated	0.04...0.07
Slide bearings, solid bronze, grease lub	0.07...0.12
Polymer slide bearing, polyamide, dry	0.2...0.3
Polymer bearing, composite, dry	0.05...0.15
Ball bearings	0.001...0.0015
Roller bearings	0.0018
Needle bearings	0.0045
Air bearings, pressurized	0.0
Hydrostatic bearings	0.001...0.002, ref viscous shearin

TACHOMETERS

3631 00,
3632 00 & 3633 00

3631 00, 3632 00 & 3633 00
Pocket Tachometers

3631 00
50 (W) × 220 (H) × 30 (D) mm
210g

3633 00
50 (W) × 240 (H) × 30 (D) mm
270g

3632 00
50 (W) × 180 (H) × 30 (D) mm   210g excludes probe

New, pocket digital tachometers provide easy one-hand operation. The 3631 and 3632 operate from photo probe, and the 3633 uses a contact rubber tip or surface speed wheel. These pocket-sized tachometers are ideal tools for safe and simple measurement of rotational speed.

3631 & 3632
- SAFE TO OPERATE WITH NO CONTACT WITH MACHINE
- CRISP TONE SOUNDS AND ◄ MARK DISPLAYED WHEN THE BEAM OF LIGHT IS ON TARGET
- ANALOG OUTPUT, AND PROBE LEAD FOR HARD TO GET AT LOCATIONS ... 3632

3633
- SURFACE SPEED WHEELS (OPTIONAL)

COMMON TO ALL MODELS
- UP TO 19,999 rpm IN TWO RANGES
- 0.1 rpm RESOLUTION UP TO 1,999.9 rpm
- SAMPLE (MEAS)/HOLD MODE SELECTOR
- PALM-SIZE PACKAGE

SPECIFICATIONS
Common to 3631 to 3633
Sample Rate: 0.5 to 1s (1s on 3633 20,000 rpm range)
Type of Display: 5-digit LCD
Maximum Reading: 19999
Overrange Indication: - - - - display
Low Battery Indication: B mark display
Mode Selector: MEAS, HOLD, or LOCK (continuous measurement)
Operating Temperature Range: 0 to 50°C (32 to 122°F)
Power Source: Single 9 V battery (IEC 6F22, Energieblock 9 V or equivalent), approx. 7 hours of continuous operation
Spares: B9691AL reflective tapes (10 sheets/unit)... for 3631 or 3632 (order q'ty: 1 unit), B9691 LA rubber tips (3 pcs /unit)... for 3633 (order q'ty: 1 unit)

Analog Output (3632 only)
Output Voltage: 0.1 V/1,000 rpm to 2.0 V/20,000 rpm
Accuracy: ±5% of range
Ripple Noise: Less than 0.1 Vp-p
Response Time: Within 1s (to reading within 90% of final value)
Output Impedance: Approx. 1 kΩ

Optional Accessories for 3633: Surface speed wheel... B9691 LD (m/min), B9691LP (mm/s)

Model	3631	3632	3633
Measurement System	Touchless, using a photo probe and reflective tape		Touch, using a contact rubber tip (standard) , or surface speed wheel (optional)
Measuring Ranges:	2,000rpm range ... 60.0 to 1,999.9rpm 20,000rpm range ... 60 to 19,999rpm		2,000rpm range ... 6.0 to 1,999.9rpm 20,000rpm range ... 1 to 19,999rpm
Resolution	0.1rpm on 2,000rpm range, 1rpm on 20,000rpm range		
Accuracy	2,000rpm range: ±0.1rpm for 60 to 400rpm ±0.2rpm for 400 to 1,200rpm ±0.3rpm for 1,200 to 1,999rpm 20,000rpm range: ±1rpm for 60 to 4,000rpm ±2rpm for 4,000 to 12,000rpm ±3rpm for 12,000 to 19,999rpm		2,000rpm range: ±0.1rpm for 6 to 160rpm ±0.2rpm for 160 to 1,000rpm ±0.3rpm for 1,000 to 1,600rpm 20,000rpm range: ±2rpm for 1 to 19,999rpm
Effective Measurement Distance between Photo Probe and Reflective Tape	*30 to 300mm	*5 to 50mm	—
	*At light projection angle of within ±30°, and reflective tape size of 10mm by 10mm		
Reflective Light Input	Buzzer sounds, and ◄ mark displayed		—
Standard Accessories	Soft case ... 1 pc, 9V battery ... (1 pc, built-in) , reflective tapes (10×90mm) ... 10 sheets, tripod adapter ... 1 pc		Soft case ... 1 pc, 9V battery ... (1 pc, built-in) , rubber tips (B9691LA) ... 3 pcs
	—	Probe fixture ... 1 set, analog output lead ... 1 set	

Figure A1: Tachometer

Loss of energy due to friction

Darcy-Weishbach equation: Head loss due to friction,

$$h_f = f\frac{L}{d}\frac{V^2}{2g} = 4C_f\frac{L}{d}\frac{V^2}{2g}$$

L: length of the pipe
V: mean velocity of the flow
d: diameter of the pipe

f is the friction factor for fully developed laminar flow:

$$f = \frac{64}{Re} \ (for \ Re < 2000)$$

$$Re = \frac{\rho u_{avg} d}{\mu}$$

C_f is the skin friction coefficient or Fanning's friction factor.

For Hagen-Poiseuille flow: $C_f = \tau_{wall} / \frac{1}{2}\rho u_{avg}^2 = \frac{16}{Re}$

For turbulent flow:

$$\frac{1}{\sqrt{f}} = 1.74 - 2.0 \ log_{10}\left[\frac{\varepsilon_p}{R} + \frac{18.7}{Re\sqrt{f}}\right]$$

Moody's Diagram

R: radius of the pipe
ε_p : degree of roughness (for smooth pipe, $\varepsilon_p = 0$)
$Re \rightarrow \infty$: completely rough pipe

- **Head loss at the entrance of the pipe:** $h_i = 0.5\frac{v^2}{2g}$,

  where *v* is the velocity of the liquid in the pipe.

- **Head loss at the exit of the pipe:** $h_0 = \frac{v^2}{2g}$,

  where *v* is the velocity of the liquid at the outlet of the pipe.

- **Head loss due to bend in pipe:** $h_b = \frac{kv^2}{2g}$,

  where *v* is the velocity of the flow, k is the coefficient of the bend which depends on the angle of the bend, radius of curvature of the bend and diameter of pipe.

- **Head loss due to pipe fittings:** $h_f = \frac{kv^2}{2g}$,

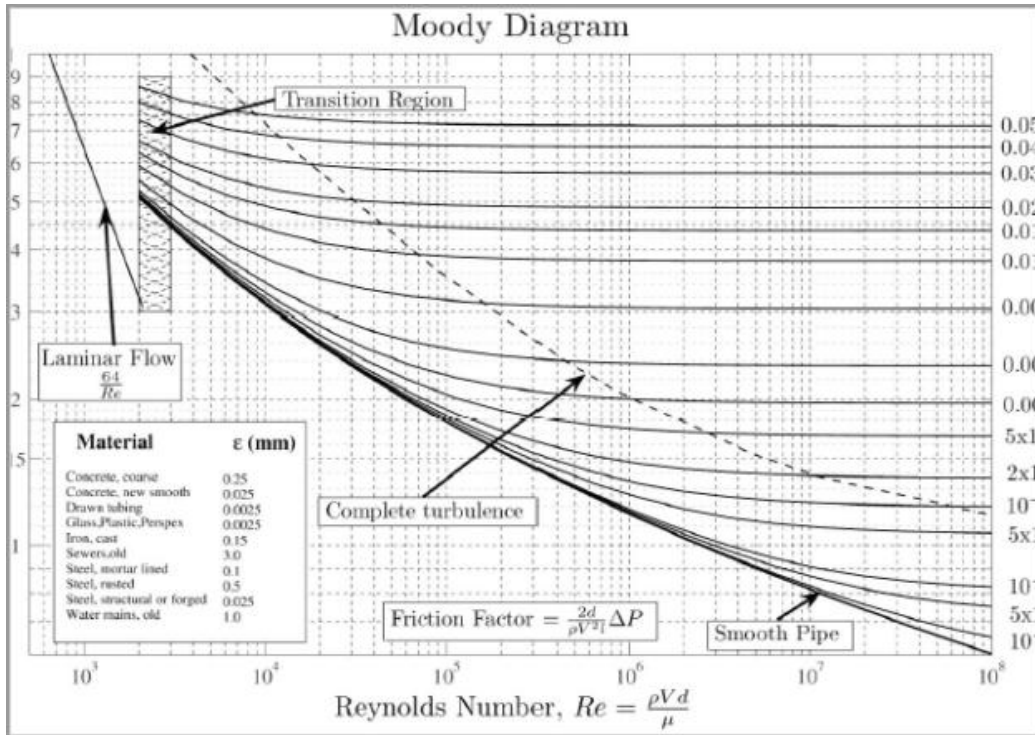 where *v* is the velocity of the flow, k is the coefficient of pipe fitting.

Figure A2: Moody Diagram (Cengel et al., 1996)

Appendix C

Experimental procedure on how to find power for loaded turbine at optimum speed.

A typical example of how to use a rope brake dynamometer and tachometer to obtain power of this turbine is as shown below. Throughout this test the hydrostatic supply head is kept constant.

You will first need to set the torque test rig as shown in figure 4.6;

Then let say the dead load W_0 = 1.5kg.

So that weighing scale readings W= 1.25kg; this is less because of friction between the rope and pulley surfaces. Then reset the weighing instrument so as to read W=0.

Switch on the flow valve shown in figure 4.2 (a). The turbine will start running as the water ejects out from the orifice tip.

As soon as the turbine start running in the anticlockwise direction the readings in the weighing instrument also begin to increase from S=0 (i.e. if the instrument had been reset to zero). As the turbine approaches its maximum speed, 'S' approaches maximum.

When the turbine angular speed is at its optimum and stable, check the readings displayed on weighing instrument and if it is no longer increasing note it down. For this case S_{max}=9.5kg. You should recall that this value is a representative of (S-W). But since W=0 (because the instrument was reset to start at zero) then you only remain with 'S' which is S_{max}=9.5kg.

Converting S_{max} into force/weight it becomes F= S_{max}*9.81=93.195N.

But from equation 4.9, T_b = F*R =F*(r_d+ r_l)= 93.195*(0.025+0.001) =**2.42307Nm.**

Use the digital tachometer to find the corresponding angular speed of the turbine. For example in this case angular speed $\omega = 2\pi\left(\frac{N}{60}\right) = 2\pi\left(\frac{135}{60}\right) =$ **7.854rads/sec.**

Therefore $P = \omega * T = 7.854 * 2.42307 = $**19.031W**.

Experimental procedure on how to find maximum torque of the turbine

Method 1; in this method, as you increase the dead load weight from zero to a certain magnitude torque also increases from zero to a certain maximum magnitude and remain constant even with a further increase of the dead load weight.

Method 2; for this method the turbine test rig for determining the maximum torque of the turbine is as shown in the diagram below;
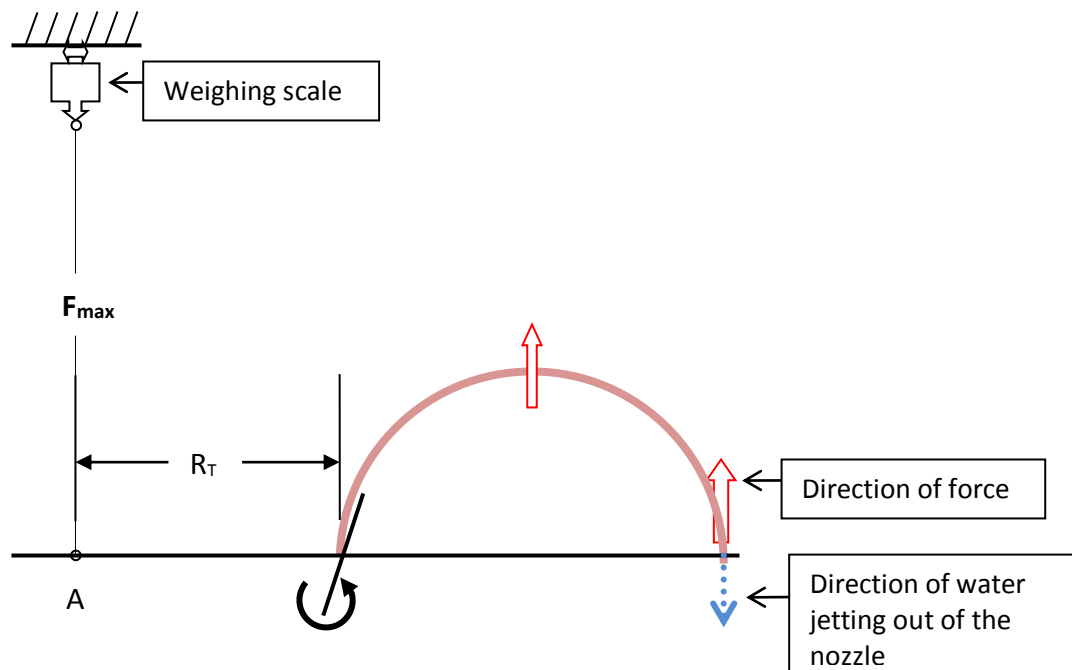

Figure A3: A turbine test rig for determining the maximum torque

After setting up the rig as shown in figure A3 (note the maximum force on the weighing scale).

Measure the distance between point A and the centre (axis of rotation).

But torque is a product of force and radius of actions. Therefore;

$T_{max} = F_{max} * R_T$

Since the turbine is strained by the weighing scale it means it can't rotate, so that $\omega = 0$ and therefore $P = \omega * T_{max} = 0\ W$

Experimental procedure on how to find maximum angular speed of the turbine

The following procedure was used to find the maximum angular speed of the turbine;

Throughout this test the hydrostatic supply head is kept constant.

Ensure that the turbine is not loaded or strained. Also ensure that there are minimal mechanical frictions.

Switch on the flow valve.

As the water exits trough the turbine nozzle it courses the turbine to start rotating anticlockwise.

With time angular speed of the turbine increases from zero to maximum

When the angular speed is stable and no longer increasing it means it is at its maximum.

Appendix D

As shown in th Figure 3.7 arbitrary spatial point P can be indicated by its coordinates x,y,z with respect to the inertial frame, or by its position vector $\vec{x}$ In other words, when we write $\vec{v}(x,y,z,t)$ or $\vec{v}(\vec{x},t)$, both representations refer to the velocity of the material in the same spatial point at time t Therefore as a short hand, the representation with the vector will be used from now on.

Applying the general definition to arrive at the time derivative of $\phi_m(t)$, we find:

$$\frac{d}{dt}[\phi_m(t)] = \lim_{\Delta t \to 0} \frac{1}{\Delta t}\left(\phi_m(t+\Delta t) - \phi_m(t)\right) = \lim_{\Delta t \to 0} \frac{1}{\Delta t}\left(\int_{V_m(t+\Delta t)} \psi(\vec{x},t+\Delta t)dV - \int_{V_m(t)} \psi(\vec{x},t)dV\right)$$

$$(2.2.3)$$

It should be clear that $\psi(\vec{x},t)$ is a quantity in a spatial point $\vec{x}$ as a function of time t. This quantity is not directly related to a certain material particle, because the fluid flows through space, and a lot of different material particles are passing that specific point. The volume $V_m(t+\Delta t)$ can be related to the volume $V_m(t)$ by the following relation (Fig 2.2.1):

$$V_m(t+\Delta t) = V_m(t) + A_m(t)(\vec{v}\bullet\vec{n})\Delta t \qquad (2.2.4)$$

The first integral of (2.2.3) can now be rewritten as:

$$\int_{V_m(t+\Delta t)} \psi(\vec{x},t+\Delta t)dV = \int_{V_m(t)} \psi(\vec{x},t+\Delta t)dV + \int_{A_m(t)(\vec{v}\bullet\vec{n})\Delta t} \psi(\vec{x},t+\Delta t)dV \qquad (2.2.5)$$

In the last integral of (2.2.5) $dV = d[A(\vec{v}\bullet\vec{n})\Delta t]$. Changing the argument leads to:

$$\int_{V_m(t+\Delta t)} \psi(\vec{x},t+\Delta t)dV = \int_{V_m(t)} \psi(\vec{x},t+\Delta t)dV + \Delta t\int_{A_m(t)} \psi(\vec{x},t+\Delta t)(\vec{v}\bullet\vec{n})dA \qquad (2.2.6)$$

Substitution of (2.2.6) into (2.2.3) gives:

$$\frac{d}{dt}[\phi_m(t)] = \lim_{\Delta t \to 0} \frac{1}{\Delta t}\left(\int_{V_m(t)} [\psi(\vec{x},t+\Delta t) - \psi(\vec{x},t)]dV\right) + \lim_{\Delta t \to 0} \frac{1}{\Delta t}\left(\Delta t\int_{A_m(t)} \psi(\vec{x},t+\Delta t)(\vec{v}\bullet\vec{n})dA\right)$$

$$(2.2.7)$$

The volume over which is integrated is not a function of Δt any more, therefore:

$$\frac{d}{dt}[\phi_m(t)] = \int_{V_m(t)} \lim_{\Delta t \to 0} \left(\frac{\psi(\vec{x}, t+\Delta t) - \psi(\vec{x}, t)}{\Delta t} \right) dV + \int_{A_m(t)} \lim_{\Delta t \to 0} \psi(\vec{x}, t+\Delta t)(\vec{v} \bullet \vec{n}) dA \quad (2.2.1$$

The integrand of the first integral is, according to the definition, equal to the spati time derivative of ψ. In the second integral the limit simply can be evaluated:

$$\frac{d}{dt}[\phi_m(t)] = \int_{V_m(t)} \frac{\partial}{\partial t}[\psi(\vec{x}, t)] dV + \int_{A_m(t)} \psi(\vec{x}, t)(\vec{v} \bullet \vec{n}) dA \quad (2.2.$$

The derivation from (2.2.3) up to (2.2.9) can be repeated, completely analogous, for spatial volume V_c. For the time derivative of $\phi_c(t)$ it follows:

$$\frac{d}{dt}[\phi_c(t)] = \int_{V_c(t)} \frac{\partial}{\partial t}[\psi(\vec{x}, t)] dV + \int_{A_c(t)} \psi(\vec{x}, t)(\vec{u} \bullet \vec{n}) dA \quad (2.2.1($$

At time t the volumes $V_m(t)$ and $V_c(t)$ overlap completely. Because $\partial \psi(\vec{x}, t)/\partial t$ is tl spatial derivative of a quantity in a certain point $\vec{x}$ and not related to the volume, tl two integrals over the volumes $V_m(t)$ and $V_c(t)$ in (2.2.9) and (2.2.10) are equa Combination of these equations yields:

$$\frac{d}{dt}[\phi_m(t)] = \frac{d}{dt}[\phi_c(t)] + \int_{A_c(t)} \psi(\vec{x}, t)(\vec{v} - \vec{u}) \bullet \vec{n} dA \quad (2.2.1)$$

Where it has been used that $A_m(t) \equiv A_c(t)$. The combination of (2.2.11) and (2.2. simply gives:

$$\frac{d}{dt}\left(\int_{V_m(t)} \rho(\vec{x}, t)\varphi(\vec{x}, t) dV \right) = \frac{d}{dt}\left(\int_{V_c(t)} \rho(\vec{x}, t)\varphi(\vec{x}, t) dV \right) + \int_{A_c(t)} \rho(\vec{x}, t)\varphi(\vec{x}, t)(\vec{v} - \vec{u}) \bullet \vec{n} dA$$

$$(2.2.1$$

Appendix E

Scaled Up Version of the Turbine (1000w)

Introduction

The turbine fabricated in this research could only produce a maximum power of 2.6W at a height of 1.85m. Conversely, when operating at a height of 11.5m it could produce a maximum of 19.5W. Therefore there is need to have a scaled up version of the turbine so as to achieve a meaningful output power. The purpose of this chapter is to scale the turbine model up to an output power of more than 1000W (1KW).

Design and Calculation

The easiest way to optimally scale up this type of turbine is by increasing the cross-sectional area of the arm conduit for more discharge. The reason why this method is the most preferred is that; increased cross-sectional area means low friction within the conduit hence relative increase in flow rate. None the less referring to the output power formula in section 3.5.5, you can as well increase the conduit radial length. By so doing it increases the centrifugal force suction effect hence increasing the flow rate. However, increasing the radial length comes with its own disadvantages like, increased friction within the conduit hence lowering the flow velocity.

If we therefore increase the internal diameter of the conduit from the current 11mm to a predetermined diameter of 120mm the cross-sectional area becomes $A_e = \pi r^2 = 0.01131m^2$. From the analysed data in chapter five we see that when the operating height is H=1.85m, the efficiency of the turbine is $\approx 0.829 = 83\%$. Figure A4 shows the design of a centrifugal reaction water turbine with a larger semicircular conduit.
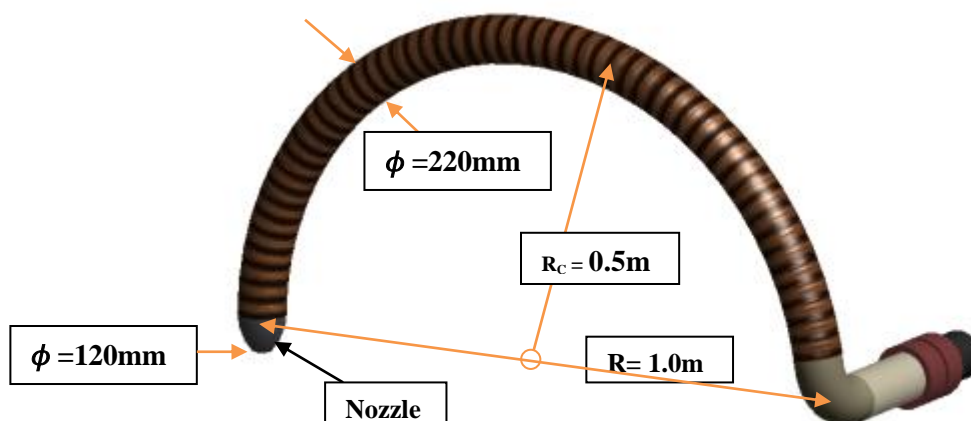

Figure A4: Scaled semicircular conduit and its dimensions

Using the same operating conditions for this scaled version and applying the formula of output power in section 3.5.5, find the output power.

Using the equation in section 3.5.1;

$$V_i A_i = (V_e - u_e cos\beta)A_e = \left(\sqrt{2gH + \omega^2 R^2 cos^2 \beta}\right) A_e = Q$$

$$Q = \left(\sqrt{2gH + \omega^2 R^2 cos^2 \beta}\right) A_e = \left(\sqrt{2(9.81 * 1.85) + (8.0634^2 * 1^2)}\right) * 0.01131$$

$$Q = 0.1138414 m^3/s$$

The equation of power from section 3.5.5 is;

$$P = -\rho Q(\omega R cos\beta)\left(\sqrt{2gH + \omega^2 R^2 cos^2 \beta}\right) + \omega R cos\beta) \rightarrow \beta = 180^0$$

$$P = 1000 * 0.1138414(8.0634 * 1)\left(\left(\sqrt{2(9.81 * 1.85) + (8.0634^2 * 1^2)}\right)\right.$$

$$\left. - 8.0634 * 1\right)$$

$$P = \mathbf{1043.262}W$$

Turbine Cost analysis

The manufacturing costs of the scaled turbine are shown in table A4.

Table A4: Cost of fabricating the turbine

Type of component	Cost of component per unit in Ksh	No of units	Total coast in Ksh
Flow control valve	850ksh/valve	1	850
Mechanical rotary lip seal device	(total= 650ksh)	_	650
Axial, Central holed shaft	2250ksh/metre	0.5	1175
Radial centre beam	300/metre	2.2	660
Semicircular PVC conduit	155ksh/metre	2	310
Nozzle	155ksh/unit	1	155
Bearings	300ksh/bearing	2	600
Turbine Frame materials	(Total= 2800ksh)	_	2800
Labour	(Total= 2600ksh)	_	2600
			TOTAL= Ksh 9800

This means that the cost of manufacturing a 1KW turbine is approximately Ksh 9800. When you compare this with conventional turbine as shown in section 2.9, it becomes clear that this type of turbine is more cost effective. Maintenance cost has not been factored in as it is more or less similar to the maintenance procedure and cost of most of the available turbines.